University of Sussex

Kinematically Redundant Parallel Robots for High Performance Applications

Nicholas Baron

Submitted for the degree of Doctor of Philosophy

University of Sussex

September 2020

Declaration

I hereby declare that this thesis has not been and will not be submitted in whole or in part to another University for the award of any other degree.

Signature:

Nicholas Baron

UNIVERSITY OF SUSSEX

Nicholas Baron

Doctor of Philosophy

Kinematically Redundant Parallel Robots for High Performance Applications

September 2020

Abstract

This thesis addresses the development of kinematically redundant parallel robots for high performance applications and methods of kinematic analyses tailored towards them. Parallel robot manipulators are well known to hold various advantages over serial manipulators, including having better speeds, accuracies, and power-to-weight ratios. However, a major disadvantage they have is that they suffer from limited workspaces and rotational capabilities; indeed, it can be argued that this is the main reason serial robots are used more frequently in many industries. This thesis aims to address this major shortcoming of parallel robots, whilst maintaining all of their advantages, by concentrating on the solution of kinematic redundancy.

Firstly, an introduction to the topic of kinematically redundant parallel robots for high performance applications is presented and a review of the relevant literature is given. In the second section, a novel kinematically redundant architecture of parallel robot is presented. The kinematic redundancy of the mechanism allows it to achieve full cycle rotations of the end-effector without encountering kinematic singularities, a feat that is not possible for non-redundant systems. The third section addresses the issue with current methods of singularity analyses of parallel robots when applied to kinematically redundant architectures. It is shown that conventional Jacobian-based methods of singularity analysis are unreliable when applied to kinematically redundant architectures. In the fourth section a novel, more robust, method of singularity analysis is presented, which is then used to develop a method of singularity avoidance. The fifth section presents a kinematically redundant architecture that is dynamically balanced, meaning that the shaking forces and moments imposed on the base by the manipulator are nullified. An issue for manipulators moving at high speeds is that shaking forces and moments generated can cause vibration and inhibit the performance of the system. By dynamically balancing the system, the manipulator is able to move at high speeds without experiencing these drawbacks.

The aim of this PhD thesis is that the work presented here can provide some of the building blocks for developers of robot manipulators to create high performance parallel

robots which exhibit high speed, strength, and dexterity, through the use of kinematic redundancy.

Preface

The following publications resulted from the work presented in this thesis.

Journals

- Baron, N., Philippides, A., and Rojas, N. (2019). A novel kinematically redundant planar parallel robot manipulator with full rotatability. Journal of Mechanisms and Robotics,11(1).
- Baron, N., Philippides, A., and Rojas, N. (2020). On the false positives and false negatives of the jacobian matrix in kinematically redundant parallel mechanisms. IEEE Transactions on Robotics, 36:951–958.
- Baron, N., Philippides, A., and Rojas, N. (2020). A robust geometric method of singularity avoidance for kinematically redundant planar parallel robot manipulators. Mechanism and Machine Theory, 151:103863.
- Baron, N., Philippides, A., and Rojas, N. (2020). A dynamically balanced kinematically redundant planar parallel robot. ASME Journal of Mechanical Design, MD-20-1506.

Conferences

- Baron, N., Philippides, A., and Rojas, N. (2018). A Geometric Method of Singularity Avoidance for Kinematically Redundant Planar Parallel Robots. In International Symposium on Advances in Robot Kinematics, pages 187–194. Springer.

Acknowledgements

I would like to thank several individuals whose help and support were vital to the completion of the research conducted for this PhD.

A great thank you has to be given to Dr Nicolas Rojas for, firstly, introducing me to the topic of parallel robotics before my PhD began, and whose knowledge and mentorship since then have been absolutely invaluable. I will forever be grateful for the endless advice and support he has provided during my PhD and for his constant availability to help. Thank you so much, Nicolas!

I would also like to acknowledge my supervisor Andy Philippides for the guidance he has given which has helped steer this PhD research. Without his support, this PhD would certainly not have been possible to complete.

Finally, I would like to thank my colleagues, most notably Angus Clark and Icey Lu, with whom I have spent many hours in the lab! In addition to the great help I have received from them on a technical front, they have also made the PhD experience much more enjoyable.

Contents

List of Figures

Chapter 1

Introduction

Robotic manipulation is an important area of robotics which has a large variety of applications, including manufacturing, packaging, medical, and many others. Most robot manipulators can be placed into one of two categories; serial robots and parallel robots. Serial robots are mechanisms for which the end-effector, the tool at the end of the robot, is connected to the base by a sequence of links connected by actuated joints; for example, a robotic arm. Serial robots are arguably the most commonly known type of manipulator and are used frequently in many applications. Parallel robots on the other hand are closed-loop mechanisms where the end-effector is joined to the base via multiple sequences of links and joints. Due to the nature of their kinematic structure, it is often the case that each sequence of links, referred to as limbs, only require a single joint to be actuated, and this is often attached to the base. This provides multiple advantages, for instance, as the actuators are connected to base, the total mass of the moving parts of the mechanism is reduced which enables the robot to achieve faster motions of the end-effector. Additionally, as no actuators are connected in series, parallel robots do not suffer from the accumulation of actuator errors along each of their limbs, instead the actuator errors are averaged. Finally, the load being carried by the robot is distributed over several limbs instead of a single one, resulting in stronger weight-carrying capabilities.

Despite these multiple advantages, serial robots are still used more frequently than parallel robots in many applications. The reason for this is that parallel robots have one major disadvantage, which is that they have considerably smaller workspaces and rotational capabilities of the end-effector. This means that for any task which requires the end-effector to move over a large distance with respect to the size of the mechanism, or is required to undergo significant rotations, parallel robots are often unsuitable. Indeed, the main reason for this shortcoming is the existence of singularities in their workspaces. Sin-

gularities, which will be explored in greater depth later in this chapter, are configurations of the mechanism in which control of the robot is lost due to an instantaneous change in the number of degrees of freedom of the mechanism. Following this, singularities must be avoided which, in practice, reduces the feasible workspace of the parallel robot. In order for parallel robots to be used for applications of high performance where larger workspaces and rotational capabilities are required, this main challenge must be overcome. In this thesis, this issue is addressed through the solution of kinematic redundancy.

A kinematically redundant parallel robot defines a mechanism for which the total number of degrees of freedom of the actuated joints exceeds the number of degrees of freedom of the end-effector, but is equal to the total degrees of freedom of the system; this is explored in further detail later in this chapter. The advantage of these types of mechanisms is that the redundant degrees of freedom can be utilised to avoid singularities, which helps to significantly increase the robot's workspace and rotational capabilities. However, until now kinematic redundancy has received relatively little attention in the literature. Kinematically redundant robots have a great potential to be used in applications of high performance, where high speed, strength, accuracy, and dexterity are required, however there are still some key areas which need to be addressed in order for this potential to be realised. This thesis aims to address some of these key challenges so that developers of robot manipulators are able to use kinematically redundant architectures for applications of high performance. This first challenge is that, currently, there are very few architectures of this type that have been proposed in the literature, which limits the amount of research that can be conducted on these types of mechanisms. In chapter 2, a novel kinematically redundant architecture is presented which has full rotational capabilities of the end-effector, a feat that is not possible for non-redundant mechanisms. The second issue, which is investigated in chapter 3, is that conventional methods of singularity analysis are unreliable when applied to kinematically redundant architectures. In chapter 4, a method of singularity analysis which is more reliable than conventional methods is presented and, additionally, a method of singularity avoidance is proposed which utilises the redundancy of the robot to move as far away from a singularity as possible. Finally, in chapter 5 a dynamically balanced architecture of a kinematically redundant parallel robot is presented which does not exhibit shaking forces or moments onto the base regardless of the speed at which the mechanism is moving, what increases its accuracy and reliability.

The remainder of the introduction comprises a review of the relevant literature of the main areas of focus of this thesis. Firstly, a background of high performance parallel

robots is given. Following this the issue of singularities in parallel robots is explored, and an overview of the solution of redundancy to this problem is given. Methods of kinematic analyses for determining how close a parallel robot is to a singularity are then reviewed. Finally, the topic of dynamic balancing of parallel robots is explored as means of enhancing the performance of these mechanisms.

1.1 High Performance Parallel Robots

As stated above, a parallel robot is a closed-loop mechanism for which the end-effector is attached to the base by multiple kinematic chains. Parallel robots have increased in popularity over the past few decades. An interest in these mechanisms began in the 1960s, firstly with the development of the Stewart-Gough platform for the application of a tire testing device Gough (1962) and a flight simulating equipment Stewart (1965); Baret (1978); Watson (1984). A parallel mechanism was used for an assembly system for the first time in MacCalion and Pham (1979). In the 1980s, the very fast moving DELTA robot was developed Clavel (1988); the manipulator consists of three arms, each of which takes advantage of parallelogram structures in order to maintain a constant orientation of the output link of the mechanism. The delta robot subsequently gained popularity, especially in the packaging industry. Indeed, the amount of research conducted on parallel robots increased significantly toward the end of the decade Mohamed and Duffy (1985); Merlet (1987, 1988).

Parallel robots have many advantages over serial robots, including strong load carrying capabilities, high speeds, accuracy, and precision Merlet (2006); Briot and Bonev (2008); Patel et al. (2012); Briot and Bonev (2007). The strong load carrying capabilities stem from the multiple kinematic chains which share the load of the moving platform, meaning the load is distributed rather than concentrated along a single chain. Serial robots, on the other hand, consist of a single chain of links connected by actuated joints, a consequence of this is that the added mass of the actuators on each of the joints leads to high inertial loads, whereas for parallel robots the actuated joints are often attached to the base and so the inertial load of each of the kinematic chains is much lower. The lower inertial properties of parallel robots compared to serial robots means that they are able to move much faster. Another issue with having actuated joints connected in series is that the errors of each of the joints are accumulated along the kinematic chain, magnifying the error in the pose of the end-effector Guan et al. (2004); Song et al. (1999). Parallel robots, on the other hand, do not suffer from this issue as the actuated joint errors are averaged rather than

accumulated, which results in a greater accuracy in the end-effector pose Wavering (1999); Miller (2004).

Parallel robots are well suited to high performance applications, that where high speed, accuracy, and precision are required, for the reasons described above. Following this, many parallel robots have been proposed for use applications of high performance. The most well known example of this is the delta robot, which is renowned for its ability to move at very high speeds Pierrot et al. (1991, 1990); Rey and Clavel (1999); Carp-Ciocardia et al. (2003) and, indeed, this has lead to its popularity in packaging applications where fast and accurate movement of the end-effector is required. The Stewart platform is a parallel robot which has gained popularity for its potential to achieve high precision Su et al. (2004); Van Silfhout (1999) and, resultantly, this mechanism has been proposed for use in surgical applications Wapler et al. (2003), radio telescope applications Jáuregui et al. (2013), and for the development of flight simulators Pradipta et al. (2013).

Despite the numerous advantages parallel robots have over serial robots, they have one main disadvantage, which limits the number of applications they can be used in. This drawback is that they have limited workspaces and rotational capabilities. The workspace of a robot manipulator describes the set of possible poses which the end-effector is able to achieve Gupta (1986); Merlet et al. (1998); Bonev and Ryu (2001). It is clear that a large workspace is desirable for many applications and vital for others, and unfortunately parallel robots often are unable to perform these tasks despite their many strengths. Additionally, parallel robots are not well suited to applications where high dexterity of the end-effector is required. Indeed, non-redundant parallel robots are incapable of performing full cycle rotations. This shortcoming limits parallel robots from being used in many high performance applications in which they are otherwise very well suited to. Parallel robots suffer in these areas largely due to the existence of singularities in their workspaces.

1.2 Singularities

The term ‘singularity’ is one that is used to describe a range of problematic configurations of robotic manipulators which result in, generally undesirable, changes in the kinematic properties of the mechanism Zlatanov (1999); Zlatanov et al. (1994). To be more precise, singularities are configurations in which the total number of degrees of freedom of the mechanism instantaneously changes Gosselin and Angeles (1990); Kumar (1992); Park and Kim (1999). A type of singularity that both serial and parallel robots suffer from is the inverse kinematic singularity, a configuration where the inverse kinematic Jacobian

of the mechanism loses rank, which corresponds to a loss in the number of degrees of freedom of the mechanism; for example, if the manipulator reaches the boundary of its workspace Gosselin and Angeles (1990); Ebrahimi et al. (2007); Lai and Yang (1986); Waldron et al. (1985). However, unlike serial robots, parallel robots also suffer from the existence of forward kinematic singularities and, indeed, it is the existence of these types of singularities which limits their workspaces and rotational capabilities.

A forward kinematic singularity is a configuration in which the forward kinematic Jacobian of the mechanism loses rank, which corresponds to an instantaneous increase in the total number of degrees of freedom of the mechanism Merlet (1989); Zlatanov et al. (1994); Park and Kim (1999). When in such a configuration, the input joint velocity vector can be equal to zero and still produce a non-zero end-effector velocity vector; equivalently, even if the acutated joints are locked, the end-effector is unable to resist forces or moments in one or more directions Daniali et al. (1995); Wen and O'Brien (2003). Because of this, direct kinematic singularities result in configurations where control of the robot is lost. Additionally, the performance of the robot will begin to deteriorate as such a configuration is approached; for example, the end-effector may experience shaking which becomes more significant as the singularity is neared. In order to avoid these effects, the workspace of the mechanism has to be reduced such that no singularities are ever crossed or neared, which in practice significantly reduces the size of the mechanism's workspace. This is a significant issue for parallel robots since many applications require the end-effector to move over large distances with respect to the size of the manipulator, and many other require the end-effector to perform large rotations. A solution to this issue is to use redundant architectures.

1.3 Redundancy in Parallel Robots

Redundancy in parallel robots refers to architectures for which the number of actuated degrees of freedom of the joints exceeds the number of degrees of freedom of the end-effector Gosselin and Schreiber (2018); Zanganeh and Angeles (1994a); Lee and Kim (1993). The benefit of redundant architectures is that the additional degrees of freedom enhance the manipulator's ability to avoid singular configurations in the workspace, increasing the size of the feasible workspace of the end-effector. There are two classes of redundancy for parallel robots, actuation redundancy and kinematic redundancy.

1.3.1 Actuation Redundancy

Redundantly actuated parallel robots refer to those for which the total number of actuated degrees of freedom of the joints exceed the total number of degrees of freedom of the mechanism Wu et al. (2009); Chakarov (2004). This results in a mechanism for which a given operational force does not correspond to a unique set of joint forces Krut et al. (2004). Such mechanisms can be obtained by taking a non-redundant architecture, where the total number of degrees of freedom of the mechanism is equal to the number of actuated degrees of freedom of the joints, and adding additional kinematic chains, also referred to as legs, between the moving platform and the base or alternatively by replacing passive joints with actuated joints Gosselin and Schreiber (2018); Luces et al. (2017); Mueller (2013); Garg et al. (2009); Dasgupta and Mruthyunjaya (1998a); Firmani and Podhorodeski (2004).

Multiple redundantly actuated architectures have been proposed in order to improve the robot's ability to avoid singularities. In Kock and Schumacher (1998), a 2-DoF planar manipulator was proposed which consists of three $\underline{\text{R}}$RR legs, that is an actuated revolute joint followed by two passive revolute joints, connected to the base which are joined together at a single point. In Marquet et al. (2001), the ARCHI architecture was proposed, using four $\underline{\text{P}}$RR legs, that is an actuated prismatic joint followed by two passive revolute joints, to produce 3-DoF planar motion. A five-bar finger was presented in Lee et al. (1998) in which the effects of varying the degree of redundancy was investigated. In Ryu et al. (1999), a 6-DoF parallel mechanism which consisted of eight actuated joints was proposed to perform rapid machining applications. In Saglia et al. (2009), a 2-DoF mechanism driven by three linear actuators was used as an ankle rehabilitation device. A 6-DoF mechanism was presented in Abedinnasab and Vossoughi (2009) which consisted of a moving platform connected to the ground by four legs, and which was driven by eight actuated joints.

The additional degrees of freedom provided by each of these redundantly actuated architectures give the robot the potential to avoid singularities and hence increase the feasible workspace of the end-effector. In Collins (1997), a method of selecting the positions of the redudnantly actuated joints such that singularity-free motions can be achieved was proposed. The use of redundancy to avoid singularities was also addressed in Notash and Podhorodeski (1994). The effect of redundancy on reducing the number of singularities in the workspace of a parallel mechanism used for sprained ankle rehabilitation was investigated in Saglia et al. (2008). In Kurtz et al. (1992), the design of a redundantly actuated spherical manipulator was optimised such that the number of singularities in

its workspace was minimised. However, the drawback of using actuation redundancy as a means to achieve singularity avoidance is that as the total number of DoF of the actuated joints is greater than the total number of DoF of the system, the mechanism is over-constrained, meaning that internal forces and moments are generated on the platform. Resultantly, complex control algorithms need to be employed in order to handle this redundancy Cheng et al. (2003); Nokleby et al. (2007); Harada and Nagase (2010); Cheng (2001); Niu et al. (2013). However, there is an alternative solution which enhances the robot's ability to avoid singularities and does not exhibit the issues associated with over-constraining the mechanism; kinematic redundancy.

1.3.2 Kinematic Redundancy

Just like architectures that are redundantly actuated, the total number of DoF of the actuated joints of kinematically redundant robots is greater than that of the end-effector. However, the difference between these two classes of redundant robots is that for kinematically redundant architectures the total number of DoF of the system is equal to the DoF of the actuated joints; in other words, the mechanism is not over constrained Zanganeh and Angeles (1994b); Huang and Kong (1995). Not many kinematically redundant architectures have been proposed in the literature. In Wang and Gosselin (2004), a planar mechanism was presented in which the moving platform was connected to the base by two RPR legs and one RRPR leg. A planar mechanism consisting of three PRRR legs was presented in Ebrahimi et al. (2007). Other variations of three-legged planar architectures were presented in Cha et al. (2007), including a 3-RRPR and a 3-RPRPR mechanism. In Wang and Gosselin (2004), 4-DoF Mechanism in which the end-effector is capable of spherical motion and a 7-DoF spatial Stewart platform are presented. Although these kinematically redundant architectures greatly reduce the number of unavoidable singularities in their respective workspaces, and without over constraining the mechanism, they all consist of actuated joints connected in series. This is problematic as it detracts from some of the fundamental advantages of parallel robots, e.g. not suffering from the accumulation of actuator errors along each kinematic chain, or the low amounts of mass and inertia added along each leg because actuators do not need to be added at each joint.

The shortcomings described above are addressed by developing architectures where each leg of the mechanism does not exhibit multiple actuators connected in series; here referred to as those with non-serially connected actuators. Such architectures were first considered in Mohamed and Gosselin (2005), where the concept of developing reconfigur-

able platforms was presented. In Gosselin et al. (2015), a planar mechanism was presented which consists of four $\underline{P}$RR legs, two of which are connected directly to the platform, the others are connected first to a additional link which is in turn connected to the moving platform via a revolute joint. A family of similar architectures was presented in Schreiber and Gosselin (2018). In each of these architectures, no more than a single joint is actuated in each leg, meaning that the key advantages of the parallel architecture are retained. Very few architectures of this type have been presented in the literature, and the ones that have all exhibit rigid sub-structures when the actuated joints are locked; e.g. the architectures consist of triads connected in cascade. Architectures which do not consist of rigid internal structures when the actuated joints are locked are described as generic architectures Rojas (2012). The development of generic kinematically redundant architectures of this type is important as such architectures can be used to develop future mechanisms and conduct future research upon.

Currently, there remains very few kinematically redundant architectures that have been proposed in the literature and so the potential of these types of parallel robots to be used in a large variety of different applications is restricted. In chapter 2, a novel kinematically redundant architecture of parallel robot is presented. The kinematic redundancy of the mechanism allows it to achieve full cycle rotations of the end-effector without encountering kinematic singularities, a feat that is not possible for non-redundant systems. In order for parallel robots to become a more viable option for a wider range of applications, the number of kinematically redundant architectures available to be used by developers of robot manipulators, and for further research to be conducted upon, must be increased. This thesis aims to address this through proposing a novel architecture of kinematically redundant robot which has full rotational capabilities of the end-effector.

1.4 Methods of Kinematic Analysis

The development of kinematically redundant architectures enhance the potential for parallel robots to be designed which have larger workspaces and rotational capabilities, due to their ability to avoid singularities. However, an additional, and important, aspect of developing such robots is being able to identify the configurations of the robot which are singular, and additionally developing metrics which can be used to determine how far the robot is from a singularity, as the robot's performance is likely to deteriorate as one is approached.

The singularity analysis of parallel mechanisms traditionally is analysed in terms of the

Jacobian matrices of the manipulator which are used to relate the input velocity vector, containing the actuated joint velocities, to the velocity of the end-effector. A classification of three different singularities of parallel mechanisms was first made in Gosselin and Angeles (1990). By defining the relationship between the input velocity vector, $\dot{\theta}$, of the mechanism and the output velocity vector, $\dot{\mathbf{x}}$, by Jacobian matrices $\mathbf{A}$ and $\mathbf{B}$, such that $\mathbf{A}\dot{\mathbf{x}}+\mathbf{B}\dot{\theta} = 0$, the three types of singularities are defined as the configurations of the mechanism when each and both of $\mathbf{A}$ and $\mathbf{B}$ are singular. A type 1 singularity corresponds to a configuration where $\mathbf{B}$ is singular, this is also referred to as an inverse kinematic singularity or singularity of redundant input Zlatanov et al. (1994). An example of a type 1 singularity is when the mechanism reaches the boundary of its workspace and so it loses a degree of freedom; note that this type of singularity exists for serial robots as well as parallel robots. A type 2 singularity, also referred to as a forward kinematic singularity or a singularity of redundant output Zlatanov et al. (1994), corresponds to a configuration of the mechanism in which the mechanism gains one or multiple degrees of freedom instantaneously. A more comprehensive singularity classification was presented in Zlatanov et al. (1994) where six different types were given.

For redundant parallel mechanisms, the literature is much less comprehensive. Just as for non-redundant robots, the Jacobian is frequently used to perform the singularity analysis of redundant parallel mechanisms. For instance, in Merlet (1996), a solution to finding the singular configurations of redundantly actuated robots, for which the number of input parameters, n, exceeds the number of degrees of freedom of the platform, m, was proposed by generating a non-square $m \times n$ Jacobian, $\mathbf{J}$, such that $\dot{\mathbf{x}} = \mathbf{J}\dot{\theta}$, where the configuration is singular if $det(\mathbf{J}\mathbf{J}^T) = 0$. A similar analysis was conducted in Liao et al. (2004), using singular value decomposition of the Jacobian, where three different singularity conditions were found.

It is commonplace to use Jacobian-based methods for performing the singularity analysis of redundant robots, however, such methods can be unreliable when applied to kinematically redundant architectures. These limitations of Jacobian-based methods had previously remained unaddressed in the literature, however in chapter 3 of this thesis these shortcomings are demonstrated and discussed. Multiple instances are shown of the Jacobian both failing to identify and incorrectly identifying singular configurations for several kinematically redundant parallel architectures with non-serially connected actuators. More specifically, it is shown that the inverse of the 2-norm condition number of the Jacobian, a traditional method of singularity analysis, either fails to identify or incor-

rectly identifies a singular configuration. Indeed, other measures, such as computing the determinant of the Jacobian, exhibit the same shortcomings. The failure of the Jacobian is verified using the principles of rigidity theory; by analysing the underlying graph of the robot and computing its rigidity matrix.

In addition to understanding the robot manipulator's proximity to a singularity, it is also useful to be able to know how to reconfigure the mechanism such that it will move further away from these troublesome configurations, this is especially important when carrying out path-planning algorithms. Indeed, in the early 2000s, many path-planning algorithms that were developed for parallel robots did not take into account the mechanism's distance to singularities and therefore are unreliable Porta et al. (2007, 2012); Han (2000); Berenson et al. (2011); Cortés and Siméon (2004); Yakey et al. (2001). In more recent years, techniques which take into account the manipulator's proximity to a singularity have been proposed. For non-redundant parallel robots, many have formulated path-planning algorithms using Jacobian-based approaches of singularity analysis. In Bhattacharya et al. (1998), an online method of singularity avoidance is proposed which aims to keep the actuator forces within their capacities by computing the determinant of the Jacobian. Others have developed path planning methods between distant configurations Dash et al. (2005); Dasgupta and Mruthyunjaya (1998b); Sen et al. (2003). In Bohigas et al. (2012) and Bohigas et al. (2013), a path-planning algorithm was developed for non-redundant robots which finds a solution to the problem by computing the *singularity-free C-space*; the region where the Jacobian is non-singular. Additionally, some path-panning algorithms have been made for kinematically redundant parallel robots. In Cha et al. (2007), an algorithm was developed for kinematically redundant variations of the 3-$\underline{\text{R}}$RR manipulator which used a local optimisation of the determinant of the Jacobian to plan the trajectory. A point-to-point motion planning scheme was proposed in Ebrahimi et al. (2008) for a 3-$\underline{\text{RP}}$RR manipulator, which utilises an index, the *normalised scaled incircle radius*, that describes how far away the geometric conditions in which the Jacobian becomes singular are from being met. Similarly, in Carretero et al. (2008) and Carretero et al. (2012) an overall motion planning scheme was developed, which aims to optimise the entire trajectory as a whole, that uses the same index as the previous reference. A method of minimising the actuator torques of a kinematically redundant robot was presented in Varalakshmi and Srinivas (2014) in which the Jacobian was used to compute the joint torques along its trajectory. These methods are effective when applied to kinematically redundant robots with serially connected actuators, however they are limited when applied to architectures

which exhibit no actuators connected in series, as it is for these architecture where the Jacobian becomes unreliable as a means of singularity analysis. In chapter 4, a method of singularity avoidance is proposed which is based upon the method of singularity analysis presented in chapter 3. The algorithm is used to optimise the redundant degree of freedom of the mechanism such that the robot moves as far away from a singularity as possible for a given pose of the end-effector. This method is an important tool for helping kinematically redundant parallel robots exploit their ability to avoid singularities, without succumbing to the downfalls of traditional Jacobian-based approaches.

1.5 Dynamic Balancing of Parallel Robots

One of the advantages of parallel robot architectures is that they are able to move at very high speeds, however, as a consequence of this, a major challenge that they face is the accumulation of shaking forces and moments on their bases. These shaking forces and moments can be especially problematic as they cause wear and fatigue of the manipulator, and possibly neighbouring manipulators, in addition to inhibiting its performance Lowen and Berkof (1968). A well known solution to this issue is to eliminate the shaking forces and moments imposed on the base by designing the manipulator such that the total linear and angular momentum of the system is zero for any trajectory of the end-effector; this is referred to as dynamically balancing the mechanism.

Much research has been carried out on the dynamic balancing of parallel mechanisms over the previous few decades Arakelian and Smith (2005a,b). In Berkof and Lowen (1969), a method of force balancing four and six bar linkages was presented, and in Berkof and Lowen (1971) the moment balancing of four bar linkages was addressed as well. In Bagci (1982), the dynamic balancing of simple parallel mechanisms was approached through the use of moment balanced idler loops. In recent years, the dynamic balancing of more complex mechanisms has been addressed. A method of static balancing 3-DoF planar parallel mechanisms was presented in Jean and Gosselin (1996) such that the weight of the manipulator does not produce any force or torque at the actuators for any configuration of the robot. In Ricard and Gosselin (2000), balanced four bar linkages were used to synthesise the legs of a dynamically balanced 3-DoF planar parallel mechanism, and a similar method was used in Gosselin et al. (2004) to balance a 3-DoF spatial mechanism. In Foucault and Gosselin (2004), a dynamically balanced planar parallel mechanism was synthesised using balanced five bar linkages. A different approach was proposed in Wu and Gosselin (2005), where a balanced parallelepiped mechanism was presented which can

be used to form the legs of balanced 3-DoF and 6-DoF mechanisms. In Van der Wijk and Herder (2012), a method of making the centre of mass of a linkage to be invariant at one of its links using pantograph mechanisms is presented. An approach based on the method of principal vectors was applied to balance a four bar linkage in van der Wijk and Herder (2012). A method of balancing each link of a double pendulum mechanism was presented in van der Wijk and Herder (2009), where counter-rotary countermasses were installed on each link; the countermasses are driven via negative transmission ratios in the opposite direction to the rotation of the link to which they are attached in order to moment balance the mechanism. This method was compared with three others in van der Wijk et al. (2009) in terms of the addition of mass and inertia contributed by each method when applied to a double pendulum. The counter-rotary countermass approach has been compared with other balancing methods by others as well Herder and Gosselin (2004); Van der Wijk et al. (2008). A high amount of mass and inertia added to the system is undesirable because this generally corresponds to higher actuators torque required to drive the mechanism Dresig et al. (1992); Kochev (2000). All of the methods of developing dynamically balanced parallel mechanisms described consist of balancing the legs of the mechanism and creating a dynamic equivalence between the moving platform and a set of point masses Wu and Gosselin (2007). This approach greatly simplifies the task of analysing the dynamics of a closed loop mechanism as it allows the system to be treated as a set of open loop mechanisms.

As is the case for many aspects of parallel robotics research, the majority of work on dynamically balanced parallel mechanisms has been focused on non-redundant architectures. In recent years, some have developed dynamically balanced redundantly actuated architectures, such as in Van Der Wijk et al. (2013) a balanced 4-$\underline{\text{R}}$RR planar parallel architecture was presented. However, dynamically balanced kinematically redundant architectures have yet to receive any attention in the literature. In order to create kinematically redundant parallel robots that are capable of high performance, dynamically balanced architectures need to be developed. In chapter 5, a dynamically balanced architecture of a kinematically redundant parallel robot is presented. The resulting mechanism allows fast, dexterous movements of the end-effector without suffering from shaking forces and moments on being imposed onto the base.

1.6 Overview of Chapters

The structure of this thesis is a hybrid between a thesis-by-paper and a conventional thesis, meaning that each chapter is based on the work presented in a journal article that is published or accepted for publication. The remainder of this thesis is structured as follows:

- Chapter 2 introduces a novel architecture of a kinematically redundant planar parallel robot which is able to complete full cycle rotations of the end-effector without encountering any singularities. Methods for presenting the inverse and forward kinematics are presented and the singularity analysis is carried out. This work was published in Baron et al. (2019).

- In chapter 3, the issues associated with using traditional, Jacobian-based methods of singularity analysis are discussed. This work was published in Baron et al. (2020b).

- In chapter 4, a novel, geometric approach of singularity analysis is introduced which is shown to be more reliable than conventional approaches. A method of singularity avoidance based on this approach is also presented, such that the kinematic redundancy of the mechanism is utilised to move as far away from a singularity as possible for a given pose of the end-effector. This work was published in Baron et al. (2020c).

- Chapter 5 presents a novel architecture of a dynamically balanced kinematically redundant planar parallel robot, which utilises a system of countermasses and counter-rotary elements to balance the mechanism. The balancing conditions are derived and an optimisation is performed such that the amount of mass and inertia added to the system is minimised. This work is under review for publication Baron et al. (2020a).

- In chapter 6, the main contributions are summarised and the prospects for future work on the topic are discussed.

Chapter 2

Novel Planar Parallel Architecture

As discussed in chapter 1, the amount of research that has been conducted on kinematically redundant parallel robots is quite small; furthermore, very few architectures with non-serially connected actuators have been presented in the literature. In order to increase the potential for these types of robot manipulators to be used for high performance applications, and to provide a platform for further research on these mechanisms to be conducted, new architectures must be proposed. In this chapter, a novel kinematically redundant planar parallel robot with non-serially connected actuators is presented; this work was published as Baron et al. (2019).

Only a few kinematically redundant architectures with non-serially connected actuators have been proposed in the literature Gosselin et al. (2015); Schreiber and Gosselin (2018). The first, presented in Gosselin et al. (2015), is composed of two R$\underline{\text{P}}$R legs connected to a common joint on the platform, along with two other similar legs connected to a revolute joint that is then connected to a second common joint on the platform. A rigid structure is obtained from this robot manipulator if and only if all four actuators are simultaneously locked. This resulting structure corresponds to three triads connected in cascade, which implies that the robot manipulator is not a fundamental truss Rojas (2012). Similarly, the architectures presented in Schreiber and Gosselin (2018) do not correspond to fundamental trusses. A parallel robot manipulator architecture corresponds to a fundamental truss if it does not exhibit internal rigid structures, beyond local elements of single limbs, when the actuators are locked, such that its rigidity is not inherited from a more general architecture or resulting from the combination of other fundamental structures. Thus, for instance, the standard 3-R$\underline{\text{R}}$RR parallel robot manipulator architecture is a fundamental truss, but the 4-R$\underline{\text{P}}$R redundant manipulator is not. The underline in this convention means that the corresponding joint is actuated.

It has been claimed that generic architectures of kinematically redundant planar parallel robot manipulators—as those corresponding to cases where the robot manipulator's architecture is a fundamental truss—cannot achieve unlimited rotation capability Schreiber and Gosselin (2018). However, in this chapter, it is shown that this is not the case; a novel fundamental kinematically redundant architecture with such a characteristic is introduced. The fundamental topology of this robot manipulator implies that, just like the 3-R$\underline{\text{P}}$R architecture, it can be used as a basis upon which future mechanisms can be developed and future research can be conducted. The proposed robot manipulator architecture consists of a moving platform connected to the base via four $\underline{\text{R}}$RR legs and a ternary link, which is joined to the ground link by a revolute joint, via two other $\underline{\text{R}}$RR legs. The robot manipulator is kinematically redundant as its degree of mobility (four) is the same as the number of actuated joints; and this value exceeds the number of degrees of freedom required to describe a pose of the end effector (three). The redundancy allows any pose to be attained within the workspace of the robot manipulator without producing a singularity and the novel architecture does not present mechanical interferences in full cycle trajectories; thus resulting in unlimited rotational capabilities of the end-effector. Although the architecture is similar to that in Schreiber and Gosselin (2018), it is novel as the two architectures represent different kinematic chains – if the corresponding graphs of the two mechanisms are compared it can be seen that they are not isomorphic. A method of identifying singular configurations and reconfiguring the robot manipulator such that they are avoided is presented in Baron et al. (2018).

In addition to presenting the novel architecture in section 2.1, methods of solving the inverse and forward kinematics of the mechanism are given in section 2.2 and section 2.3, respectively. The method of singularity analysis used to determine whether or not a configuration of the mechanism is singular is presented in section 2.4. An example trajectory is examined in section 2.5 showing that the mechanism is capable of performing full cycle rotations of the end-effector without encountering singularities.

2.1 Robot Architecture

The robot architecture, as exemplified in the instance shown in Fig. 2.1, consists of a moving platform ($P_{10}P_{11}$) that is connected to the base ($P_1P_2P_3$), and one ternary link ($P_3P_4P_5$), via four $\underline{\text{R}}$RR legs; where R denotes a passive revolute joint and $\underline{\text{R}}$ denotes an actuated revolute joint. The moving platform is connected to the base, or ground link, directly via two of the legs, and to the ternary link via the other two legs. The ternary

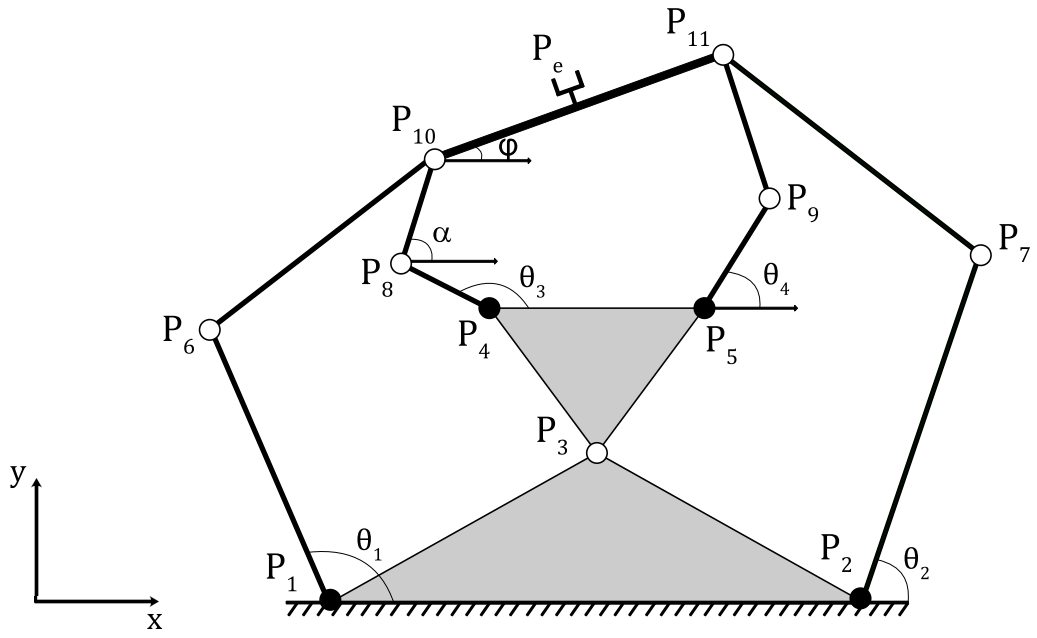

Figure 2.1: Kinematic diagram of the proposed robot mechanism. The architecture consists of a moving platform connected directly to the base via two RRR legs and connected to a ternary link, which is joined to the base by a passive revolute joint, via two other RRR legs.

link is connected to the base via a passive revolute joint and the legs are attached to the ternary link and the base via actuated revolute joints. Two of the legs are attached to a common passive revolute joint on the moving platform and the other two are connected to another common passive joint on it. The actuators are not serially connected and although two of them are attached to the ternary link, what increases the inertial properties of this part, the mechanism does not suffer from the accumulation of actuator errors along the limbs.

The proposed robot mechanism is, in general, rigid when the four actuators are locked; meaning that the links are unable to move with respect to the base or each other. This can be shown, for instance, by calculating its structural mobility, M, via the extended Chebychev-Kutzbach-Grübler formula Rojas and Dollar (2016). According to this criterion, the structural mobility of a mechanism is

$$M = F - \sum_{i=1}^{\lambda} t_i \tag{2.1}$$

where $\lambda = J - L + 1$ is the number of independent closed-loops in the kinematic chain and t_i is the motion type of the i^{th} independent closed-loop ($t_i = 3$ in the planar case), with J, the total number of joints, L, the number of links, and F, the total number of degrees

of freedom of the joints. Since the proposed architecture consists of 13 joints (counting twice the ternary joints of the platform), 11 links (including the base) and 13 degrees of freedom (as each revolute joint has one degree of freedom), its resulting structural mobility is 4. This result implies that in order for the mechanism to be rigid (*i.e.*, to have a mobility of zero), four of the joints need to be actuated. It is known that the structural mobility, which is a function only of structural parameters, is a lower bound of the total mobility of a mechanism; however, it has been proven that if M is computed using the extended Chebychev-Kutzbach-Grübler formula, it is unlikely that the structural mobility is different to the total mobility when a kinematic chain is selected at random Müller (2009).

The proposed architecture is fundamental, which implies that the robot manipulator, once the actuators are locked, does not exhibit rigid sub-structures beyond subcomponents in a single leg. Thus, the rigidity of a fundamental parallel robot manipulator is not inherited from a more general architecture or resulting from the combination of other fundamental structures. For the case of the proposed robot mechanism, this can be proven by systematically analysing the kinematic chains formed by subsets of the set of joints, taking into account that rigid elements of an $\underline{\text{R}}$RR leg do not contribute to general rigidity since these limbs are equivalent to an R$\underline{\text{P}}$R leg when the actuators are activated, that is, they can be modelled as a line segment connecting the centres of the two end revolute joints. Since the introduced robot mechanism has three independent loops, $\lambda = 3$, there are only two fundamental structures that could be present, namely, a triad (*i.e.* a one-loop structure composed of three links connected by revolute joints, $\lambda = 1$) or a pentad (*i.e.* a two-loop structure composed of two ternary links connected between them by binary links, all of them jointed by revolute kinematic pairs, $\lambda = 2$). Neither triads nor pentads that contribute to general rigidity are detected in the proposed robot mechanism.

In the instance of the introduced kinematically redundant planar parallel manipulator that is shown in Fig. 2.1, the robot manipulator is designed such that the end-effector is able to complete full rotations without encountering mechanical interferences. Moreover, the link which is the upper component of the left leg connected to the ternary link, the shortest link, is made to be able to complete a full rotation with respect to the platform; this characteristic is vital for the process of avoiding singularities as it is further discussed in section 2.4.

2.2 Inverse Kinematics

The inverse kinematics problem refers to the determination of the required values of the actuated joints in order to produce a given pose of the moving platform. Fig. 2.1 shows a schematic of the proposed architecture where the robot manipulator is depicted in terms of the centres of rotation of its kinematic pairs (joints) and the line segments connecting them (links); each centre has been labelled, from P_1 to P_{11}, and the sought values of the actuated joints are θ_1 to θ_4. Since this mechanism is kinematically redundant with one extra degree of freedom, there are an infinite number of solutions to the inverse kinematics. However, if an additional condition is set, such as the orientation of the link defined by P_8 and P_{10}, to name one, then the number of solutions reduces to a finite number. The orientation of this link is given by α – this angle has been chosen to control the redundancy as opposed to, say, the orientation of the ternary link because it makes the method of singularity avoidance more straightforward. With this condition set, the positions of the joints can be found using, for instance, analytic geometry and trigonometric relations; here the bilateration method is used instead.

The bilateration method consists of finding the possible positions of an unknown point, P_k, if the distances between this point and two points whose positions are known, P_i and P_j, are known. $\mathbf{p}_{i,k}$, which is the vector going from P_i to P_k, is found by taking the matrix-vector product between the bilateration matrix, $\mathbf{Z}_{i,j,k}$, and $\mathbf{p}_{i,j}$, the vector going from P_i to P_j Rojas (2012). That is,

$$\mathbf{p}_{i,k} = \mathbf{Z}_{i,j,k}\mathbf{p}_{i,j} \tag{2.2}$$

where

$$\mathbf{Z}_{i,j,k} = \frac{1}{2s_{i,j}} \begin{bmatrix} s_{i,j} + s_{i,k} - s_{j,k} & -4A_{i,j,k} \\ 4A_{i,j,k} & s_{i,j} + s_{i,k} - s_{j,k} \end{bmatrix}$$

and

$$A_{i,j,k} = \pm\frac{1}{4}\sqrt{(s_{i,j} + s_{i,k} + s_{j,k})^2 - 2(s_{i,j}^2 + s_{i,k}^2 + s_{j,k}^2)},$$

with $s_{i,j} = d_{i,j}^2$ denoting the squared distance between the points P_i and P_j and $A_{i,j,k}$, the orientated area of the triangle defined by points P_i, P_j and P_k. The $\pm$ sign implies that $\mathbf{p}_{i,k}$ can point in one of two different directions; when positive, $\mathbf{p}_{i,k}$ points to the left of $\mathbf{p}_{i,j}$ and, when negative, it points to the right.

According to the notation of Fig. 2.1, the desired position and orientation of the

platform can be represented by P_{10} and ϕ. Then, the vector $\mathbf{p}_{10,11}$ can be computed as

$$\mathbf{p}_{10,11} = d_{10,11} \begin{bmatrix} cos(\phi) \\ sin(\phi) \end{bmatrix}, \tag{2.3}$$

where ϕ is the angle between the platform and the x-axis. By setting the value of α, the position of P_8 is found using basic trigonometry. The positions of the remaining points are found by applying the bilateration method, using equation (2.2). The position of P_4 is determined using the bilateration matrix $\mathbf{Z}_{3,8,4}$ and selecting an orientation of $\mathbf{p}_{3,4}$ by choosing the sign of $A_{3,8,4}$. P_5 is obtained from $\mathbf{Z}_{3,4,5}$ and since the orientation of $A_{3,4,5}$ is known, P_5 has a definite position. P_6, P_7 and P_9 are determined with $\mathbf{Z}_{10,1,6}$, $\mathbf{Z}_{11,2,7}$ and $\mathbf{Z}_{5,11,9}$, and by selecting the orientations of their respective areas.

The above procedure computes the location of all joint centres. The values of the actuated joints, that is, the angles θ_1, θ_2, θ_3 and θ_4, can then be computed using the arccosines of $\frac{\mathbf{p}_{1,6}\cdot[1,0]^T}{d_{1,6}}$, $\frac{\mathbf{p}_{2,7}\cdot[1,0]^T}{d_{2,7}}$, $\frac{\mathbf{p}_{4,8}\cdot\mathbf{p}_{4,5}}{d_{4,8}d_{4,5}}$, and $-\frac{\mathbf{p}_{5,9}\cdot\mathbf{p}_{5,4}}{d_{5,9}d_{4,5}}$, respectively.

2.3 Forward Kinematics

The forward kinematics problem consists of finding the feasible Cartesian poses of the moving platform once the actuators are fixed at particular values. A common method for solving this problem is to formulate the characteristic polynomial of the mechanism, which involves manipulating the kinematic equations of the system so that a single equation in terms of one variable is formed—this is usually called a closed-form solution Rojas and Thomas (2011). Solving this polynomial gives, or leads to obtain, the feasible poses of the platform given the known geometric parameters, such as link lengths, and the actuator values. Additionally, the degree of the polynomial shows the maximum number of solutions to the forward kinematics. For example, when the actuators of the 3-R<u>P</u>R robot manipulator are locked a sextic polynomial is obtained, thus implying that up to 6 different configurations can be calculated; a proof of this feasible number of solutions is given in Hunt (1983). Here, the bilateration method is used for formulating the characteristic polynomial of the proposed kinematically redundant planar parallel robot manipulator. To this end, the equivalent kinematic model shown in Fig. 2.2 is used. This model results from the fact that once the actuators are fixed at a given value, each of the <u>R</u>RR legs of the parallel robot manipulator can be represented by a line segment of known distance that connects the centres of the two end revolute joints. Looking back to the model presented in Fig. 2.1, once the values of θ_1, θ_2, θ_3 and θ_4 are fixed, the distances $d_{3,6}$, $d_{3,7}$ and $d_{6,7}$ can be calculated, as can $d_{3,8}$, $d_{3,9}$ and $d_{8,9}$; resultantly, P_3, P_6 and P_7, and P_3, P_8 and P_9

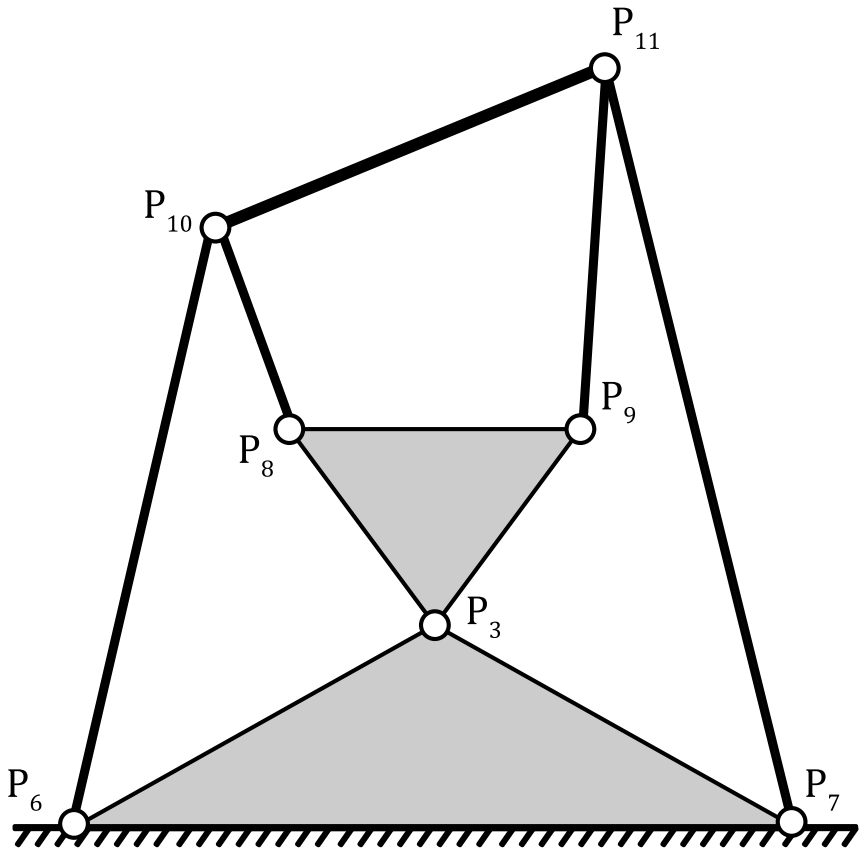

Figure 2.2: Equivalent kinematic model used for solving the forward kinematics; it corresponds to the mechanism obtained when the robot actuators are fixed at particular values. This model also applies for a robot manipulator with type R$\underline{\text{P}}$R legs.

form two triads. As these two triads are rigid structures, the robot manipulator can be modelled, when the actuator values are fixed, by the diagram shown in Fig. 2.2, where the triads represent the base and the ternary link, respectively, and the lower links of the legs to which they are attached. The moving platform is joined to these triads via four single links with passive joints at each end; which represent the upper links of the legs. Note that this equivalent model is also applicable to a mechanism with type R$\underline{\text{P}}$R legs. Now, instead of directly calculating the Cartesian pose of the platform, the bilateration method is used firstly to determine the set of values of an unknown squared distance of the system, such as $s_{6,8}$, according to the notation of Fig. 2.2, that are compatible with the known geometric parameters of the mechanism. Following this approach, the characteristic polynomial is obtained as follows. Firstly, using a sequence of bilaterations, an equation is formed which computes a single vector between two points whose distance is known, in this case $\mathbf{p}_{10,11}$, in terms of one of the two vectors that result from the unknown squared distance used

as variable, in this case $\mathbf{p}_{6,8}$. This vector equation has to take into account all distance constraints in the mechanism. Thus, the following system of equations is obtained.

$$\mathbf{p}_{6,10} = \mathbf{Z}_{6,8,10}\mathbf{p}_{6,8}, \tag{2.4}$$

$$\mathbf{p}_{6,7} = \mathbf{Z}_{6,3,7}\mathbf{Z}_{6,8,3}\mathbf{p}_{6,8}, \tag{2.5}$$

$$\mathbf{p}_{6,9} = (-\mathbf{Z}_{8,3,9}\mathbf{Z}_{8,6,3} + \mathbf{I})\mathbf{p}_{6,8}, \tag{2.6}$$

$$\mathbf{p}_{7,9} = \mathbf{p}_{6,9} - \mathbf{p}_{6,7}, \tag{2.7}$$

$$\mathbf{p}_{7,11} = \mathbf{Z}_{7,9,11}\mathbf{p}_{7,9}, \tag{2.8}$$

$$\mathbf{p}_{6,11} = \mathbf{p}_{6,7} + \mathbf{p}_{7,11}, \tag{2.9}$$

$$\mathbf{p}_{10,11} = \mathbf{p}_{6,11} - \mathbf{p}_{6,10}, \tag{2.10}$$

with $s_{i,j} = \|\mathbf{p}_{i,j}\|^2$ and $\mathbf{I}$ denoting the 2-by-2 identity matrix, and taking into account that the orientation of the triangles defined by the revolute centres P_6, P_7, and P_3; and P_3, P_8, and P_9 is known. Rewriting the above system of equations in terms of $\mathbf{p}_{6,8}$ we obtain

$$\mathbf{p}_{10,11} = \mathbf{Q}\mathbf{p}_{6,8}, \tag{2.11}$$

where

$$\begin{aligned}\mathbf{Q} = (&-\mathbf{Z}_{6,8,10} + \mathbf{Z}_{6,3,7}\mathbf{Z}_{6,8,3} \\ &+ \mathbf{Z}_{7,9,11}(-\mathbf{Z}_{6,3,7}\mathbf{Z}_{6,8,3} - \mathbf{Z}_{8,3,9}\mathbf{Z}_{8,6,3} + \mathbf{I})).\end{aligned}$$

Then, by the scaling property of bilateration matrices, we get that

$$\det(\mathbf{Q}) = \frac{s_{10,11}}{s_{6,8}}. \tag{2.12}$$

By eliminating the square roots involved in equation (2.12), a 14th-degree characteristic polynomial in terms of $s_{6,8}$ is finally obtained. The real roots of this polynomial correspond to the compatible values of $s_{6,8}$ for the geometric parameters and actuator values of the robot manipulator.

Finally, the feasible assembly modes of the parallel manipulator can be computed, for instance, by substituting the real values of $s_{6,8}$ into (2.12) along with each possible combination of orientations for the orientated areas $A_{6,8,10}$, $A_{6,8,3}$, and $A_{7,9,11}$; if the equation holds, then the corresponding assembly mode is feasible. Then for each of the detected assembly modes, a reference frame is introduced and the positions of the base joints, P_6, P_7 and P_3 are designated. The resulting configuration from the positions of the

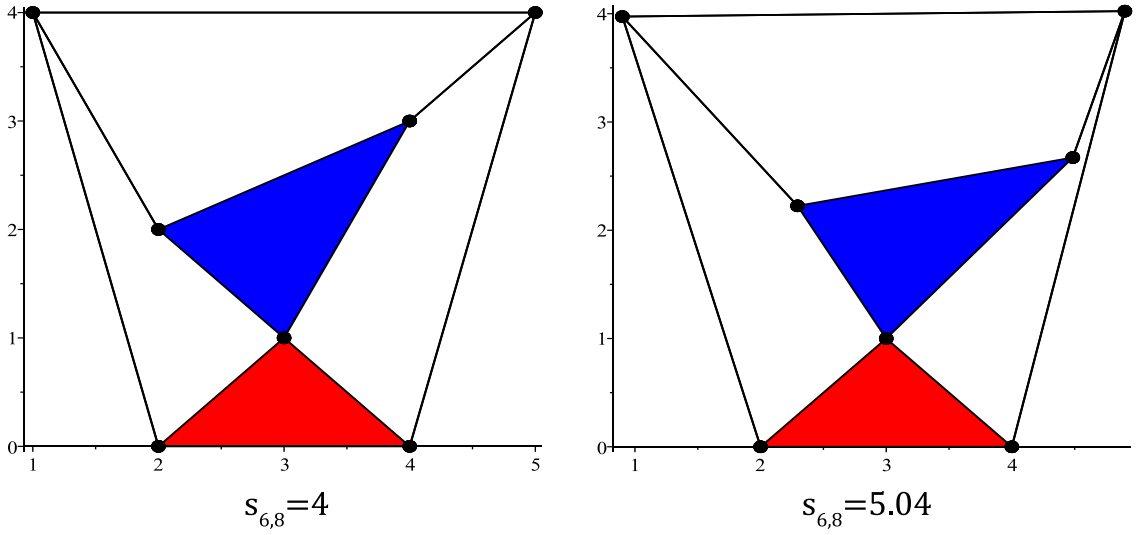

Figure 2.3: Resulting configurations of the example used in the forward kinematic analysis.

remaining joints are then found by computing the following sequence of bilaterations

$$\mathbf{p}_{6,8} = \mathbf{Z}_{6,3,8}\mathbf{p}_{6,3}, \tag{2.13}$$

$$\mathbf{p}_{3,9} = \mathbf{Z}_{3,8,9}\mathbf{p}_{3,8}, \tag{2.14}$$

$$\mathbf{p}_{6,10} = \mathbf{Z}_{6,8,10}\mathbf{p}_{6,8}, \tag{2.15}$$

$$\mathbf{p}_{7,11} = \mathbf{Z}_{7,9,11}\mathbf{p}_{7,9}. \tag{2.16}$$

The sign of $A_{6,3,8}$ is the opposite of the sign of $A_{6,8,3}$.

As an example of the method described above; consider the mechanism with link lengths $d_{6,7} = 2$, $d_{3,6} = \sqrt{2}$, $d_{6,10} = \sqrt{17}$, $d_{3,7} = \sqrt{2}$, $d_{7,11} = \sqrt{17}$, $d_{7,8} = \sqrt{2}$, $d_{7,9} = \sqrt{5}$, $d_{8,9} = \sqrt{5}$, $d_{8,10} = \sqrt{5}$, $d_{9,11} = \sqrt{2}$ and $d_{10,11} = 4$, the following base joint positions: $P_6 = (2,0)^T$, $P_7 = (4,0)^T$ and $P_3 = (3,1)^T$, and with the oriented area $A_{3,8,9}$ being negative. The following characteristic polynomial is then obtained.

$$\sum_{i=0}^{14} k_i s_{6,8}^i, \tag{2.17}$$

where $k_0 = 6.11 \times 10^{17}$, $k_1 = -2.39 \times 10^{17}$, $k_2 = -3.41 \times 10^{16}$, $k_3 = 3.86 \times 10^{16}$, $k_4 = -1.00 \times 10^{16}$, $k_5 = 5.54 \times 10^{14}$, $k_6 = 4.42 \times 10^{14}$, $k_7 = -1.66 \times 10^{14}$, $k_8 = 3.08 \times 10^{13}$, $k_9 = -3.51 \times 10^{12}$, $k_{10} = 2.72 \times 10^{11}$, $k_{11} = -1.59 \times 10^{10}$, $k_{12} = 7.24 \times 10^{8}$, $k_{13} = -2.22 \times 10^{7}$ and $k_{14} = 3.20 \times 10^{5}$. The real roots of this polynomial are 4 and 5.04. The values of these roots, and the coefficients in the polynomial, are given to 2 decimal places. The resulting configurations of this example are depicted in Fig. 2.3.

2.4 Singularity Analysis

It is well known that the singularities of a standard 3-RPR mechanism can be determined geometrically by finding the configurations in which the lines that pass through the three legs of the robot manipulator intersect at a common point. In this section, a similar set of geometrical conditions are developed in order to determine if the proposed mechanism is in a singular configuration.

Singular configurations are those in which a mechanism of mobility zero ($M = 0$), which is generally rigid, loses its rigidity; this implies multiple problems for parallel robot manipulators such as loss of controllability and large actuation forces. The most commonly used method of identifying if a parallel robot manipulator is in a singular configuration is by formulating the relationship between the Cartesian velocities and the joint velocities of the robot manipulator in terms of Jacobian matrices; the robot manipulator is considered to be in a singular configuration when these matrices are not of full rank Gosselin et al. (2015).

Here, the method used to determine if the robot manipulator is in a singular configuration is based on the properties of instantaneous centres of rotation (ICRs). The benefit of carrying out the singularity analysis by using this approach is that it gives a geometrical interpretation of the conditions which lead to the the production of a singularity, as opposed to a purely mathematical description as that obtained from Jacobian matrices. The ICR between two rigid bodies that are moving relatively to one another is the point at which the absolute velocities of both bodies are equal Daniali (2005). Using ICRs, it can be seen that there are certain configurations where an $M = 0$ mechanism loses its rigidity when the $M = 1$ sub-mechanisms whose union composes the system are considered.

For instance, according to the notation of Fig. 2.4, in a 3-RPR parallel manipulator, which is rigid when the actuators are fixed at particular values, there exist three $M = 1$ sub-mechanisms whose collection generates the original kinematic chain, namely, the sub-mechanisms obtained when links 2, 3, and 4 are removed, respectively.

For each of these sub-mechanisms, the platform (link 5) is able to move relative to the base (link 1); implying that the ICR between the platform and the base can be found, that is, ICR(1,5). Herein, the notation ICR(i,j) will be used to denote the ICR between links i and j.

An effective way of determining the position of ICR(1,5) for each of the sub-mechanisms is through the use of a bookkeeping system for $M = 1$ mechanisms, first presented in Hartenberg and Denavit (1964). The system involves constructing what is called a

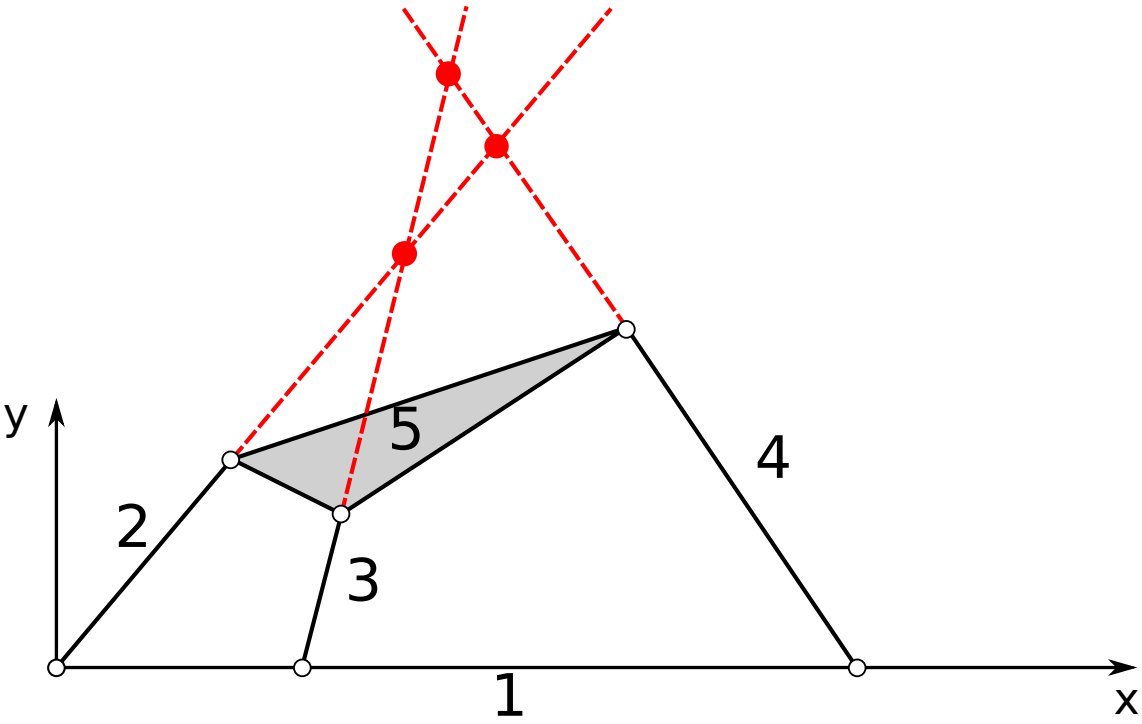

Figure 2.4: Kinematic diagram of 3-RPR mechanism with the links numbered and with the ICRs of the $M = 1$ sub-mechanisms shown (links 1, 2, 3, and 5; links 1, 2, 4, and 5; and links 1, 3, 4, and 5).

circle diagram (also known as the auxiliary polygon derived from the Aronhold-Kennedy theorem on ICRs), shown in Fig. 2.5 for the 3-RPR robot manipulator depicted in Fig. 2.4, which details all the links in the mechanism by number and a known ICR between two links is denoted by a solid line drawn between them. An unknown ICR between two links, denoted by a dotted-line, can be found if this dotted-line is the common side of two triangles otherwise made up of solid lines. The geometrical location of this unknown ICR is found by drawing two lines, each of which pass through the two known ICRs of each triangle. The point at which these two lines intersect is the position of the ICR; note that if the lines are parallel, the ICR is positioned at infinity.

Following the above procedure, the positions of ICR(1,5) for each sub-mechanism of the 3-RPR robot manipulator can be obtained as shown geometrically in Fig. 2.4. As long as these points are separate the robot mechanism is rigid; however, if they coincide, the platform is able to, instantaneously, rotate relative to the base about this point and hence the mechanism loses its rigidity. This corresponds to a singular configuration. It is important to highlight that the information provided by the $M = 1$ sub-mechanism created by removing link 2 (links 1, 3, 4, and 5) is redundant. The geometric conditions which cause the ICR(1,5) of this sub-mechanism to coincide with that of the others are,

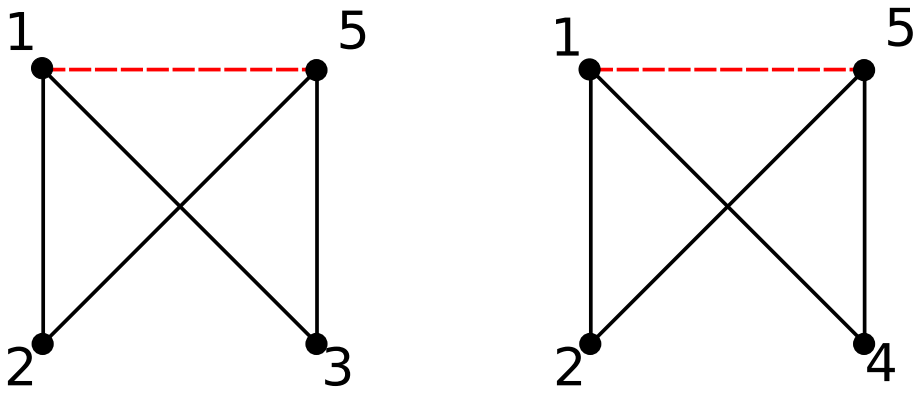

Figure 2.5: Circle diagram for $M = 1$ sub-mechanism with link 4 removed (left) and link 3 removed (right) for the case of the 3-R$\underline{P}$R robot manipulator. See text for details.

generally, the same as the conditions which cause the positions of ICR(1,5) for the other two sub-mechanisms to coincide with each other. The only exception to this, an instance where two of the ICR(1,5)s are coincident but the third is not, is when one of the sub-mechanisms is itself in a singular configuration, however under these conditions it can still be verified that the entire system is in a singularity because the total degrees of freedom of one of the sub-mechanisms has increased, therefore the mobility of the robot manipulator also increases.

The same analysis is now carried out on the proposed kinematically redundant architecture using the equivalent mechanism when the actuators are locked; in this case, according to the notation of Fig. 2.6, four $M = 1$ sub-mechanisms can be detected, namely, the sub-mechanisms obtained when we remove (i) link 3, (ii) link 4, (iii) link 5, and (iv) link 6. Fig. 2.7 shows the circle diagrams used to determine the construction lines needed to find the ICR between the platform and the base for the $M = 1$ sub-mechanisms (ii) and (iii); similar to the case of the 3-R$\underline{P}$R robot manipulator, the conditions resulting from the other sub-mechanisms are redundant.

The position of ICR(1,7) of sub-mechanism (iii), shown in the left hand diagram of Fig. 2.7, is given by the point of intersection between the lines which pass through links 3 and 4. The case of sub-mechanism (ii), shown in the right hand diagram of Fig. 2.7, is slightly different. In this case, before the ICR between the platform and the base can be found, an additional unknown ICR must be determined since the dotted line which connects links 1 and 7 is not the common side of any two otherwise known triangles. Then, ICR(2,7) needs to be found first, which is given by the point at which the lines that pass through links 5 and 6 intersect. ICR(1,7) is then obtained by finding where the line which passes through ICR(1,2) and ICR(2,7) intersects with the line which passes through link 3.

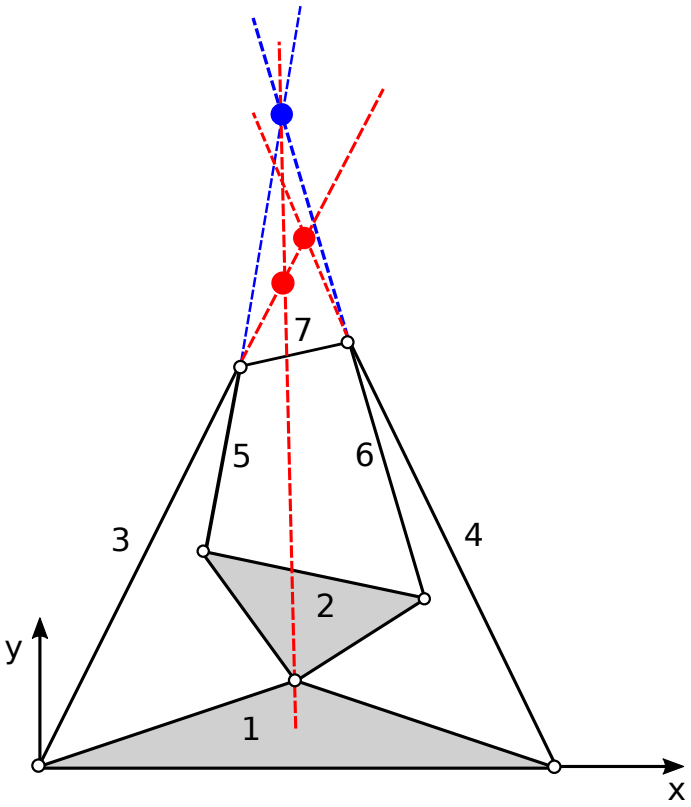

Figure 2.6: Kinematic diagram of proposed mechanism with links numbered. ICR(1,7) for the sub-mechanisms (ii) and (iii) is shown.

A singular configuration in the kinematically redundant robot manipulator occurs either when the ICR(1,7) of these sub-mechanisms coincide, or when the position of one or more of these ICRs cannot be calculated. Following this, the distance, d, between the ICR(1,7) of two sub-mechanisms can be used to determine whether or not the robot manipulator is in a singularity; the robot manipulator is therefore in a singular configuration when the value of d is zero or cannot be calculated – coresponding to the instances where the ICR(1,7)s are coincident and where one (or more) of the sub-mechanisms is itself in a singularity, respectively. A similar approach is used in Ebrahimi et al. (2008), where the proximity to a singularity is measured by comparing the incircle radius of the triangle created by the three construction lines of the mechanism with the maximum possible incircle radius.

A verification of this method is shown in Fig. 2.8, where the distance, d, between the ICR(1,7)s of sub-mechanisms (ii) and (iii) is plotted for a full rotation of the moving platform, along with the inverse of the (2-norm) condition number of the Jacobian matrix, $1/k(\mathbf{J})$. The Jacobian matrices $\mathbf{J}$ and $\mathbf{K}$ are used to relate the Cartesian velocities of the moving platform, denoted by the vector $\dot{\mathbf{c}}$, to the actuated joint velocities, denoted by the

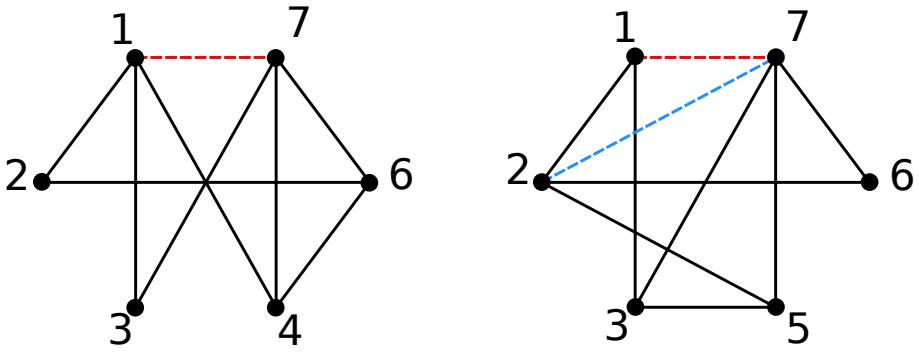

Figure 2.7: Circle diagram for $M = 1$ sub-mechanism with link 5 removed (left) and link 4 removed (right) for the case of the introduced kinematically redundant architecture.

vector $\dot{\mathbf{q}}$, such that

$$\mathbf{J}\dot{\mathbf{c}} = \mathbf{K}\dot{\mathbf{q}}. \tag{2.18}$$

For the proposed robot architecture it can be shown that

$$\mathbf{J} = \begin{bmatrix} (\mathbf{p}_{10} - \mathbf{p}_6)^T & (\mathbf{p}_{10} - \mathbf{p}_6)^T \mathbf{E}\mathbf{v}_{10} \\ (\mathbf{p}_{11} - \mathbf{p}_7)^T & (\mathbf{p}_{11} - \mathbf{p}_7)^T \mathbf{E}\mathbf{v}_{11} \\ & (\mathbf{p}_9 - \mathbf{p}_3)^T \mathbf{N}\mathbf{G} \end{bmatrix},$$

where $\mathbf{p}_i$ denotes the vector from the origin to the point P_i, $\mathbf{v}_{10}$ and $\mathbf{v}_{11}$ denote the vectors from the centre of the moving platform to points P_{10} and P_{11}, respectively,

$$\mathbf{E} = \begin{bmatrix} 0 & -1 \\ 1 & 0 \end{bmatrix},$$

$$\mathbf{N} = \begin{bmatrix} \frac{d_{3,8}}{d_{3,9}} (\mathbf{p}_{10} - \mathbf{p}_8)^T \mathbf{M} \\ (\mathbf{p}_{11} - \mathbf{p}_9)^T \end{bmatrix}^{-1},$$

$$\mathbf{G} = \begin{bmatrix} (\mathbf{p}_{10} - \mathbf{p}_8)^T & (\mathbf{p}_{10} - \mathbf{p}_8)^T \mathbf{E}\mathbf{v}_{10} \\ (\mathbf{p}_{11} - \mathbf{p}_9)^T & (\mathbf{p}_{11} - \mathbf{p}_9)^T \mathbf{E}\mathbf{v}_{11} \end{bmatrix}, \text{ and}$$

$$\mathbf{M} = \begin{bmatrix} cos(\delta) & -sin(\delta) \\ sin(\delta) & cos(\delta) \end{bmatrix},$$

with δ being the angle taken anticlockwise from the vector $(\mathbf{p}_9 - \mathbf{p}_3)$ to the vector $(\mathbf{p}_8 - \mathbf{p}_3)$. The above computation of the the 3×3 Jacobian Matrix, $\mathbf{J}$, can be obtained adapting, for instance, the method used in Schreiber and Gosselin (2018). It is well known that the robot manipulator is considered to be in a singular configuration when $1/k(\mathbf{J})$ is equal to zero; Fig. 2.8 shows that d and $1/k(\mathbf{J})$ vanish for the same robot manipulator configurations. However, it should be noted that there are some inconsistencies with this Jacobian in some configurations where $\mathbf{N}$ is singular, in which the value of $1/k(\mathbf{J})$ equals zero but the robot

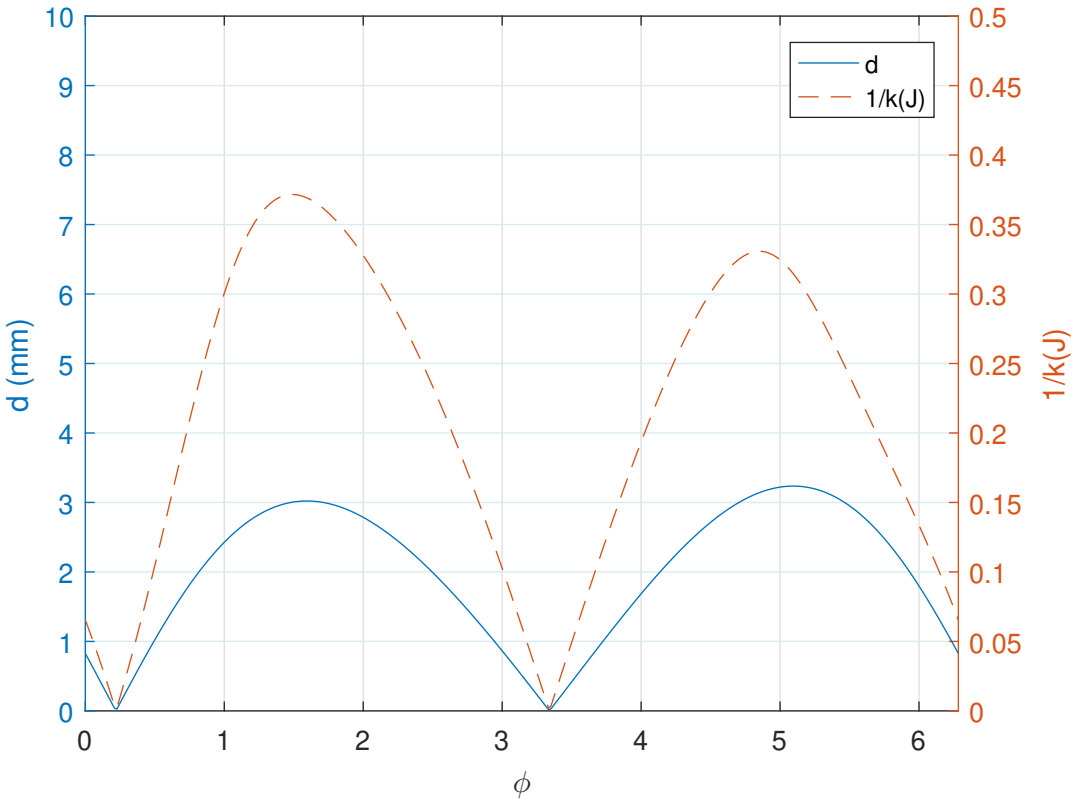

Figure 2.8: A comparison between d and the inverse of the condition number of the Jacobian, $1/k(\mathbf{J})$, of the proposed mechanism with RPR legs.

is not physically in a singular configuration; these cases are explored in chapter 3. In such circumstances d is calculated to be non-zero. Indeed, it can be verified that the robot is certainly not in a singularity by computing the rigidity matrix of the corresponding graph of the mechanism and calculating its rank Hendrickson (1992).

The architecture of the robot manipulator for the results of Fig. 2.8 is that of the robot manipulator shown in Fig. 2.1, with: base joint positions $P_1 = (0, 0)^T$, $P_2 = (10, 0)^T$ and $P_3 = (3, 2)^T$, and link lengths $d_{1,6} = 5$, $d_{2,7} = 5$, $d_{3,4} = 6$, $d_{3,5} = 7$, $d_{4,5} = 11$, $d_{4,8} = 5$, $d_{5,9} = 5$, $d_{6,10} = 5$, $d_{7,11} = 5$, $d_{8,10} = 5$, $d_{9,11} = 5$ and $d_{10,11} = 1$; all values are given in mm. The test trajectory is a full rotation of the moving platform about point $(5, 6)^T$. The configurations at which d and $1/k(\mathbf{J})$ equal zero are the points at which the robot manipulator is in a singularity.

2.5 Experimental Results

In this section, an example trajectory is tested on an example mechanism both theoretically through the use of a simulation and experimentally by implementing a physical prototype. In both cases, the trajectory of the end-effector is predefined and the configuration of the robot manipulator at each stage along this trajectory is calculated subsequently. A basic procedure to avoid singularities was implemented.

According to the notation of Fig. 2.1, the value of α is selected such that the robot manipulator always stays away from a singular configuration for the given pose of the end-effector. An appropriate value of α is identified by varying it between 0 and 2π and calculating the positions of all joints via inverse kinematics. The dimensions of the mechanism were selected carefully such that the link between P_8 and P_{10} is able to rotate fully around P_{10} at any point along the end-effector's trajectory. For each configuration, the positions of the ICR(1,7) of each sub-mechanism are determined and the distance between them, d, is calculated. If $d = 0$ the corresponding configuration is singular.

The test trajectory is a full rotation of the moving platform about the position $(100, 200)^T$; by following this trajectory, the robot manipulator demonstrates its rotational capabilities. For the reported numerical and experimental results, the following numerical values were used for the geometric parameters of the robot manipulator (all values are given in mm): the coordinates of the base joints are $P_1 = (-50, 50)^T$, $P_2 = (-100, 325)^T$ and $P_3 = (350, 175)^T$; the length of the links are $d_{1,6} = 175$, $d_{2,7} = 175$, $d_{3,4} = 150$, $d_{3,5} = 150$, $d_{4,5} = 150$, $d_{4,8} = 225$, $d_{5,9} = 200$, $d_{6,10} = 175$, $d_{7,11} = 175$, $d_{8,10} = 75$, $d_{9,11} = 200$, and $d_{10,11} = 100$.

For the physical prototype, shown in Fig. 2.9, four Herkulex drs-0601 servo motors were used for the actuated joints with centres P_1, P_2, P_4 and P_5. Each of the links (including the ternary link) were 3D-printed from ABS (Acrylonitrile Butadiene Styrene) plastic. Ball bearings were used for all the passive revolute joints in the robot manipulator; each passive joint consists of a bolt passing through the ball bearing joint attached to each link. Wheels were attached to the bottom of the ternary link for support. The passive joint of the ternary link, at centre P_3, consists of a bolt fixed to the base which passes through a ball bearing fixed to the ternary link. An Arduino Mega 2560 was used to control the system. The base joint positions, P_1, P_2, and P_3, were chosen such that the workspace of the mechanism is large enough to perform full rotations of the end-effector.

Fig. 2.10 displays the d value as the robot manipulator completes the full rotation, both for the numerical simulation and the physical prototype, in which the final con-

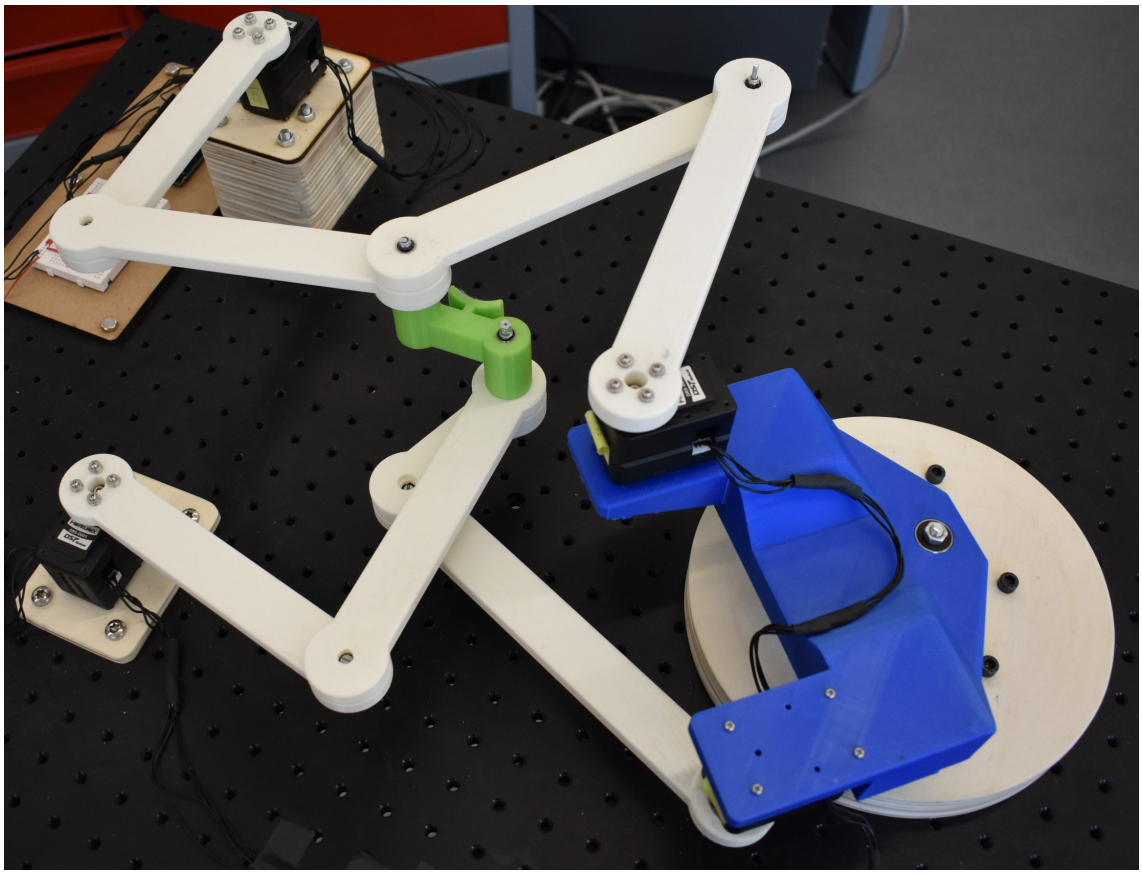

Figure 2.9: Prototype of the novel kinematically redundant planar parallel robot manipulator. An online video of this prototype completing a 2π rotation about a single point, avoiding singularities, and performing a pick-and-place trajectory of full rotation can be seen at https://www.youtube.com/watch?v=J_F8eW-K8KI&feature=youtu.be.

figuration of the mechanism is the same as the initial configuration. The experimental d values were obtained by measuring the positions of the joints using motion tracking cameras and then calculating the positions of the required ICRs using the method presented in section 2.4. The graph shows that, since d never goes to zero, the robot manipulator is able complete the full rotation without encountering a singularity. This is confirmed numerically, and the experimental validation is provided as well, showing that the full rotation is achievable without encountering mechanical interferences. An online video of the prototype of the robot manipulator completing the rotation can be seen at https://www.youtube.com/watch?v=J_F8eW-K8KI&feature=youtu.be. In the video, the rigidity of the robot manipulator is physically demonstrated during the rotation to show that it never moves into a singularity. The video also consists of an example of singularity avoidance and a pick-and-place trajectory of full rotation to demonstrate the robot manipulator's workspace.

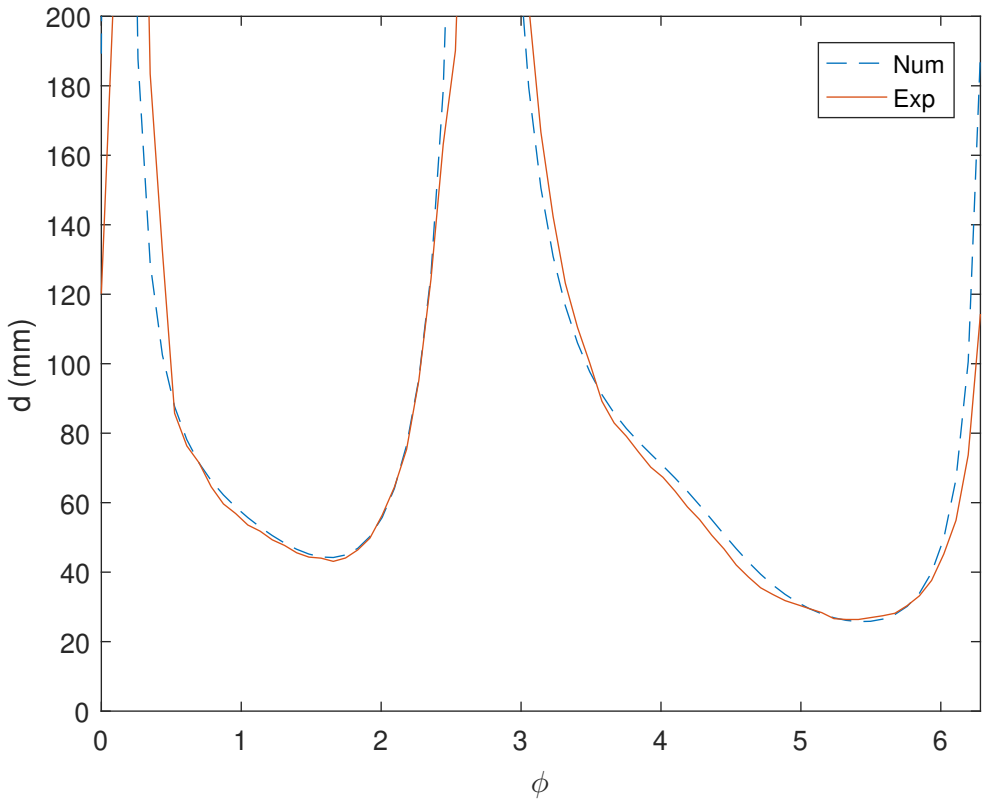

Figure 2.10: Graph displaying d, the distance between the two ICR(1,7)s, against ϕ, the angular displacement of the end-effector along the rotation trajectory.

Chapter 3

On the False Positives and False Negatives of the Jacobian Matrix in Kinematically Redundant Parallel Mechanisms

In chapter 2, a novel architecture of a kinematically redundant parallel mechanism was presented which is capable of performing full rotations of the end-effector without encountering singularities. Developers of robot manipulators could adopt this architecture for applications where the strengths of parallel robots are needed, e.g. high speed and strength, but high dexterity is also a requirement. Once the robot is developed, full cycle rotations can be achieved by employing a method of singularity analysis to identify which configurations of the mechanism correspond to singularities and to then avoid them by utilising the redundancy of the mechanism. As discussed in the chapter 1, the conventional method of performing singularity analysis on parallel mechanisms is to use Jacobian-based approaches, e.g. by computing the determinant of the Jacobian. In this chapter, it is shown that such methods are unreliable when applied to kinematically redundant architectures with non-serially connected actuators. The problems arise from the need to eliminate redundant variables when forming it, resulting in both situations where the Jacobian incorrectly identifies singularities (*false positive*), and where it fails to identify singularities (*false negative*). These issues have thus far remained unaddressed in the literature. These limitations are highlighted here by demonstrating several cases using numerical examples of both planar and spatial architectures. The work presented in this chapter is based on

that published in Baron et al. (2020b)

The issues associated with using Jacobian-based methods of singularity analysis manifest when applied to kinematically redundant architectures with non-serially connected actuators. When conducting the kinematic analysis of these mechanisms, it is commonplace to formulate the so-called forward kinematic Jacobian by eliminating the additional passive joint velocity which describes the kinematically redundant degree of freedom—see for instance Gosselin et al. (2015); Schreiber and Gosselin (2018); Gosselin and Schreiber (2016). However, there are problems associated with this method which, to the authors' knowledge, have yet to be discussed in the literature. Such problems arise when using Jacobian-based methods of singularity analysis on these mechanisms. Herein, the term singularity is used to describe the so-called forward kinematics singularity. In this chapter, the Jacobians of three kinematically redundant parallel robots with non-serially connected actuators (two planar and one spatial) are calculated following the standard approach, and particular instances of each architecture are examined. It is shown that the inverse of the 2-norm condition number of the Jacobian, a traditional method of singularity analysis, either fails to identify or incorrectly identifies a singular configuration. Indeed, other measures, such as computing the determinant of the Jacobian, exhibit the same shortcomings. This phenomenon is distinct from the constraint singularity Zlatanov et al. (2002), in that the Jacobian is either failing to identify (false negative), or incorrectly identifying (false positive), direct kinematic singularities. The failure of the Jacobian is verified using the principles of rigidity theory; by analysing the underlying graph of the robot and computing its rigidity matrix.

The rest of this chapter is structured as follows. In section 3.1, a summary of the principles of rigidity theory is given, including how a parallel robot can be analysed in terms of its underlying graph and how its rigidity, or lack thereof, can be determined by computing the rank of its rigidity matrix. In section 3.2, a family of kinematically redundant parallel mechanisms with non-serially connected actuators is presented, and in section 3.3, the methods used to calculate the Jacobian for these mechanisms are presented. In section 3.4, three example configurations of these architectures where the Jacobian fails as a means of singularity analysis are demonstrated. Finally, in section 3.5 the results are discussed.

3.1 The Rigidity Matrix of Parallel robots

Rigidity theory provides a useful set of mathematical tools which can be leveraged for the analysis of parallel robots Hendrickson (1992); Asimow and Roth (1978, 1979). A graph $G = (V, E)$ is a set of $|V|$ vertices and $|E|$ edges, where each edge joins two vertices and is associated with a real number. A realisation of a graph is an assignment of coordinates to each vertex such that the Euclidean distances between any adjacent vertices equals the number associated with the corresponding edge. A framework, denoted by $p(G)$, is the combination of a graph and a realisation. A framework that can be continuously deformed whilst maintaining all of the distance constraints between the vertices is *flexible*, else it is *rigid* Hendrickson (1992). Parallel robots can be analysed using these principles through modelling the joints of the mechanism as the vertices of a graph and the links that join them as the edges Merlet (2006). A given configuration of a particular architecture can then be described as a framework, and the rigidity of the physical mechanism can be analysed by inspecting this framework.

A finite flexing of a framework $p(G)$ is defined as a family of realisations of G such that if the position of each vertex is differentiable with respect to time, the distance constraint $(p_i(t) - p_j(t))^2 = constant$ holds for each vertex pairing $(i, j) \in E$, and differentiating leads to

$$(v_i - v_j) \cdot (p_i - p_j) = 0 \tag{3.1}$$

where v_i is the instantaneous velocity of vertex i. An infinitesimal motion of a framework is a set of vertex velocities for which (3.1) holds for every paring of adjacent vertices; for generic graph realisations, infinitesimal motions correspond to finite flexings Hendrickson (1992). Finite flexings can be categorised as either trivial or non-trivial. Trivial finite flexings correspond to translations or rotations of the Euclidean space itself, non-trivial finite flexings are those that do not fit this description. If there exists a non-trivial infinitesimal motion, the framework is described as flexible, otherwise it is described as rigid.

In d-dimensional Euclidean space, a set of n vertices have nd possible independent motions. A d-dimensional body has d possible translations and $d(d-1)/2$ rotations, whereas a d'-dimensional body for which $d' < d$ has $d'(2d - d' - 1)/2$ rotations. The total number of allowed motions, $S(n, d)$, for the framework is given by the total number of independent motions of the vertices, nd, minus the number of rigid body motions, this is

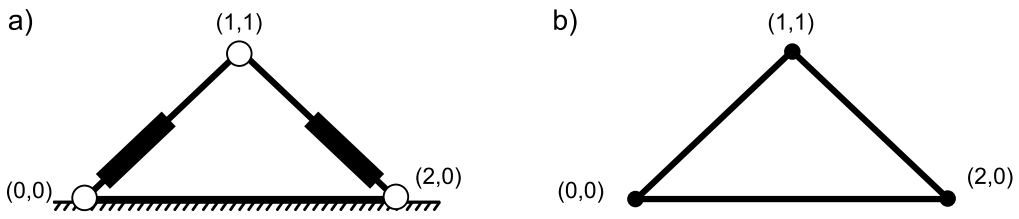

Figure 3.1: Mechanism, a), whose graph, b), corresponds to three vertices, positioned at $P_1 = (0,0)^T$, $P_2 = (2,0)^T$, and $P_3 = (1,1)^T$, and three edges.

formulated by

$$S(n,d) = \begin{cases} nd - d(d+1)/2 & \text{if } n >= d, \\ n(n-1)/2 & \text{otherwise.} \end{cases} \tag{3.2}$$

If each edge adds one independent constraint, then $S(n,d)$ edges are required for the system to become rigid.

A method of testing the rigidity of a graph is by forming its rigidity matrix, which is comprised of the set of equations (3.1) for each edge. The matrix has m rows, each of which corresponds to an edge and nd columns, each of which corresponds to a coordinate of a vertex. If an element in the matrix is in a row corresponding to an edge and in a column of a vertex that is part of that edge, then the value of that element is the difference between that vertex and the other vertex in the edge in terms of the coordinates dictated by the column. For example, consider the planar case depicted in Fig. 3.1 where two prismatic actuators are joined together by a revolute joint and also to the ground via two other revolute joints; assuming the actuators are locked, this mechanism can be modelled by a graph composed of three vertices, located at the positions of the revolute joints, joined by three edges, which correspond to the length between each pair of joints. For the case where the vertices are positioned at $P_1 = (0,0)^T$, $P_2 = (2,0)^T$, and $P_3 = (1,1)^T$, as displayed in Fig. 3.1, the corresponding rigidity matrix is

$$M = \begin{array}{c} \\ e_{1,2} \\ e_{1,3} \\ e_{2,3} \end{array} \begin{array}{c} \begin{array}{cccccc} x_1 & y_1 & x_2 & y_2 & x_3 & y_3 \end{array} \\ \begin{pmatrix} -2 & 0 & 2 & 0 & 0 & 0 \\ -1 & -1 & 0 & 0 & 1 & 1 \\ 0 & 0 & 1 & -1 & -1 & 1 \end{pmatrix} \end{array}. \tag{3.3}$$

The example given above is straightforward since it is a planar linkage where all of the passive joints are revolute. If the revolute joints of this mechanism were replaced by spherical joints, such that the corresponding spatial mechanism was formed, the 3-dimensional graph would again consist of three vertices connected by three edges. The

Figure 3.2: A family of kinematically redundant parallel robots with non-serially connected actuators proposed in the literature. The architectures, from left to right, were first presented in Baron et al. (2018), Schreiber and Gosselin (2018), and Gosselin and Schreiber (2016), respectively.

spatial manipulator examined in this chapter consists of revolute and universal joints in addition to spherical joints, the corresponding sub-graphs for each of these joints are addressed here. A revolute joint in a spatial mechanism corresponds to two vertices which lie along the joint's axis. If the revolute joint is attached to a spherical joint, each vertex is connected to the vertex corresponding to the spherical joint in addition to each other Rojas and Thomas (2018). A universal joint attached to the base corresponds to three adjacent vertices, two attached to the base, forming the base revolute axis, and the third, able to move with respect to the base, forming the moving revolute axis with one of the other two vertices. If the universal joint is connected to a revolute joint, then the vertices that form the moving axis are each connected to both of the vertices corresponding to the revolute joint.

A framework is rigid if, and only if, the row rank, herein referred to as rank, of its corresponding rigidity matrix is equal to $S(n, d)$. This is because as all infinitesimal motions must be in the null space of M, and $S(n, d)$ represents the size of the rigidity matrix without any trivial infinitesimal motions, it follows that if there exists any non-trivial motions within the null space of M, its rank must be less than $S(n, d)$. Therefore for a parallel robot, which is generally rigid, its corresponding rigidity matrix should be of full rank except for singular configurations in which it loses its inherent rigidity. In section 3.4, computing the rank of the rigidity matrix is used as a steadfast method of determining whether or not a parallel robot has entered a singularity.

3.2 Kinematic Redundant Parallel Robots with Non-Serially Connected Actuators

Kinematically redundant architectures can be categorised into two different types: those which contain serial connected actuators and those which do not. Architectures with serially connected actuators can be obtained by taking a non-redundant architecture and adding extra actuated joints to the existing limbs. Architectures which don't exhibit actuators connected in series contain at least two limbs that share a kinematic constraint between the base and the moving platform. Fig. 3.2 displays three instances of non-serially actuated kinematically redundant parallel architectures that have been proposed in the literature.

The architecture displayed on the left-hand side of Fig. 3.2 is the equivalent of the planar mechanism presented in chapter 2, but with R$\underline{\text{P}}$R legs instead of $\underline{\text{R}}$RR legs; that is an actuated prismatic joint with a passive revolute joint at each of its ends, two of which join the end-effector to the base directly, and the the other two join the end-effector to a ternary link, which itself is connected to the base via a passive revolute joint. The second architecture, presented in Schreiber and Gosselin (2018), is also a planar mechanism that consists of four R$\underline{\text{P}}$R legs. Two of the legs are connected to the base and the end-effector at separate points, the other two legs are joined to the end-effector at separate points and to a binary link at the same point, which in turn is connected to the base via a passive revolute joint. The third architecture, presented in Gosselin and Schreiber (2016), consists of a moving platform which is connected to the base by multiple redundant and non-redundant legs. A non-redundant leg consists of a prismatic joint which is joined to the platform via a spherical joint and to the base via a universal joint. A redundant leg consists of two prismatic actuators joined to the base at different points via universal joints, and to each other via a revolute joint, which in turn is connected to the platform via a spherical joint. The instance of the manipulator shown in Fig. 3.2 consists of three pairings of redundant and non-redundant legs, where the universal joints of each pairing are positioned upon of the same line. The six spherical joints connecting the legs to platform are located at three different positions; each position shares a joint between a redundant and non-redundant leg from different pairings.

The kinematically redundant architectures with non-serially connected actuators presented in Fig. 3.2 benefit from the advantages provided by kinematic redundancy, i.e the singularity locus in the robot's workspace is significantly reduced, but additionally they do not suffer from the accumulation of actuator errors along each of the limbs. In the

following section, the method of calculating the Jacobian matrices, relating the robot's input joint velocity vector to the output velocity vector, is demonstrated for each of these three architectures.

3.3 Calculation of the Jacobian

The relationship between the input joint velocities and the output velocity of the end-effector of a parallel robot can be described by the Jacobian matrices, **J** and **K**, such that

$$\mathbf{J}\dot{\mathbf{c}} = \mathbf{K}\dot{\mathbf{q}} \tag{3.4}$$

where $\dot{\mathbf{c}}$ and $\dot{\mathbf{q}}$ denote the output and input velocity vectors, respectively. Traditionally, the robot is determined to be in a type-II singularity if **J** is singular. In this section, the method of calculating **J** for each of the three kinematically redundant parallel robots with non-serially connected actuators displayed in Fig. 3.2 is demonstrated. Unlike for non-redundant architectures, the method requires the elimination of at least one redundant output velocity variable in order to form the row(s) corresponding to the branches of the mechanism which join between the end-effector and the base; e.g. when two legs are joined to common link which, in turn, is joined to the base. This process of eliminating the redundant output variable(s) generates issues when performing singularity analysis, these problems are discussed in section 3.4.

The methods of calculating the Jacobian for each of these three mechanisms is summarised below. The aim of this section is to highlight the need for the elimination of redundant joint velocities, the aim is not to give a detailed account of how the Jacobian is calculated from start to finish. For a more comprehensive detailing of each method, the reader is referred to the detailed Jacobian calculations in appendix A.

3.3.1 Architecture 1 - 1^{st} Planar Case

Firstly, let's consider the robot architecture displayed on the left-hand side of Fig. 3.2, the corresponding kinematic diagram of this architecture is shown in Fig. 3.3. The moving platform (P_6P_7) is connected directly to the base via two R$\underline{\text{P}}$R legs at P_1 and P_2, namely legs 1 and 2, and to the ternary link via the two other R$\underline{\text{P}}$R legs at P_4 and P_5, namely legs 3 and 4, which is connected to the base itself via a revolute joint at P_3. A fixed reference frame, Oxy, is attached to the base and a moving frame, $P_ex'y'$, is attached to the moving platform. The orientation of the platform, ϕ, is given by the angle taken

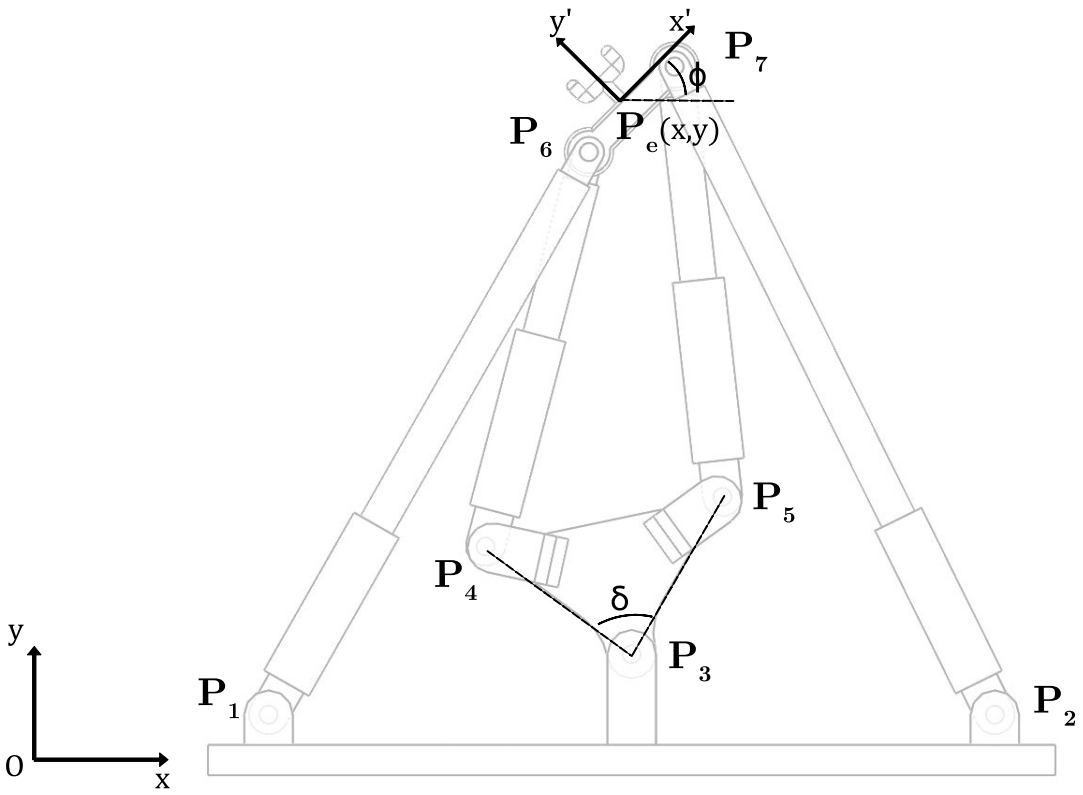

Figure 3.3: The corresponding Kinematic diagram of the architecture displayed in the left-hand side of Fig. 3.2, that of the mechanism presented in Baron et al. (2018).

anti-clockwise from the horizontal axis of the fixed frame to that of the moving frame, centred at $P_e(x, y)$. After forming the vector loop equations along each of the four legs, and taking the derivative with respect to time for each of them, we obtain

$$\mathbf{p}_{1,6}^T(\dot{\mathbf{p}}_e - \dot{\mathbf{p}}_{6,e}) = \rho_1\dot{\rho}_1, \tag{3.5}$$

$$\mathbf{p}_{2,7}^T(\dot{\mathbf{p}}_e - \dot{\mathbf{p}}_{7,e}) = \rho_2\dot{\rho}_2, \tag{3.6}$$

$$\mathbf{p}_{4,6}^T(\dot{\mathbf{p}}_e - \dot{\mathbf{p}}_{3,4} - \dot{\mathbf{p}}_{6,e}) = \rho_3\dot{\rho}_3, \tag{3.7}$$

$$\mathbf{p}_{5,7}^T(\dot{\mathbf{p}}_e - \dot{\mathbf{p}}_{3,5} - \dot{\mathbf{p}}_{7,e}) = \rho_4\dot{\rho}_4. \tag{3.8}$$

where $\mathbf{p}_{i,j}$ denotes the vector from P_i to P_j, $\mathbf{p}_e$ denotes the position vector of P_e, ρ_i denotes the length of the prismatic actuators of the i^{th} leg of the manipulator, and dot notation is used to indicate a derivative with respect to time.

Since the output of the robot is the 3-dimensional velocity vector, $\dot{\mathbf{c}} = (\dot{x}, \dot{y}, \dot{\phi})^T$, and the input is the 4-dimensional velocity vector, $\dot{\mathbf{q}} = (\dot{\rho}_1, \dot{\rho}_2, \dot{\rho}_3, \dot{\rho}_4)^T$, the Jacobian matrices, $\mathbf{J}$ and $\mathbf{K}$, are of dimension 3×3 and 3×4, respectively. The first two rows are formed by equations (3.5) and (3.6), whereas the third row is formed by combining equations (3.7) and (3.8) through the elimination of $\dot{\mathbf{p}}_{3,5}$; the vector which corresponds to the redundant

output variable.

Since P_3, P_4, and P_5 are all connected to the same ternary link, the following relation exists:

$$\mathbf{p}_{3,4} = \frac{d_{3,4}}{d_{3,5}} \begin{bmatrix} cos(\delta) & -sin(\delta) \\ sin(\delta) & cos(\delta) \end{bmatrix} \mathbf{p}_{3,5} = \lambda \mathbf{M} \mathbf{p}_{3,5} \tag{3.9}$$

where

$$\lambda = \frac{d_{3,4}}{d_{3,5}}, \tag{3.10}$$

$$\mathbf{M} = \begin{bmatrix} cos(\delta) & -sin(\delta) \\ sin(\delta) & cos(\delta) \end{bmatrix}, \tag{3.11}$$

and δ is the angle taken anti-clockwise from $\mathbf{p}_{3,5}$ to $\mathbf{p}_{3,4}$. Using this relation, equations (3.7) and (3.8) can be combined to produce the following equation

$$\begin{bmatrix} \mathbf{p}_{4,6}^T(\dot{\mathbf{p}}_e - \dot{\mathbf{p}}_{6,e}) - \rho_3\dot{\rho}_3 \\ \mathbf{p}_{5,7}^T(\dot{\mathbf{p}}_e - \dot{\mathbf{p}}_{7,e}) - \rho_4\dot{\rho}_4 \end{bmatrix} = \begin{bmatrix} \mathbf{p}_{4,6}^T\lambda\mathbf{M} \\ \mathbf{p}_{5,7}^T \end{bmatrix} \dot{\mathbf{p}}_{3,5}, \tag{3.12}$$

and then $\dot{\mathbf{p}}_{3,5}$ can be made the subject by

$$\dot{\mathbf{p}}_{3,5} = \mathbf{N} \begin{bmatrix} \mathbf{p}_{4,6}^T(\dot{\mathbf{p}}_e - \dot{\mathbf{p}}_{6,e}) - \rho_3\dot{\rho}_3 \\ \mathbf{p}_{5,7}^T(\dot{\mathbf{p}}_e - \dot{\mathbf{p}}_{7,e}) - \rho_4\dot{\rho}_4 \end{bmatrix}, \tag{3.13}$$

where

$$\mathbf{N} = \begin{bmatrix} \mathbf{p}_{4,6}^T\lambda\mathbf{M} \\ \mathbf{p}_{5,7}^T \end{bmatrix}^{-1}.$$

Since the distance between P_3 and P_5 is constant,

$$\mathbf{p}_{3,5}^T\dot{\mathbf{p}}_{3,5} = 0. \tag{3.14}$$

The redundant output variable, $\dot{\mathbf{p}}_{3,5}$, is then eliminated by substituting (3.13) into (3.14). By expanding the velocity vectors, we obtain

$$\mathbf{p}_{3,5}^T\mathbf{N} \begin{bmatrix} \mathbf{p}_{4,6}^T \\ \mathbf{p}_{5,7}^T \end{bmatrix} \begin{bmatrix} \dot{x} \\ \dot{y} \end{bmatrix} - \mathbf{p}_{3,5}^T\mathbf{N} \begin{bmatrix} \mathbf{p}_{4,6}^T\mathbf{E}\mathbf{p}_{6,e} \\ \mathbf{p}_{5,7}^T\mathbf{E}\mathbf{p}_{7,e} \end{bmatrix} \dot{\phi} = \mathbf{p}_{3,5}^T\mathbf{N} \begin{bmatrix} \rho_3\dot{\rho}_3 \\ \rho_4\dot{\rho}_4 \end{bmatrix}, \tag{3.15}$$

where

$$\mathbf{E} = \begin{bmatrix} 0 & -1 \\ 1 & 0 \end{bmatrix}.$$

By similarly expanding the velocity vectors of equations (3.5) and (3.6), the Jacobian matrices $\mathbf{J}$ and $\mathbf{K}$ can be formed, such that $\mathbf{J}$ is given by

$$\mathbf{J} = \begin{bmatrix} \mathbf{p}_{1,6}^T & -\mathbf{p}_{1,6}^T\mathbf{E}\mathbf{p}_{6,e} \\ \mathbf{p}_{2,7}^T & -\mathbf{p}_{2,7}^T\mathbf{E}\mathbf{p}_{7,e} \\ \mathbf{p}_{3,5}^T\mathbf{N} \begin{bmatrix} \mathbf{p}_{4,6}^T \\ \mathbf{p}_{5,7}^T \end{bmatrix} & -\mathbf{p}_{3,5}^T\mathbf{N} \begin{bmatrix} \mathbf{p}_{4,6}^T\mathbf{E}\mathbf{p}_{6,e} \\ \mathbf{p}_{5,7}^T\mathbf{E}\mathbf{p}_{7,e} \end{bmatrix} \end{bmatrix}. \tag{3.16}$$

3.3.2 Architecture 2 - Spatial Case

Here the Jacobian is calculated for the kinematically redundant spatial manipulator displayed in the right-hand side of Fig. 3.2, the corresponding kinematic diagram of which is displayed in Fig. 3.4. As mentioned above, the manipulator consists of a moving platform attached to the base by three redundant and three non-redundant legs. The non-redundant legs consist of an actuated prismatic joint which is connect to the base via a universal joint, at point A_i, and to the moving platform via a spherical joint, at point B_i, where $i = 4, 5, 6$. The redundant legs consist of two actuated prismatic joints joined to the base at points $A_{i,1}$ and $A_{i,2}$, to each other via a revolute joint at S_i, and to the moving platform via a spherical joint at B_i, where $i = 1, 2, 3$. The six spherical joints attached to the platform are positioned in coincident pairs. A fixed reference frame $Oxyz$ is attached to the base and a moving reference frame $Px'y'z'$ is attached to the moving platform. In Gosselin and Schreiber (2016), the Jacobian is calculated for a manipulator with an unspecified number of redundant legs, here the same method is simplified for a manipulator with three redundant and three non-redundant legs. The position vectors of the universal joints on the base, $A_{i,j}$ and A_i for the redundant and non-redundant legs respectively, are denoted by $\mathbf{a}_{i,j}$ and $\mathbf{a}_i$. The position vectors for the spherical joints, B_i, on the platform are given by $\mathbf{b}_i$, and the position vectors of each revolute joint, S_i, are denoted by $\mathbf{s}_i$. The Jacobian, $\mathbf{J}$, of this robot is a 6×6 matrix, where three of the rows correspond to the redundant legs and three correspond to the non-redundant legs. Here, the steps required to compute the rows corresponding the redundant legs are shown as this is where the elimination of the redundant variables occurs.

The position of the i^{th} platform joint in terms of $\mathbf{Q}$, the matrix denoting the orientation of the platform, and $\mathbf{v}_{i,0}$, the position of the joint in the moving frame,is given by

$$\mathbf{b}_i = \mathbf{p} + \mathbf{Q}\mathbf{v}_{i,0}, i = 1, ..., 6. \tag{3.17}$$

For the i^{th} redundant leg, the following constraint equations are written

$$(\mathbf{s}_i - \mathbf{a}_{i,j})^T(\mathbf{s}_i - \mathbf{a}_{i,j}) = \rho_{i,j}^2, \tag{3.18}$$

$$(\mathbf{s}_i - \mathbf{b}_i)^T(\mathbf{s}_i - \mathbf{b}_i) = l_i^2, \tag{3.19}$$

where l_i denotes the length of the link which joins S_i and B_i, and $j = 1, 2$. Given that the joints $A_{i,1}$, $A_{i,2}$, S_i, and B_i are coplanar, if we define a unit vector $\mathbf{e}_i$ which passes through the base joints of redundant leg i, the following relationship must hold

$$[(\mathbf{b}_i - \mathbf{a}_{i,1}) \times \mathbf{e}_i]^T(\mathbf{s}_i - \mathbf{a}_{i,1}) = 0. \tag{3.20}$$

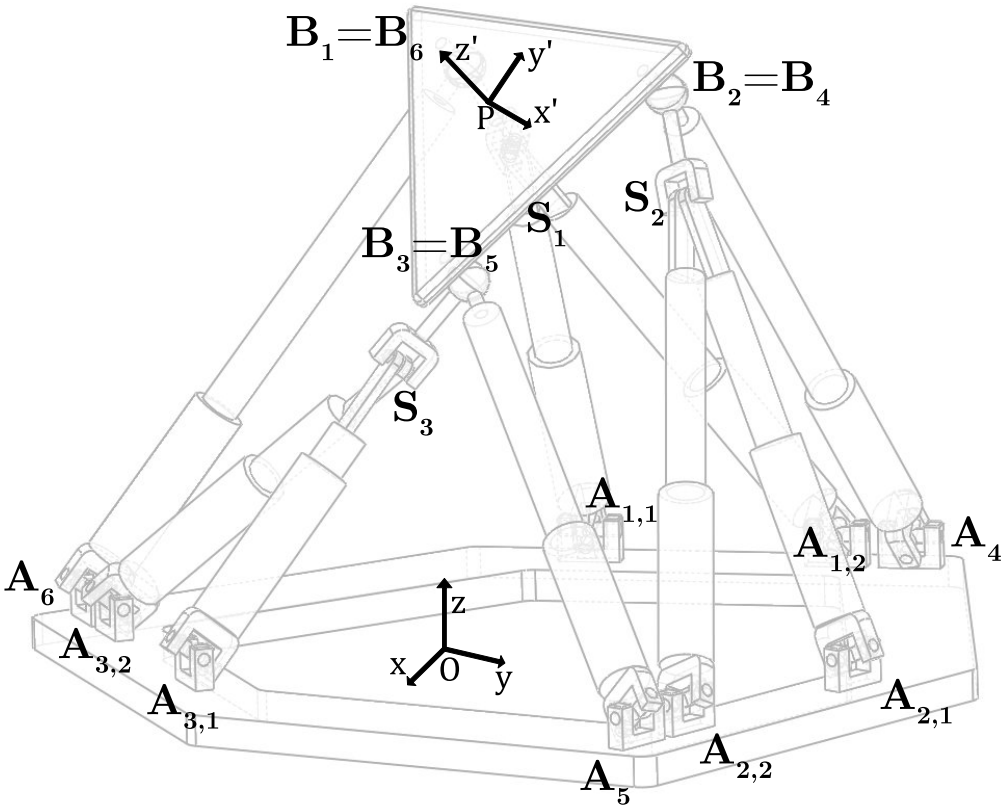

Figure 3.4: The corresponding kinematic diagram of the architecture displayed in the right-hand side of Fig. 3.2, that of the mechanism presented in Gosselin and Schreiber (2016).

By differentiating equations (3.18) and (3.20), the following is obtained

$$\begin{bmatrix} (\mathbf{s}_i - \mathbf{a}_{i,1})^T \\ (\mathbf{s}_i - \mathbf{a}_{i,2})^T \\ [(\mathbf{b}_i - \mathbf{a}_{i,1}) \times \mathbf{e}_i]^T \end{bmatrix} \dot{\mathbf{s}}_i = \mathbf{H}_i \dot{\mathbf{s}}_i = \begin{bmatrix} \rho_{i,1}\dot{\rho}_{i,1} \\ \rho_{i,2}\dot{\rho}_{i,2} \\ [(\mathbf{s}_i - \mathbf{a}_{i,1}) \times \mathbf{e}_i]^T \dot{\mathbf{b}}_i \end{bmatrix}. \tag{3.21}$$

Equation (3.21) is solved for $\dot{\mathbf{s}}_i$ by taking the matrix inverse of $\mathbf{H}_i$, such that

$$\dot{\mathbf{s}}_i = \mathbf{H}_i^{-1} \begin{bmatrix} \rho_{i,1}\dot{\rho}_{i,1} \\ \rho_{i,2}\dot{\rho}_{i,2} \\ [(\mathbf{s}_i - \mathbf{a}_{i,1}) \times \mathbf{e}_i]^T \dot{\mathbf{b}}_i \end{bmatrix}, \tag{3.22}$$

where $\mathbf{H}_i^{-1}$ can be expressed as

$$\mathbf{H}_i^{-1} = \frac{Adj(\mathbf{H}_i)}{det(\mathbf{H}_i)}, \tag{3.23}$$

$Adj(\mathbf{H}_i)$ is the adjoint of matrix $\mathbf{H}_i$ and $det(\mathbf{H}_i)$ is the determinant, which herein will be denoted by μ_i. These can be expressed algebraically by

$$det(\mathbf{H}_i) = \mu_i = [(\mathbf{s}_i - \mathbf{a}_{i,1}) \times (\mathbf{s}_i - \mathbf{a}_{i,2})]^T [(\mathbf{b}_i - \mathbf{a}_{i,1}) \times \mathbf{e}_i] \tag{3.24}$$

and

$$Adj(\mathbf{H}_i) = \begin{bmatrix} \mathbf{h}_{i,1} & \mathbf{h}_{i,2} & \mathbf{h}_{i,3} \end{bmatrix} \tag{3.25}$$

where

$$\mathbf{h}_{i,1} = (\mathbf{s}_i - \mathbf{a}_{i,2}) \times [(\mathbf{b}_i - \mathbf{a}_{i,1}) \times \mathbf{e}_i], \tag{3.26}$$

$$\mathbf{h}_{i,2} = [(\mathbf{b}_i - \mathbf{a}_{i,1}) \times \mathbf{e}_i] \times (\mathbf{s}_i - \mathbf{a}_{i,1}), \tag{3.27}$$

$$\mathbf{h}_{i,3} = (\mathbf{s}_i - \mathbf{a}_{i,1}) \times (\mathbf{s}_i - \mathbf{a}_{i,2}). \tag{3.28}$$

Now equation (3.22) can be rewritten as

$$\dot{\mathbf{s}}_i = \frac{1}{\mu_i}(\mathbf{h}_{i,1}\rho_{i,1}\dot{\rho}_{i,1} + \mathbf{h}_{i,2}\rho_{i,2}\dot{\rho}_{i,2} + \mathbf{h}_{i,3}[(\mathbf{s}_i - \mathbf{a}_{i,1}) \times \mathbf{e}_i]^T\dot{\mathbf{b}}_i). \tag{3.29}$$

By taking the derivative of (3.19), one obtains

$$(\mathbf{s}_i - \mathbf{b}_i)^T\dot{\mathbf{s}}_i = (\mathbf{s}_i - \mathbf{b}_i)^T\dot{\mathbf{b}}_i, \tag{3.30}$$

and substituting (3.29) and the derivative of (3.17) into (3.30) gives

$$(\mathbf{s}_i - \mathbf{b}_i)^T\dot{\mathbf{p}} + [\mathbf{Q}\mathbf{v}_{i,0} \times (\mathbf{s}_i - \mathbf{b}_i)]^T\boldsymbol{\omega} = (\mathbf{s}_i - \mathbf{b}_i)^T\mathbf{m}_i\dot{\rho}_{i,1} + (\mathbf{s}_i - \mathbf{b}_i)^T\mathbf{n}_i\dot{\rho}_{i,2} \tag{3.31}$$

where

$$\mathbf{m}_i = \frac{\rho_{i,1}}{\mu_i}[(\mathbf{s}_i - \mathbf{a}_{i,2}) \times [(\mathbf{b}_i - \mathbf{a}_{i,1}) \times \mathbf{e}_i]], \tag{3.32}$$

$$\mathbf{n}_i = \frac{\rho_{i,2}}{\mu_i}[[(\mathbf{b}_i - \mathbf{a}_{i,1}) \times \mathbf{e}_i] \times (\mathbf{s}_i - \mathbf{a}_{i,1})]. \tag{3.33}$$

The output velocity vector of the manipulator is given by $\dot{\mathbf{c}} = (\dot{\mathbf{p}}^T, \boldsymbol{\omega}^T)^T$ and the vector of actuated joint velocities is given by $\dot{\mathbf{q}} = (\dot{\rho}_{1,1}, \dot{\rho}_{1,2}, \dot{\rho}_{2,1}, \dot{\rho}_{2,2}, \dot{\rho}_{3,1}, \dot{\rho}_{3,2}, \dot{\rho}_4, \dot{\rho}_5, \dot{\rho}_6)^T$. Equation (3.31) is used to construct the first three rows of the Jacobian which correspond to the redundant legs of the manipulator. Then, along with the latter three rows which correspond to the non-redundant legs, the Jacobian matrices $\mathbf{J}$ and $\mathbf{K}$ can be computed. Matrix $\mathbf{J}$ is given by

$$\mathbf{J} = \begin{bmatrix} (\mathbf{s}_1 - \mathbf{b}_1)^T & [\mathbf{Q}\mathbf{v}_{1,0} \times (\mathbf{s}_1 - \mathbf{b}_1)^T] \\ (\mathbf{s}_2 - \mathbf{b}_2)^T & [\mathbf{Q}\mathbf{v}_{2,0} \times (\mathbf{s}_2 - \mathbf{b}_2)^T] \\ (\mathbf{s}_3 - \mathbf{b}_3)^T & [\mathbf{Q}\mathbf{v}_{3,0} \times (\mathbf{s}_3 - \mathbf{b}_3)^T] \\ (\mathbf{b}_4 - \mathbf{a}_4)^T & [\mathbf{Q}\mathbf{v}_{4,0} \times (\mathbf{b}_4 - \mathbf{a}_4)^T] \\ (\mathbf{b}_5 - \mathbf{a}_5)^T & [\mathbf{Q}\mathbf{v}_{5,0} \times (\mathbf{b}_5 - \mathbf{a}_5)^T] \\ (\mathbf{b}_6 - \mathbf{a}_6)^T & [\mathbf{Q}\mathbf{v}_{6,0} \times (\mathbf{b}_6 - \mathbf{a}_6)^T] \end{bmatrix}. \tag{3.34}$$

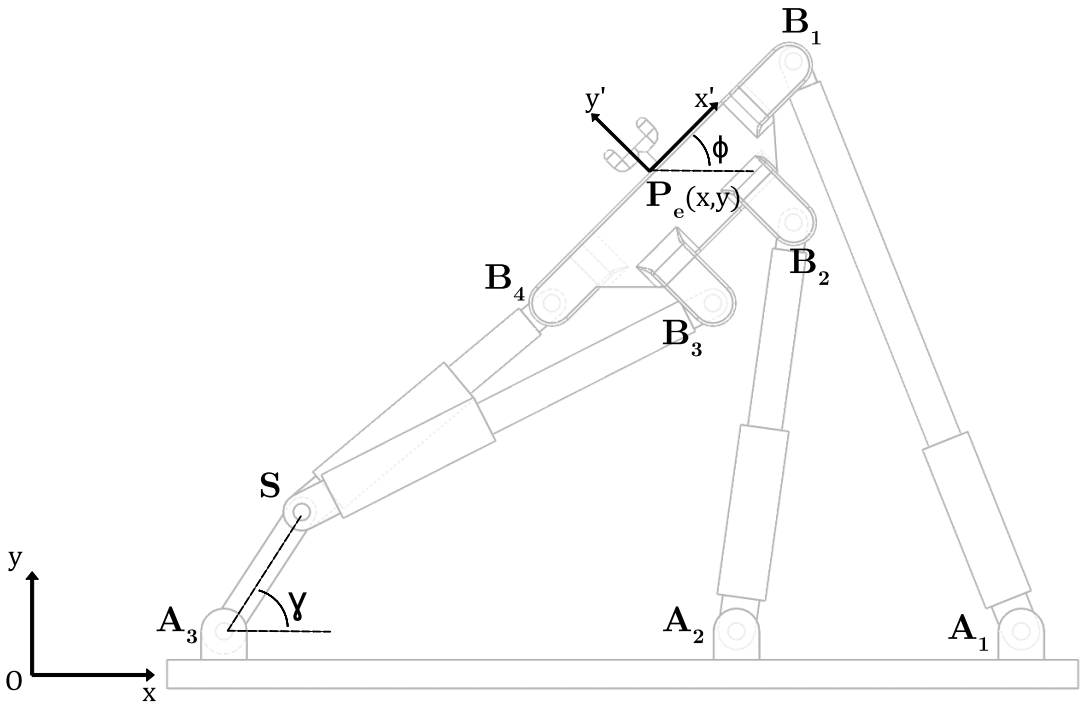

Figure 3.5: The corresponding Kinematic diagram of the architecture displayed in the centre of Fig. 3.2, that of the mechanism presented in Schreiber and Gosselin (2018).

3.3.3 Architecture 3 - 2^{nd} Planar Case

The final mechanism under inspection, displayed in the centre of Fig. 3.2, is the kinematically redundant planar parallel architecture presented in Schreiber and Gosselin (2018), the kinematic diagram of which is shown in Fig. 3.5. The architecture consists of four R$\underline{\text{P}}$R legs, two which of are joined to the base at points A_1 and A_2, and to the moving platform at B_1 and B_2. The other two are joined to the platform at points B_3 and B_4, and are joined to an additional link at the same point, S, which in turn is connected to the base via a revolute joint centred at A_3. A fixed reference frame Oxy is attached to the base, and a moving reference frame $Px'y'$ is attached to the platform at point $P(x, y)$; the orientation of the platform, ϕ, is defined by the angle taken anti-clockwise from the horizontal axis of the fixed reference frame to that of the moving reference frame. The position vectors of points A_i, B_i, S, and P are denoted by $\mathbf{a}_i$, $\mathbf{b}_i$, $\mathbf{s}$, and $\mathbf{p}$ respectively. The Cartesian coordinates of the platform are given by $\mathbf{c} = (x, y, \phi)^T$. The distance between joints A_i and B_i, $i = 1, 2$, and S and B_i, $i = 3, 4$, is denoted by ρ_i, corresponding to the lengths of the prismatic actuators. The orientation of link A_3S relative to the fixed reference frame is given by γ. Firstly, the constraint equations in terms of the square of the length of each prismatic actuator, ρ_i^2, and the square of the length of link A_3S, l_i^2, are formed, and their

derivatives are obtained as

$$(\mathbf{b}_i - \mathbf{a}_i)^T(\dot{\mathbf{p}} + \dot{\phi}\mathbf{E}\boldsymbol{\nu}_i) = \rho_i\dot{\rho}_i, i = 1, 2, \tag{3.35}$$

$$(\mathbf{b}_i - \mathbf{s})^T(\dot{\mathbf{p}} + \dot{\phi}\mathbf{E}\boldsymbol{\nu}_i - \dot{\mathbf{s}}) = \rho_i\dot{\rho}_i, i = 3, 4 \tag{3.36}$$

$$(\mathbf{s} - \mathbf{a}_3)^T\dot{\mathbf{s}} = 0 \tag{3.37}$$

where $\boldsymbol{\nu}_i = \mathbf{Q}\boldsymbol{\nu}_{0,i}$. Equations (3.36) are then combined to form the matrix equation

$$\mathbf{G}\dot{\mathbf{c}} - \mathbf{h} = \mathbf{H}\dot{\mathbf{s}} \tag{3.38}$$

such that

$$\begin{bmatrix} \mathbf{f}^T & \mathbf{f}^T\mathbf{E}\boldsymbol{\nu}_3 \\ \mathbf{m}^T & \mathbf{m}^T\mathbf{E}\boldsymbol{\nu}_4 \end{bmatrix} \dot{\mathbf{c}} - \begin{bmatrix} \rho_3\dot{\rho}_3 \\ \rho_4\dot{\rho}_4 \end{bmatrix} = \begin{bmatrix} \mathbf{f}^T \\ \mathbf{m}^T \end{bmatrix} \dot{\mathbf{s}}$$

where $\mathbf{f}^T = (\mathbf{b}_3 - \mathbf{s})^T$ and $\mathbf{m}^T = (\mathbf{b}_4 - \mathbf{s})^T$. Equation (3.38) is then rearranged to make $\dot{\mathbf{s}}$ the subject by taking the inverse of matrix $\mathbf{H}$, such that

$$\dot{\mathbf{s}} = \mathbf{N}(\mathbf{G}\dot{\mathbf{c}} - \mathbf{h}) \tag{3.39}$$

where

$$\mathbf{N} = \mathbf{H}^{-1} = \frac{1}{\mathbf{f}^T\mathbf{E}\mathbf{m}} \begin{bmatrix} \mathbf{E}\mathbf{m} & -\mathbf{E}\mathbf{f} \end{bmatrix}.$$

The redundant variable, $\dot{\mathbf{s}}$, is then eliminated by substituting (3.39) into (3.37), such that

$$(\mathbf{s} - \mathbf{a}_3)^T\mathbf{N}\mathbf{G}\dot{\mathbf{c}} = (\mathbf{s} - \mathbf{a}_3)^T \begin{bmatrix} \frac{\mathbf{E}\mathbf{m}\rho_3}{\mathbf{f}^T\mathbf{E}\mathbf{m}} & \frac{-\mathbf{E}\mathbf{f}\rho_4}{\mathbf{f}^T\mathbf{E}\mathbf{m}} \end{bmatrix} \begin{bmatrix} \dot{\rho}_3 \\ \dot{\rho}_4 \end{bmatrix} \tag{3.40}$$

where

$$\mathbf{N}\mathbf{G} = \frac{\mathbf{E}}{\mathbf{f}^T\mathbf{E}\mathbf{m}} \begin{bmatrix} (\mathbf{m}\mathbf{f}^T - \mathbf{f}\mathbf{m}^T) & (\mathbf{m}\mathbf{f}^T\mathbf{E}\boldsymbol{\nu}_3 - \mathbf{f}\mathbf{m}^T\mathbf{E}\boldsymbol{\nu}_4) \end{bmatrix}. \tag{3.41}$$

This may be further simplified to

$$\mathbf{N}\mathbf{G} = \begin{bmatrix} \mathbf{I} & \mathbf{E}(\mathbf{s} - \mathbf{p}) \end{bmatrix} \tag{3.42}$$

where $\mathbf{I}$ denotes the 2×2 identity matrix. The details of this simplification are given in the detailed Jacobian calculations in appendix A, however this is not the focus; if either (3.41) or (3.42) are used to form the Jacobian, the same problems still manifest themselves. These issues are generated through performing the matrix inverse, $\mathbf{H}^{-1}$, and the elimination of the redundant variable, $\dot{\mathbf{s}}$. The first two rows of the Jacobian Matrices, $\mathbf{J}$ and $\mathbf{K}$, can then be formed from (3.35), and the third row can be obtained by substituting (3.42) into (3.40), such that matrix $\mathbf{J}$ is given by

$$\mathbf{J} = \begin{bmatrix} (\mathbf{b}_1 - \mathbf{a}_1)^T & (\mathbf{b}_1 - \mathbf{a}_1)^T\mathbf{E}\boldsymbol{\nu}_1 \\ (\mathbf{b}_2 - \mathbf{a}_2)^T & (\mathbf{b}_2 - \mathbf{a}_2)^T\mathbf{E}\boldsymbol{\nu}_2 \\ (\mathbf{s} - \mathbf{a}_3)^T & (\mathbf{s} - \mathbf{a}_3)^T\mathbf{E}(\mathbf{s} - \mathbf{p}) \end{bmatrix}. \tag{3.43}$$

3.4 Limitations of the Jacobian

In this section, some examples of the problems with using Jacobian-based methods of singularity analysis for kinematically redundant robots with non-serially connected actuators are demonstrated. The Jacobian is computed for each of the three architectures presented in Fig. 3.2 whilst in configurations where these problems manifest themselves. The singularity analysis is conducted using the inverse of the 2-norm condition number of the Jacobian, and the results are assessed by constructing the rigidity matrix and calculating its rank. The rigidity matrices for each of the three mechanisms are provided in appendix B.

3.4.1 1^{st} Planar Case - False Positive of the Jacobian

In this first example, we consider a mechanism which has the same architecture as that presented in the left-hand side of Fig. 3.2. Let's consider the configuration of this mechanism where $\mathbf{p}_1 = (0,0)^T$, $\mathbf{p}_2 = (3,0)^T$, $\mathbf{p}_3 = (2.5,1)^T$, $\mathbf{p}_4 = (1.79,1.71)^T$, $\mathbf{p}_5 = (2.5,2)^T$, $\mathbf{p}_6 = (1.41,2.63)^T$, and $\mathbf{p}_7 = (2.88,2.92)^T$; the corresponding kinematic diagram is shown in Fig. 3.6. The Jacobian, $\mathbf{J}$, is obtained by inputting these values into (3.16). The inverse of the 2-norm condition number of the obtained Jacobian is zero, suggesting that the robot is in a singularity. However, the rigidity matrix of the mechanism in this configuration has full rank, this indicates that the robot is not in a singularity, despite the fact that the inverse of the condition number of the Jacobian suggests the robot is in a singularity.

3.4.2 Spatial Case - False Negative of the Jacobian

Now we turn our attention to the spatial manipulator. In this case, the issue is that it is possible to have a configuration where the robot enters a singularity, indicated by the fact that the rigidity matrix loses rank, but the determinant of the Jacobian is non-zero. In Gosselin and Schreiber (2016), where the architecture is presented and the Jacobian is calculated, the authors state that an assumption of this mechanism is that the legs never lie in the base plane. However, since the inverse of the condition number of the Jacobian does not approach zero as the robot nears such a configuration, it does not act as a reliable method of analysing how the performance of the robot deteriorates near all singularities, making it a bad basis for path planning algorithms. In the following example, the robot is initially in a non-singular pose and the platform follows a trajectory towards the configuration in which the revolute joint of one of the redundant legs, $\mathbf{s}_3$, lies on the line passing through the base joints $\mathbf{a}_{3,1}$ and $\mathbf{a}_{3,2}$.

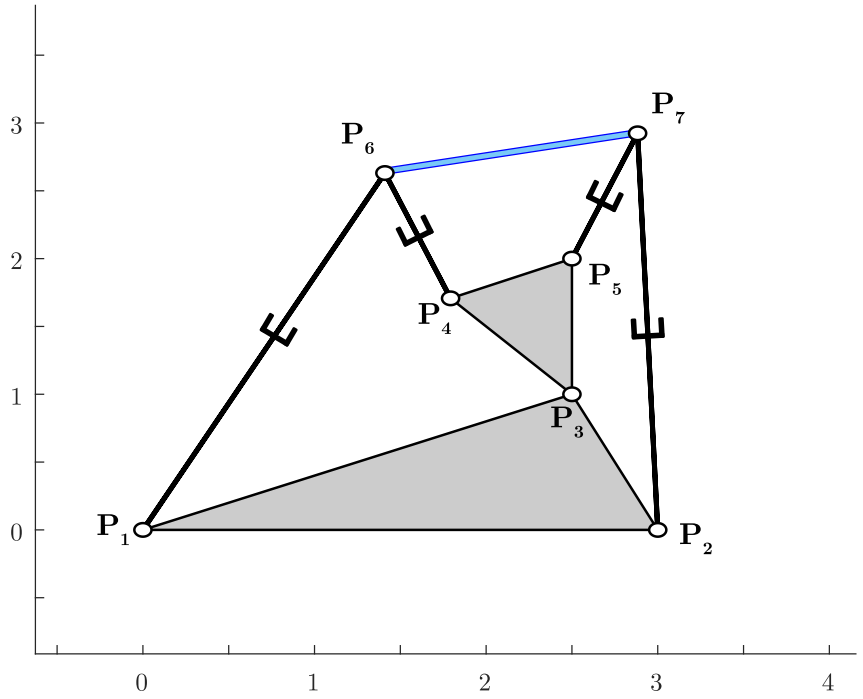

Figure 3.6: Configuration of the robot proposed in Baron et al. (2018) where the inverse of the condition number of the Jacobian is zero, suggesting that the configuration is singular, but the rigidity matrix is of full rank, indicating that the mechanism is not in a singularity.

A fixed reference frame is attached to the base and the base joints are positioned at: $\mathbf{a}_{1,1} = (-1.4, 0, 0)^T$, $\mathbf{a}_{1,2} = (-1.0, -0.69, 0)^T$, $\mathbf{a}_{2,1} = (0.7, 1.21, 0)^T$, $\mathbf{a}_{2,2} = (-0, 1, 1.21, 0)^T$, $\mathbf{a}_{3,1} = (0.7, -1.21, 0)^T$, $\mathbf{a}_{3,2} = (1.1, -0.52, 0)^T$, $\mathbf{a}_4 = (-1.5, 0.17, 0)^T$, $\mathbf{a}_5 = (0.9, 1.21, 0)^T$, and $\mathbf{a}_6 = (0.6, -1.39, 0)^T$. When in the initial pose, the platform joints are positioned at: $\mathbf{b}_1 = (-1.18, -0.43, 1.68)^T$, $\mathbf{b}_2 = (-1.18, 0.43, 1.68)^T$, and $\mathbf{b}_3 = (0.35, 0, 1.15)^T$, and the revolute joints on the redundant legs are positioned at: $\mathbf{s}_1 = (-0.23, -0.43, 1.59)^T$, $\mathbf{s}_2 = (-0.15, 0.47, 1.59)^T$, and $\mathbf{s}_3 = (0.39, -0.06, 1.07)^T$; all coordinates are given to two decimal places.

The platform follows a linear trajectory such that the final pose of the platform is given by $\mathbf{b}_1 = (0.33, -1.24, 0.60)^T$, $\mathbf{b}_2 = (0.33, -0.38, 0.60)^T$, and $\mathbf{b}_3 = (0.86, -0.81, 0.07)^T$. The revolute joints of the redundant links are positioned throughout the trajectory such that the line passing through the link $\mathbf{b}_i\mathbf{s}_i$ passes through the midpoint of base joints $\mathbf{a}_{i,1}$ and $\mathbf{a}_{i,2}$; their positions at the end of the trajectory are $\mathbf{s}_1 = (0.25, -1.19, 0.57)^T$, $\mathbf{s}_2 = (0.33, -0.28, 0.57)^T$, and $\mathbf{s}_3 = (0.90, -0.87, 0)^T$. Fig. 3.7 shows the initial and final pose of the manipulator during this trajectory.

The trajectory is discretised into 101 steps, and the value of $1/\kappa(J)$ (the inverse of the

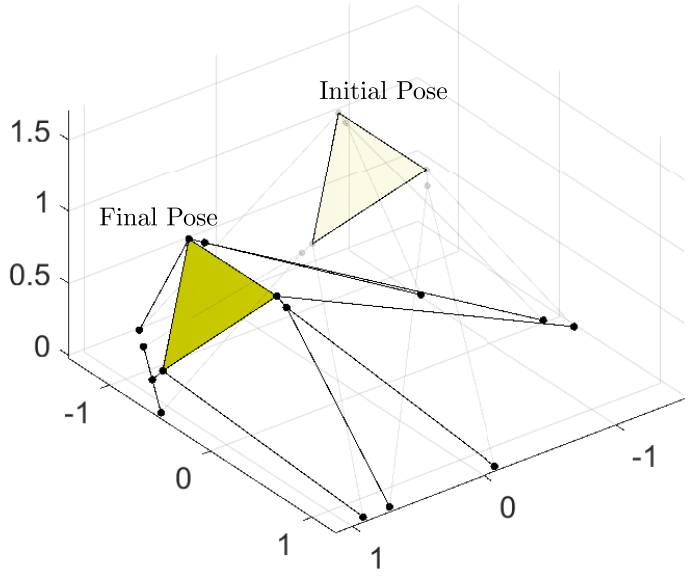

Figure 3.7: The initial and final configurations of the example kinematically redundant spatial manipulator as it moves from a non-singular pose into a singularity.

2-norm condition number of J), is displayed at each step in Fig. 3.8. The value of $1/\kappa(J)$ does not go to zero as the manipulator reaches the final pose of the trajectory, where the revolute joint $\mathbf{s}_3$ lies directly between $\mathbf{a}_{3,1}$ and $\mathbf{a}_{3,2}$. However, in this configuration the manipulator is in a type-II singularity, this is determined by formulating the rigidity matrix of the mechanism and computing its rank at each step. The rank of the rigidity matrix at each step is 88, except for the last step at which it drops to 87, indicating that the mechanism has entered a type-II singularity at this point and lost its rigidity.

3.4.3 2^{nd} Planar Case - False Negative of the Jacobian

In this final example, the 2^{nd} planar architecture is examined as it moves from an initial non-singular configuration through a singularity. The trajectory is depicted in Fig. 3.9, the transparent instances show the initial and final non-singular configurations of the mechanism whereas the opaque instance shows the singular configuration. The base joints are positioned at: $\mathbf{a}_1 = (12, 15)^T$, $\mathbf{a}_2 = (8, 0)^T$, and $\mathbf{a}_3 = (-2, 1)^T$, and joint S is always positioned at $\mathbf{s} = (0, 2.5)^T$ throughout the trajectory. In the initial configuration, the platform joints are positioned at $\mathbf{b}_1 = (-3, 10)^T$, $\mathbf{b}_2 = (-3, 7)^T$, $\mathbf{b}_3 = (-6.5, 7)^T$, and $\mathbf{b}_4 = (-6.5, 10)^T$. The platform then moves along a horizontal trajectory to the right, passing through a configuration where the links $SB3$ and $SB4$ become collinear. The value

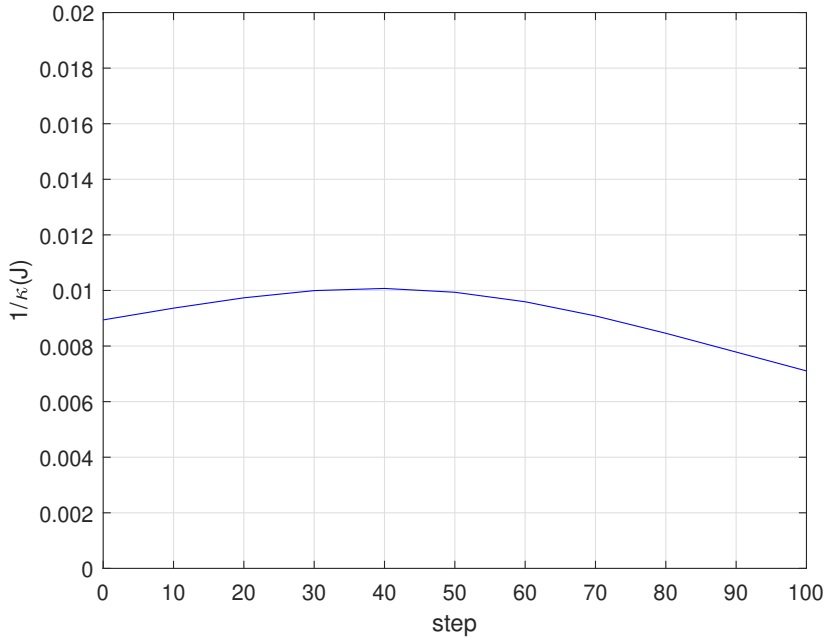

Figure 3.8: Inverse of the condition number of the Jacobian, $1/\kappa(J)$, for spatial manipulator at each step of the trajectory, showing that the Jacobian does not approach becoming singular as the robot moves into a type-II singularity.

of the inverse of the 2-norm condition number, $1/\kappa(J)$, is plotted against the x coordinate of platform joint $\mathbf{b}_1$ in Fig. 3.10. This case is similar to that reported in example 2, in that the value of $1/\kappa(J)$ does not approach zero as the robot nears a singularity, when $x_0 = 3.5$.

3.5 Discussion

It is clear that these shortcomings of the Jacobian as a means of singularity detection have serious implications in terms of path planning algorithms for kinematically redundant parallel robots with non-serially connected actuators. For cases similar to the first example, the feasible workspace of the mechanism would needlessly be restricted since the Jacobian becomes singular in configurations where the robot is not in a singularity. Whereas for cases similar to the second two examples, any path planning algorithms based on the Jacobian would run the risk of moving the robot into a configuration where its performance may deteriorate significantly.

The issues are generated by the need to eliminate a, or multiple, redundant variables. For the first example, the determinant of the Jacobian becomes singular because the matrix that is inverted to obtain $\mathbf{N}$, in equation (3.13), itself becomes singular due to a linear

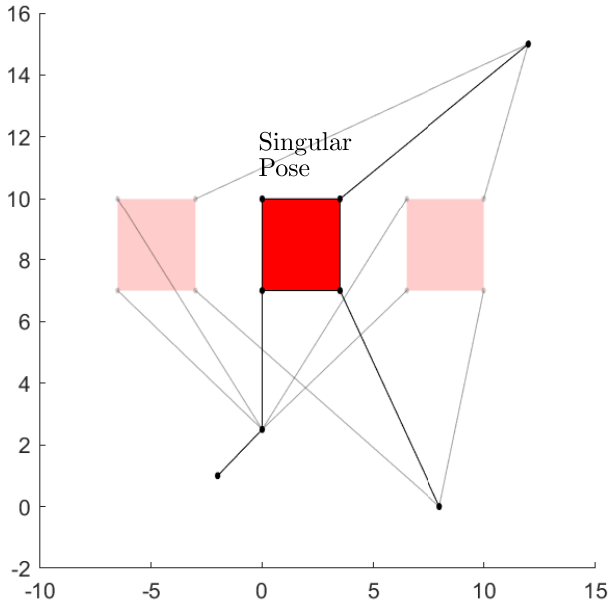

Figure 3.9: Trajectory of the example kinematically redundant planar parallel robot, passing through a type-II singularity for which the Jacobian stays non-singular.

dependence between its rows. Although this accounts for the singularity from a mathematical perspective, it does not translate into a physical meaning for the singularity. The geometric conditions for this instance to occur are that if the line which passes through leg 3 of the manipulator is rotated by δ in the clockwise direction, and the result is a collinearity with the line which passes through leg 4. In addition to computing the rank of the corresponding rigidity matrix, it is also possible to verify that this configuration is non-singular by performing the singularity analysis via instantaneous centres of rotation Baron et al. (2019); Daniali (2005); Di Gregorio (2009), and in chapter 4, such a method is presented. The result is that, when in the configuration detailed in example 1, the instantaneous centres of rotation between the platform and the base, for each of the four equivalent mechanisms where all but one of the actuators are locked, are all determinable and do not coincide with one another, indicating that the robot is not in a singularity.

The failure of the Jacobian in examples 2 and 3 is different to example 1; the inverse of the condition number of the Jacobian is non-zero, but we know that the robot is in a singularity as the corresponding rigidity matrix is rank deficient. Although the architectures in examples 2 and 3 correspond to spatial and planar cases respectively, the reasons which cause the Jacobian to fail in both examples are similar and so we will treat them

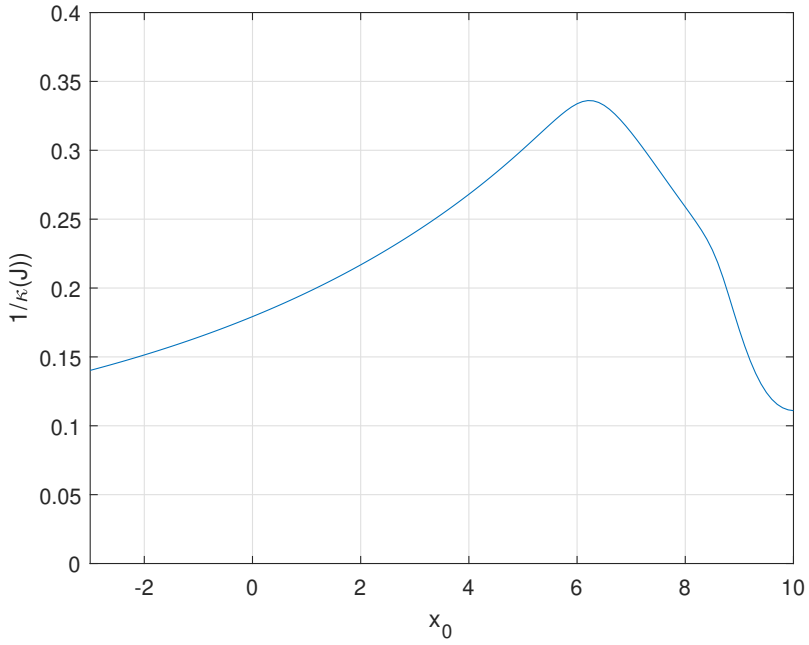

Figure 3.10: Value of $1/\kappa(J)$ as the planar parallel robot passes through the singularity; the configuration where the limbs joined to the platform and the redundant link become collinear, occurring at $x_0 = 3.5$.

both here. In example 2, the redundant variable $\mathbf{s}_i$ is eliminated by taking the inverse of matrix $\mathbf{H}_i$ so that equation (3.22) can be substituted into (3.30). In order to perform this matrix inverse, the determinant of $\mathbf{H}_i$, denoted μ_i, is taken; which equals zero when the prismatic actuators along $A_{i,1}S$ and $A_{i,2}S$ are collinear. It can be seen that (3.31) is obtained by substituting (3.29), that which contains μ_i, into (3.30). However, since the third term of the right-hand side of (3.29) is orthogonal to $(\mathbf{s}_i - \mathbf{b}_i)$, the product of them equals zero and hence μ_i does not feature in the Jacobian matrix, $\mathbf{J}$. Similarly in example 3, the term $\mathbf{NG}$ in (3.41) is simplified to (3.42), such that the coefficient $1/\mathbf{f}^T\mathbf{Em}$ is cancelled. An alternative is to not perform these simplifications such that the determinants of of matrices $\mathbf{H}_i$ and $\mathbf{H}$, respectively, remain present in the Jacobian; however this means that although $det(\mathbf{J}) = 0$ when the robot is in this configuration, it does not smoothly approach zero as the robot approaches the configuration; therefore unless, the robot is positioned precisely in such a pose, the singularity will not be detected. It is also possible to detect these singularities by generating the so-called 'extended Jacobian', by including the time derivative of the redundant variable in the cartesian velocity vector Schreiber and Gosselin (2018, 2019). However, the use of this technique for path planning algorithms is limited as the time derivative of the redundant variable must also be selected in order to

solve the inverse kinematics.

The findings presented above are summarised by advising developers of kinematically redundant parallel robots with non-serially connected actuators to use non-Jacobian based methods of path planning and singularity analysis. Computing the rank of rigidity matrix of the underlying graph of the mechanism is a reliable method of determining whether or not a particular configuration is singular or not, but does not help with informing how close the robot is to a singularity. It is clear that other methods need to be developed which do not exhibit the issues detailed above. A video summarising the work presented in this chapter can be viewed at https://www.youtube.com/watch?v=-fmpNin_Zgs.

Chapter 4

A Robust Method of Singularity Avoidance

In the previous chapter, it has been made clear that conventional, Jacobian-based methods of singularity analysis can be very unreliable when applied to kinematically redundant architectures with non-serially connected actuators. This has massive implications for path planning algorithms used on kinematically redundant architectures as this can lead to algorithms missing some (false negative) singularities, risking the failure of the robot in some configurations, and also leading to needlessly restricting the size of the workspace to avoid false positive singularities. In this chapter, a method of singularity analysis is proposed which does not exhibit the same shortcomings as Jacobian-based methods, as exemplified in the previous chapter. This approach is then used as a basis upon which a method of singularity avoidance is developed, such that the redundancy of the mechanism is optimised for a given pose of the end-effector to move as far away from a singularity as possible. The work presented in this chapter is based on that published in Baron et al. (2020c).

The method of singularity avoidance for kinematically redundant parallel robots presented here is a geometric approach, which firstly determines the manipulator's proximity to a singularity and then computes how the kinematically redundant degree(s) of freedom should be optimised for the given pose of the end-effector. The singularity analysis is conducted by examining the mechanism in terms of the instantaneous centres of rotation (ICRs) of its corresponding mobility one sub-mechanisms when all but one of the actuators are locked. The position of the ICR between the platform and the base of each sub-mechanism is computed and the manipulator is in a type-II singularity when these ICRs either are indeterminable or coincide with one another. The robot manipulator's

proximity to a singularity is measured by computing the in-circle radii of the triangles formed by these ICRs, and finding the minimum of these radii, r_{min}. This is different to the method presented in chapter 2, where the robot manipulator's proximity to a singularity is given by the minimum distance between two ICRs. The avoidance of singularities is carried out by determining the configuration of the robot for which r_{min} is optimised, and is reachable without crossing a singularity. A predictor-corrector method to compute the optimum value of the parameter which describes the degree of kinematic redundancy of the robot manipulator such that r_{min} is maximised without passing through a singular configuration, that where r_{min}=0. The method of singularity avoidance is carried out numerically on an example mechanism. Finally, it is shown that the geometric method of singularity analysis is more reliable than Jacobian-based approaches by examining two example mechanisms, which are in configurations where the Jacobian both incorrectly identifies and fails to identify singularities, but the proposed method does not; this is verified by computing the robots' corresponding rigidity matrices whilst in these configurations, as it is known that the rank of the rigidity matrix drops in a singular configuration Hendrickson (1992); Asimow and Roth (1978, 1979).

The remainder of this chapter is structured as follows. In section 4.1, the principles of instantaneous centres of rotation are discussed and the method of determining their positions is presented. In section 4.2, the singularity analysis is performed, such that the value of r_{min} for a given configuration of the robot manipulator can be obtained and a predictor-corrector algorithm is then employed to increase this value without crossing a singularity or changing the pose of the end-effector. Section 4.3 gives a numerical example to demonstrate this process. In section 4.4, the proposed method of singularity analysis is compared with a conventional Jacobian based method; the advantages the former has over the latter are shown with the aid of two examples.

4.1 Review of Basic Tools

In this section, the background tools used to conduct the proposed method are briefly reviewed. Firstly, as the method is intended to be implemented on kinematically redundant planar parallel robots with non-serially connected actuators, a set of four example architectures that have been proposed in recent years are presented in Fig. 4.1. This includes the two planar architectures presented in chapter 3 and two additional architectures. Architecture a) was first presented in Baron et al. (2018), b) and c) in Schreiber and Gosselin (2018), and d) in Gosselin et al. (2015), although this architecture is less unique than the

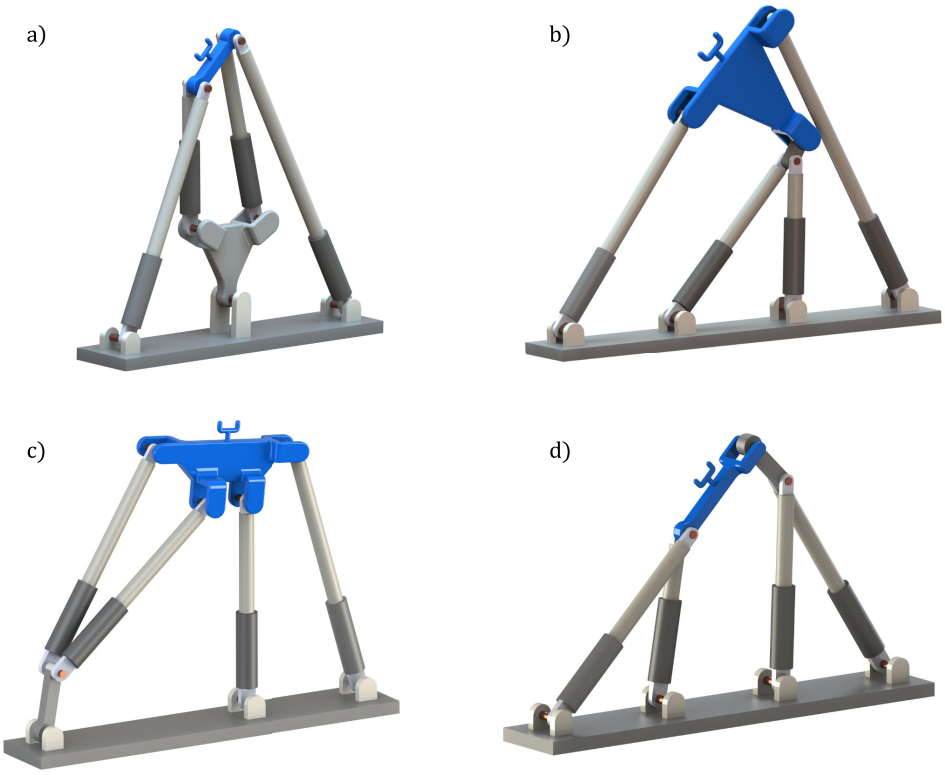

Figure 4.1: A family of kinematically redundant planar parallel robots. All of these architectures consist of four R<u>P</u>R legs, two of which directly connect the end-effector to the ground. In architecture a) the remaining two R<u>P</u>R legs join the end-effector to a ternary link which itself is connected to the base via a revolute joint. In architecture b), the remaining two R<u>P</u>R legs join the base to a binary link which is joined to the end-effector via a revolute joint. In architecture c), the remaining two R<u>P</u>R legs join the end-effector to a binary link which is connected to the ground via a revolute joint. Finally, architecture d) is a specialised case of b) in which two of the joints attached to the end-effector are coincident.

others because it can be considered as a specialised case of architecture b). The method of singularity analysis presented in section 4.2.1 is applicable on all planar parallel robots, however the method of singularity avoidance, presented in section 4.2.2, is tailored for redundant robots such as those shown in Fig. 4.1.

The singularity analysis is performed by inspecting the mechanism in terms of its instantaneous centres of rotation (ICRs), where the manipulator is determined to be in a singularity if these ICRs coincide or become indeterminable Daniali (2005); Baron et al. (2018); Di Gregorio (2009). The method of carrying out this analysis is briefly reviewed

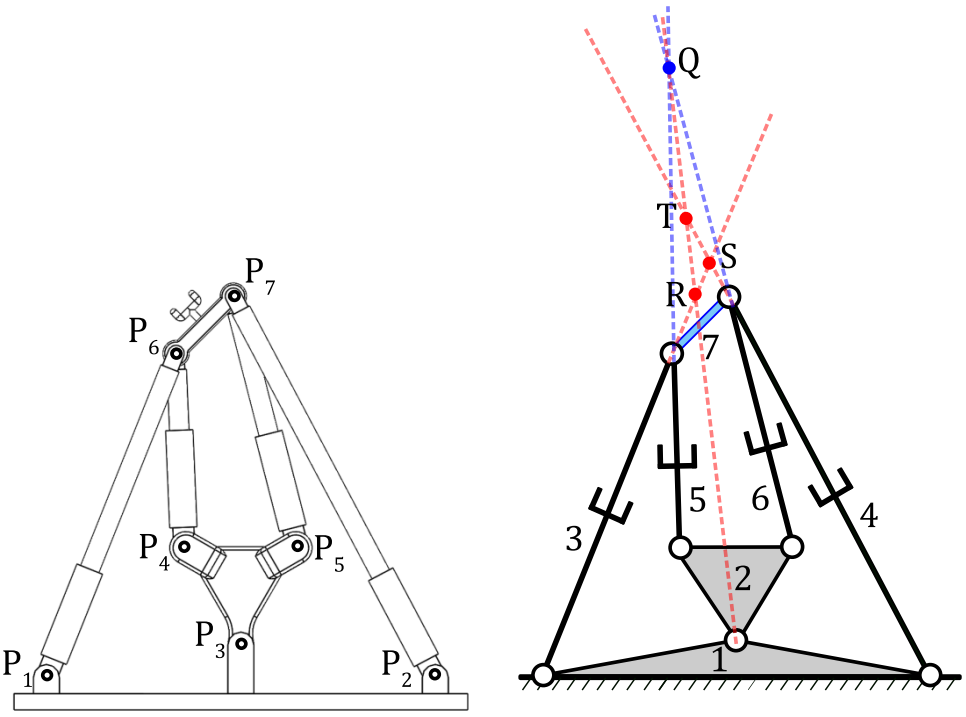

Figure 4.2: Kinematically redundant planar parallel architecture presented in Baron et al. (2018) with the relevant ICRs displayed.

here, a more comprehensive description is given in chapter 2. Firstly, the mechanism is treated as the union of its corresponding sub-mechanisms with a mobility of one (M=1) where all but one of the actuated joints are locked. Then the ICR between the end-effector and the base of each sub-mechanism can be found by applying the Aronhold-Kennedy theorem; which states that for any three rigid bodies moving relative to one another in a plane, the three ICRs between them lie upon the same line. If the positions of two of the ICRs between three rigid bodies are known, then the third ICR must lie upon the line which passes through them; following this, the position of an ICR can be determined if it lies upon two known lines – the ICR between the end-effector and the base for each sub-mechanism is found using this principle. An effective system for keeping track of which ICRs between two rigid links of the mechanism are known is to construct *Circle Diagrams* (also known as the auxiliary polygon derived from the Aronhold-Kennedy theorem on ICRs), first presented in Hartenberg and Denavit (1964). For example, Fig. 4.2 displays the architecture in Fig. 4.1 a) with the relevant ICRs depicted, and the corresponding *Circle Diagrams* are given in Fig. 4.3.

The mechanism consists of an end-effector (link 7) which is connected to the base (link 1) directly by two RPR legs (links 3 and 4), and also by two other RPR legs (links 5 and 6) that are connected to a ternary link (link 2) which itself is connected to the base via

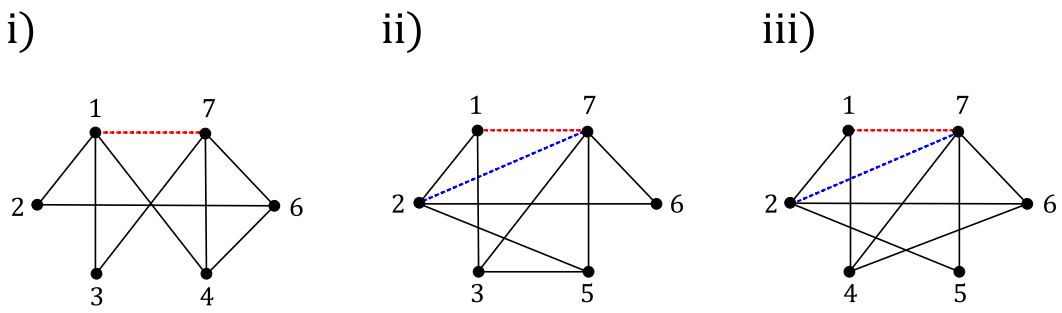

Figure 4.3: Circle Diagrams used to determine the positions of the ICRs for the mechanism displayed in Fig. 4.2.

a revolute joint. Links 4 and 6 are connected to the end-effector at a single point, as are links 5 and 7.

The M=1 sub-mechanisms are obtained by removing the constraints imposed by each of the four legs in turn; it can be verified that each of the following mechanisms have a mobility of one by using the extended Chebychev-Kutzbach-Grübler formula Rojas and Dollar (2016), which is given by

$$M = F - \sum_{i=1}^{\lambda} t_i \tag{4.1}$$

where $\lambda = J - L + 1$ is the number of independent closed-loops in the mechanism, t_i is the motion type of the i^{th} independent closed-loop ($t_i = 3$ in the planar case), J is the total number of joints, L is the number of links, and F is the total number of degrees of freedom of the joints. The *Circle Diagrams* for the sub-mechanisms are given in Fig. 4.3 where all the links are denoted by number and the black, filled lines denote that the corresponding links share a physical joint. The circle diagram for the sub-mechanism where link 6 is removed is not shown because it gives the same result as the sub-mechanism where link 5 is removed. A desired ICR is denoted by a dashed line, and it is possible to find its position if this line is the common side of two other triangles that are otherwise made up of lines denoting known ICRs and joints.

The aim is to obtain the position of ICR(1,7) for each sub-mechanism; from herein the ICR between links i and j will be denoted by ICR(i,j). For sub-mechanism i), it can be seen that the dashed line on the circle diagram between links 1 and 7 is the common side of two triangles otherwise made up of filled in lines. The position of ICR(1,7) is therefore given by the point of intersection between the lines that pass through the joints between links 1 & 3 and links 3 & 7, and the joints between links 1 & 4 and links 4 & 7; this is displayed as point **S** on Fig. 4.2. Sub-mechanisms ii) and iii) follow the same logic, but since ICR(1,7) is not initially the common side of two triangles, an additional ICR has to

be calculated beforehand, this is ICR(2,7) and it is shown as point **Q** in Fig. 4.2. Now ICR(1,7), for both sub-mechanism ii) and iii), is the common side of two triangles, its position can be found by finding the point of intersection of the relevant lines.

4.2 Geometric Method of Singularity Avoidance

4.2.1 Proximity to a Singularity

After the ICRs between the base and the platform for each M=1 sub-mechanism have been determined using the methods detailed in section 4.1, the robot manipulator's proximity to a singularity is analysed by determining how close two of these ICRs are to coinciding or how close one of the sub-mechanisms is to being in a singularity itself. In order to measure both of these criteria, the method used is to find sets of three ICRs and calculate the in-circle radius of the triangle whose vertices correspond to the positions of these points. The computation of the in-circle radius has previously been used for performing a Jacobian-based method of singularity analysis of the 3-RPRR manipulator Ebrahimi et al. (2008).

The first objective is to determine the triangles that need to be formed in order to measure the robot manipulator's proximity to a singularity. A robot manipulator is in a singularity if either two or more of the ICRs between the base and the end-effector of each sub-mechanism coincide, or if one or more of the sub-mechanisms themselves move into a singularity; a configuration where the ICR between the base and the end-effector cannot be determined due to the collinearity of construction lines. The former is done by calculating the number of triangles that can be formed by the total number of ICRs between the base and the end-effector; e.g. if there are three, one triangle needs to be formed. The latter is done by making sure that every pair of construction lines used to compute the position of any virtual ICR is included in a triangle; if there exists a pair that are not, then a triangle must be formed with one of its vertices corresponding to the position of the ICR determined by these lines, and the remaining two corresponding to the centres of the physical joints which lie on each of the lines. The in-circle radius of each triangle is then calculated, and the obtained value is then normalised using the maximum possible in-circle radius of that triangle, which is dependent on the pose of the end-effector.

Two examples are shown in Fig. 4.4 which correspond to each of these situations. The first example, displayed in Fig. 4.4 a), shows a set of three ICRs whose positions

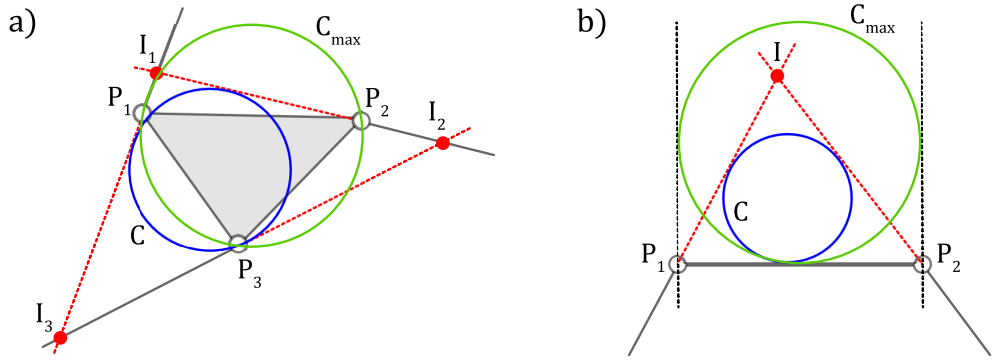

Figure 4.4: Different maximum in-circles: Example a) shows the in-circle, C, of the triangle formed by three ICRs (I_1, I_2, and I_3) and the maximum sized in-circle, C_{max}, given by that which passes through each of the physical joints (P_1, P_2, and P_3), example b) shows the in-circle of the triangle formed by one ICR and two physical joints, and the maximum sized in-circle whose radius is given by half the distance between the physical joints.

are determined by the construction lines passing through three links, which are joined to three revolute joints separated by fixed distances; the positions of the ICRs are given by the red points. The in-circle of the triangle formed by these points, C, is shown in blue. The maximum sized circle, C_{max}, is the maximum in-circle that can be obtained by reorienting the three links, corresponding to the circle which passes through the three physical joints Ebrahimi et al. (2008). Note that this example is not showing how the ICRs are computed just for the case of the 3-RPRR parallel robot (as computed in Ebrahimi et al. (2008)), but for any mechanism where three joints are separated by fixed lengths and whose ICRs are positioned at the intersection points of the three construction lines that pass through each of the joints. Fig. 4.4 b) shows the in-circle of the triangle formed by a single virtual ICR and two physical joints separated by a fixed distance. It can be seen that the maximum value of the radius of this circle is given by half of the fixed distance between the physical joints.

For the case shown in Fig. 4.4 a), the in-circle radius of the triangle formed by the the three ICRs, denoted by $\mathbf{I}_1$, $\mathbf{I}_2$, and $\mathbf{I}_3$, is calculated below; the x and y coordinates of ICR $\mathbf{I}_i$ are given by $I_{i,x}$ and $I_{i,y}$ respectively. The coordinates of the centre of the in-circle are calculated by taking the angle bisectors of two of the vertices of the triangle and calculating the point of intersection of these lines. Firstly, the gradients of the lines connecting each pair of points are computed as

$$m_{i,j} = \frac{I_{i,y} - I_{j,y}}{I_{i,x} - I_{j,x}} \tag{4.2}$$

where (i, j) is $(1, 2)$, $(1, 3)$, and $(2, 3)$. Two points that lie upon the angle bisectors of two of the vertices of the triangle, say $\mathbf{I}_1$ and $\mathbf{I}_2$, are given by

$$\mathbf{I}_{1,bi} = \mathbf{I}_1 + \mathbf{I}_1\mathbf{I}_2 \left\|\mathbf{I}_1\mathbf{I}_3\right\| + \mathbf{I}_1\mathbf{I}_3 \left\|\mathbf{I}_1\mathbf{I}_2\right\| \tag{4.3}$$

$$\mathbf{I}_{2,bi} = \mathbf{I}_2 + \mathbf{I}_2\mathbf{I}_3 \left\|\mathbf{I}_2\mathbf{I}_1\right\| + \mathbf{I}_2\mathbf{I}_1 \left\|\mathbf{I}_2\mathbf{I}_3\right\| \tag{4.4}$$

where $\mathbf{I}_i\mathbf{I}_j$ denotes the vector from $\mathbf{I}_i$ to $\mathbf{I}_j$. The gradients, $m_{1,bi}$ and $m_{2,bi}$, of the lines passing through points $\mathbf{I}_1$ and $\mathbf{I}_{1,bi}$, and $\mathbf{I}_2$ and $\mathbf{I}_{2,bi}$ are calculated using (4.2). The coordinates of the centre of the in-circle is given by the point of intersection of these two lines, calculated as

$$C_x = \frac{I_{1,y} - m_{1,bi}I_{1,x} - I_{2,y} + m_{2,bi}I_{2,x}}{m_{2,bi} - m_{1,bi}} \tag{4.5}$$

$$C_y = m_{2,bi}C_x + I_{2,y} - m_{2,bi}I_{2,x} \tag{4.6}$$

and $\mathbf{C} = (C_x, C_y)^T$. The in-circle radius, r, is then found by

$$r = \frac{\left\|\mathbf{I}_2\mathbf{C} \times \mathbf{I}_2\mathbf{I}_1\right\|}{\left\|\mathbf{I}_2\mathbf{I}_1\right\|} \tag{4.7}$$

Equations (4.2)-(4.7) are also used to compute the in-circle radius of the triangle for the case shown in Fig. 4.4 b), by replacing the set of points ($\mathbf{I}_1$, $\mathbf{I}_2$, $\mathbf{I}_3$), with ($\mathbf{I}$, $\mathbf{P}_1$, $\mathbf{P}_2$), as the vertices of the triangle in this case correspond to points $\mathbf{I}$, $\mathbf{P}_1$, and $\mathbf{P}_2$. The normalised in-circle radius, r_{norm}, is then obtained by dividing r by its maximum possible value, r_{max}. The value of r_{max} depends on the physical constraints of the ICRs and the construction lines. The maximum possible radius of the in-circle displayed in Fig. 4.4 a), that which passes through all three physical joints, denoted by $\mathbf{P}_1$, $\mathbf{P}_2$, and $\mathbf{P}_3$, is given by equation (4.8)

$$r_{a,max} = \sqrt{\frac{b^2 + c^2 - 4ad}{4a^2}} \tag{4.8}$$

where

$$a = x_1(y_2 - y_3) - y_1(x_2 - x_3) + x_2y_3 - x_3y_2,$$

$$b = (x_1^2 + y_1^2)(y_3 - y_2) + (x_2^2 + y_2^2)(y_1 - y_3) + (x_3^2 + y_3^2)(y_2 - y_1),$$

$$c = (x_1^2 + y_1^2)(x_2 - x_3) + (x_2^2 + y_2^2)(x_3 - x_1) + (x_3^2 + y_3^2)(x_1 - x_2),$$

$$d = (x_1^2 + y_1^2)(x_3y_2 - x_2y_3) + (x_2^2 + y_2^2)(x_1y_3 - x_3y_1) + (x_3^2 + y_3^2)(x_2y_1 - x_1y_2),$$

and the x and y coordinates of $\mathbf{P}_i$ are given by x_i and y_i respectively. The maximum possible radius of the in-circle displayed in Fig. 4.4 b), $r_{b,max}$, is given by half the distance between the two fixed points.

The robot manipulator is in a singularity if any of these r_{norm} values are equal to zero. In order to analyse how close the entire system is to being in a singularity, fuzzy logic is applied; such that the proximity to a singularity is given by the minimum r_{norm} value. In order for the derivative of this value to be continuous, the minimum r_{norm} is computed using the p-norm, where p is a 'large' integer, such that

$$r_{min} = \frac{1}{(\frac{1}{r_{1,norm}}^p + ... + \frac{1}{r_{n,norm}}^p)^{\frac{1}{p}}}. \tag{4.9}$$

Throughout this chapter, p is set equal to 20.

4.2.2 Singularity Avoidance

Once the kinematically redundant robot's proximity to a singularity has been computed, the next step is to determine how its links can be reconfigured such that the robot moves further away from a singularity without changing the pose of the end-effector. Since the robot's distance from a singularity is given by the minimum normalised radius of these in-circles, the robot can reliably be moved further away from a singularity by increasing the value of r_{min}.

The method of singularity avoidance for kinematically redundant planar parallel robots is performed in three steps:

1. Identify which ICRs are able to be repositioned without changing the pose of the end-effector, and determine the triangles necessary to detect all possible singularities.

2. Formulate the value of r_{min} in terms of the redundant variable.

3. Find a greater value of r_{min} by using a predictor-corrector method.

This method is demonstrated below using the mechanism displayed in Fig. 4.2. For this mechanism, the joints whose positions are constant for any given pose of the end-effector are $\mathbf{P}_1$, $\mathbf{P}_2$, $\mathbf{P}_3$, $\mathbf{P}_6$, and $\mathbf{P}_7$; which means that the constant ICR is point $\mathbf{S}$ since its position is determined by the orientation of the links that pass through points $\mathbf{P}_1$ and $\mathbf{P}_6$, and $\mathbf{P}_2$ and $\mathbf{P}_7$, respectively. The moveable joints for a given pose of the end-effector are $\mathbf{P}_4$ and $\mathbf{P}_5$. ICRs $\mathbf{Q}$, $\mathbf{R}$, and $\mathbf{T}$ are identified as the ICRs that can be repositioned; this is because $\mathbf{Q}$ is dependent on the positions of $\mathbf{P}_4$ and $\mathbf{P}_5$, and both $\mathbf{R}$ and $\mathbf{T}$ are dependent on $\mathbf{Q}$.

To complete step one,the necessary triangles for detecting all possible singularities must be identified. The robot is in a singularity when two of ICRs **R**, **S**, and **T** become coincident, or when the construction lines used to determine the position of any ICR become collinear. Following this, the in-circles of only two triangles are needed; the triangle made from **R**, **S**, and **T**, and the triangle made from $\mathbf{P}_6$, $\mathbf{P}_7$, and **Q**, called triangles 1 and 2, respectively. The in-circle of triangle 1 describes both how close the ICRs are to coinciding, and also how close any pair of construction lines are to becoming collinear for these three points. The in-circle of triangle 2 describes how close the construction lines which determine **Q** are to becoming collinear, which is the only remaining possible singularity.

The next step is to formulate the value of r_{min} in terms of the redundant variable. For this robot, the redundant variable, denoted by α, is the orientation of the ternary link $\mathbf{P}_3\mathbf{P}_4\mathbf{P}_5$ – the anticlockwise angle taken from the horizontal axis to the link that joins $\mathbf{P}_3$ and $\mathbf{P}_4$. The pose of the end-effector is given by $(\mathbf{P}_e^T, \phi)^T$, where $\mathbf{P}_e$ denotes the position of the end-effector and ϕ denotes the anticlockwise angle taken from the horizontal axis to the link joining $\mathbf{P}_6$ and $\mathbf{P}_7$.

If $\mathbf{P}_e$, ϕ, and α, are known, along with the position of the base joints $\mathbf{P}_1$, $\mathbf{P}_2$, and $\mathbf{P}_3$, then the position of every joint of the robot and also every ICR can be determined. Firstly, $\mathbf{P}_6$, $\mathbf{P}_7$, and $\mathbf{P}_4$ are calculated by

$$\mathbf{P}_j = \mathbf{P}_i + \mathbf{p}_{i,j}, \tag{4.10}$$

where $(i, j) = (e, 6)$, $(e, 7)$, and $(3, 4)$, respectively, and $\mathbf{p}_{e,6} = -d_{e,6}(cos(\phi), sin(\phi))^T$, $\mathbf{p}_{e,7} = d_{e,7}(cos(\phi), sin(\phi))^T$, and $\mathbf{p}_{3,4} = d_{3,4}(cos(\alpha), sin(\alpha))^T$.

The vector from $\mathbf{P}_3$ to $\mathbf{P}_5$, denoted by $\mathbf{p}_{3,5}$, is determined by multiplying the vector from $\mathbf{P}_3$ to $\mathbf{P}_4$, $\mathbf{p}_{3,4}$, by the bilateration matrix $\mathbf{Z}_{3,4,5}$

$$\mathbf{p}_{3,5} = \mathbf{Z}_{3,4,5}\mathbf{p}_{3,4} \tag{4.11}$$

where

$$\mathbf{Z}_{3,4,5} = \frac{1}{2s_{3,4}} \begin{bmatrix} s_{3,4} + s_{3,5} - s_{4,5} & -4A_{3,4,5} \\ 4A_{3,4,5} & s_{3,4} + s_{3,5} - s_{4,5} \end{bmatrix}$$

and

$$A_{3,4,5} = \pm\frac{1}{4}\sqrt{(s_{3,4} + s_{3,5} + s_{4,5})^2 - 2(s_{3,4}^2 + s_{3,5}^2 + s_{4,5}^2)},$$

with $s_{i,j} = d_{i,j}^2$ denoting the squared distance between the points $\mathbf{P}_i$ and $\mathbf{P}_j$ and $A_{3,4,5}$, the signed area of the triangle defined by points $\mathbf{P}_3$, $\mathbf{P}_4$ and $\mathbf{P}_5$ Rojas and Thomas (2012).

The positions of the ICRs are found by finding the points of intersection between their respective construction lines. If the lines pass through points $\mathbf{P}_i$ and $\mathbf{P}_j$, and $\mathbf{P}_k$ and $\mathbf{P}_l$, respectively, then the x and y coordinates of the ICR, $\mathbf{I}_m$, are given by

$$I_{m,x} = \frac{y_k - m_{k,l}x_k - y_i + m_{i,j}x_i}{m_{i,j} - m_{k,l}}, \tag{4.12}$$

$$I_{m,y} = m_{i,j}I_{m,x} + y_i - m_{i,j}x_i, \tag{4.13}$$

where the gradients $m_{i,j}$ and $m_{k,l}$ are obtained using equation (4.2).

The positions of ICRs $\mathbf{Q}$, $\mathbf{R}$, $\mathbf{S}$, and $\mathbf{T}$ are calculated by replacing ($\mathbf{P}_i$, $\mathbf{P}_j$, $\mathbf{P}_k$, and $\mathbf{P}_l$) with ($\mathbf{P}_4$, $\mathbf{P}_6$, $\mathbf{P}_5$, and $\mathbf{P}_7$), ($\mathbf{P}_1$, $\mathbf{P}_6$, $\mathbf{P}_3$, and $\mathbf{Q}$), ($\mathbf{P}_1$, $\mathbf{P}_6$, $\mathbf{P}_2$, and $\mathbf{P}_7$), and ($\mathbf{P}_2$, $\mathbf{P}_7$, $\mathbf{P}_3$, and $\mathbf{Q}$), respectively. The in-circle radii of triangles 1 and 2, r_1 and r_2, are then obtained in terms of the redundant parameter, α, by inputting ($\mathbf{R}$, $\mathbf{S}$, and $\mathbf{T}$) and ($\mathbf{P}_6$, $\mathbf{P}_7$, and $\mathbf{Q}$) into equations (4.2-4.7). $r_{1,norm}$ is obtained by firstly obtaining $r_{1,max}$ by inputting the coordinates of the base joints P_3, P_6, and P_7 into (4.8), as the maximum in-circle radius for any given pose of the end-effector is given by that of the circle which passes through these joints, and $r_{2,max}$ is given by half the distance between P_6 and P_7.

The initial r_{min} value is calculated, using (4.9), given the initial value of α. In order to move further away from a singularity, the value of α which gives the maximum value of r_{min} must be obtained, with the additional condition that a singularity, a point where r_{min}=0, cannot be crossed. This is accomplished by using a predictor-corrector method Gomes et al. (2009), which will be described here continuing with the same example. The first step is to differentiate both $r_{1,norm}$ and $r_{2,norm}$ with respect to α. Given an initial known value of α, r_{min} will either lie on the curve of $r_{1,norm}$ or $r_{2,norm}$. The tangent vector at the initial point, $\mathbf{x}_i$, on the curve is obtained, and a new point $\mathbf{p}_i$, the predicted point, is determined by translating along this tangent by a small amount, h, such that

$$\mathbf{p}_i = \mathbf{x}_i + h\mathbf{t}_i \tag{4.14}$$

where

$$\mathbf{t}_i = \frac{1}{\sqrt{1 + f'(\alpha_i)^2}} \begin{bmatrix} sign(f'(\alpha_i)) \\ |f'(\alpha_i)| \end{bmatrix},$$

$f(\alpha)$ denotes the function of α that provides the value of r_{min}, and $f'(\alpha)$ denotes its derivative with respect to α.

$\mathbf{t}_i$ is formulated such that the the predicted point moves higher up on the curve than the initial point. The corrector step of the algorithm then maps $\mathbf{p}_i$ back onto the curve by

repeating equation (4.15) until the difference between the α value of the current $\mathbf{p}_i$ and the previous one becomes less than a chosen threshold value.

$$\mathbf{p}_{i+1} = \mathbf{p}_i - \begin{bmatrix} f'(\alpha_i) \\ -1 \end{bmatrix} \frac{f(p_{i,\alpha}) - p_{i,r}}{f'(\alpha_i)^2 + 1} \tag{4.15}$$

where $\mathbf{p}_i$ is defined by the coordinates $(p_{i,\alpha}, p_{i,r})^T$.

r_{min} is recalculated with this new α value to see if it is still on the same curve; if not, the next predicted point is computed using the tangent of the current curve. This process is repeated until the gradient changes sign; i.e. the local maximum point on the curve has been reached.

4.3 Numerical Example

In this section, a numerical example is used to demonstrate the method detailed above, using a mechanism with the same architecture as that used above. The positions of the base joints and the joints attached to the moving platform are $\mathbf{P}_1 = (0, 0)^T$, $\mathbf{P}_2 = (4, 0)^T$, $\mathbf{P}_3 = (1, 1)^T$, $\mathbf{P}_6 = (0.75, 5)^T$, and $\mathbf{P}_7 = (2, 5.5)^T$. The dimensions of the ternary link, that formed by joints $\mathbf{P}_3$, $\mathbf{P}_4$, and $\mathbf{P}_5$, are $d_{3,4} = 2$, $d_{3,5} = 2$, and $d_{4,5} = 2$. The orientation of the ternary link is described by the angle α, which is the angle taken in the anticlockwise direction from the horizontal axis which passes through $\mathbf{P}_3$, to the vector from $\mathbf{P}_3$ to $\mathbf{P}_4$; the initial value of α is 0.3. The vector from $\mathbf{P}_3$ to $\mathbf{P}_5$ is at an angle $pi/3$ in the clockwise direction from the vector from $\mathbf{P}_3$ to $\mathbf{P}_4$.

The four ICRs are calculated using (4.2) and (4.12-4.13) as $\mathbf{Q} = (2.22, 2.67)^T$, $\mathbf{R} = (-0.07, -0.46)^T$, $\mathbf{S} = (1.17, 7.79)^T$, and $\mathbf{T} = (2.76, 3.40)^T$. The initial in-circle radii are calculated, using equations (4.2-4.7), and then are normalised to obtain values of $r_{1,norm} = 0.43$ and $r_{2,norm} = 0.78$; hence, initially, $r_{min} = 0.43$. The predictor-corrector method is then used to find the value of α that provides an improved r_{min} value, and hence gives a configuration of the mechanism that is further away from a singularity. The algorithm returns a value of $\alpha = 1.19$, corresponding to a minimum normalised radius of $r_{min} = 0.57$. Fig. 4.5 shows $r_{1,norm}$ and $r_{2,norm}$ plotted against α between 0 and 2π, along with the initial and improved values of α found by the predictor-corrector method.

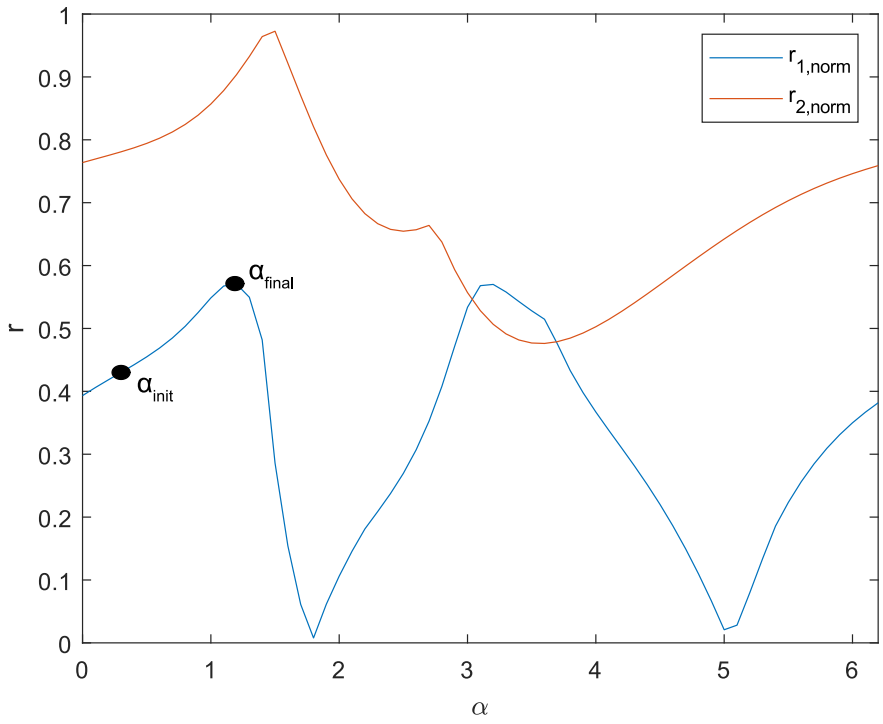

Figure 4.5: Normalised in-circle radii $r_{1,norm}$ and $r_{2,norm}$ against α for the example mechanism. The initial and final values of α are shown.

4.4 Comparison to the Jacobian

In this section, the geometric method of singularity analysis is compared with the inverse of the condition number of the Jacobian matrix. Firstly, let's consider the mechanism presented in chapter 2 in a configuration which results in its Jacobian being in a false positive singularity. Let's consider the configuration of this mechanism where the joints are positioned at $\mathbf{P}_1 = (2, 0)^T$, $\mathbf{P}_2 = (8, 0)^T$, $\mathbf{P}_3 = (6, 2)^T$, $\mathbf{P}_4 = (3.17, 4.83)^T$, $\mathbf{P}_5 = (4.96, 5.86)^T$, $\mathbf{P}_6 = (2.60, 8.79)^T$, and $\mathbf{P}_7 = (6.45, 9.58)^T$ (all values are given to two decimal places); this is shown in Fig. 4.6. If the Jacobian is calculated using equation (3.16), the inverse of its 2-norm condition number is equal to zero. The rigidity matrix of the mechanism is given by the formula in appendix B. By equating the positions of the revolute joints with those of the corresponding vertices, the rank of the rigidity matrix is computed as eleven, meaning it is of full rank. This indicates that the robot manipulator is in a non-singular configuration, meaning that the Jacobian has incorrectly determined that the mechanism is in a singularity.

The proposed method, on the other hand, is able to successfully determine that the mechanism is not in a singularity. Firstly, the positions of ICRs **Q**, **R**, **S**, and **T** are determined just as in the example given in section 4.3; here they are computed as **Q** =

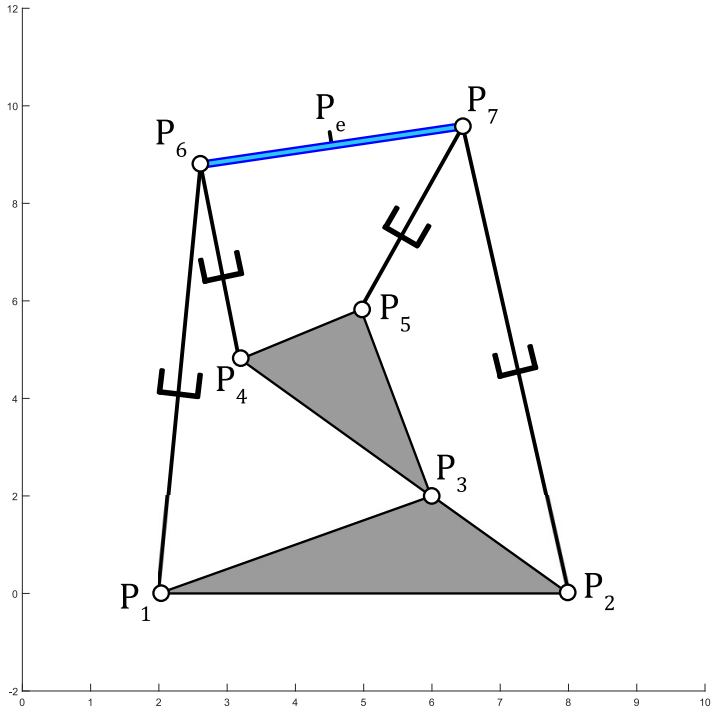

Figure 4.6: Configuration of the robot proposed in chapter 2 where the inverse of the condition number of the Jacobian is zero, but the mechanism's corresponding rigidity matrix is of full rank.

$(3.54, 2.29)^T$, $\mathbf{R} = (2.17, 2.46)^T$, $\mathbf{S} = (3.79, 26.06)^T$, and $\mathbf{T} = (7.71, 1.80)^T$. Following this, the normalised in-circle radii are calculated as $r_{1,norm} = 0.62$, and $r_{2,norm} = 0.71$, hence $r_{min} = 0.62$ which indicates the robot manipulator is not in a singularity, agreeing with the rank of the rigidity matrix.

In this second example, let's consider a different robot manipulator, the mechanism presented in section 3.2 of Schreiber and Gosselin (2018) (displayed in Fig. 4.7). The mechanism consists of a moving platform connected to two RPR legs via revolute joints, centred at B_1 and B_2, which are connected to the base via revolute joints centred at A_1 and A_2. Two other RPR legs, joined to the platform at B_3 and B_4, are joined to a common revolute joint, centred at S, which is in turn connected to the base via a revolute joint at A_1. The Jacobian, $\mathbf{J}$, of this robot manipulator is given by

$$\mathbf{J} = \begin{bmatrix} (\mathbf{b}_1 - \mathbf{a}_1)^T & (\mathbf{b}_1 - \mathbf{a}_1)^T \mathbf{E} \boldsymbol{\nu}_1 \\ (\mathbf{b}_2 - \mathbf{a}_2)^T & (\mathbf{b}_2 - \mathbf{a}_2)^T \mathbf{E} \boldsymbol{\nu}_2 \\ (\mathbf{s} - \mathbf{a}_3)^T & (\mathbf{s} - \mathbf{a}_3)^T \mathbf{E} (\mathbf{s} - \mathbf{p}) \end{bmatrix}, \tag{4.16}$$

where $\mathbf{a}_i$, $\mathbf{b}_i$, and $\mathbf{s}$, denote the position vectors of A_i, B_i, and S, respectively, $\mathbf{p}$ denotes the position vector of a chosen reference point on the platform, $\boldsymbol{\nu}_i$ denotes the vector

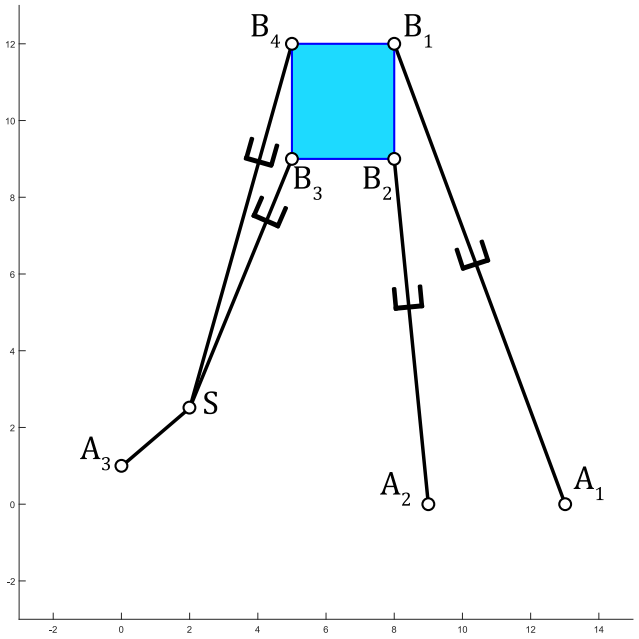

Figure 4.7: Instance of the kinematically redundant planar parallel architecture proposed in Schreiber and Gosselin (2018).

$\mathbf{b}_i - \mathbf{p}$, and

$$\mathbf{E} = \begin{bmatrix} 0 & -1 \\ 1 & 0 \end{bmatrix}.$$

It is noted by the authors that the robot manipulator is in a singularity when joint $\mathbf{S}$ lies upon the line which passes through $\mathbf{B}_3$ and $\mathbf{B}_4$. However, if the robot manipulator follows a trajectory such that $\mathbf{S}$ approaches such a position, the value of $1/k(J)$ does not approach zero, but rather it only becomes zero when $\mathbf{S}$ lies directly upon the line. An example of this is considered below.

The base joints are positioned at $\mathbf{a}_1 = (13, 0)^T$, $\mathbf{a}_2 = (9, 0)^T$, and $\mathbf{a}_3 = (0, 1)^T$. The revolute joint at $\mathbf{S}$ is positioned at $\mathbf{s} = (2, 2.5)^T$ throughout the trajectory. The platform joints are initially positioned at $\mathbf{b}_1 = (0, 12)^T$, $\mathbf{b}_2 = (0, 9)^T$, $\mathbf{b}_3 = (-3, 9)^T$, and $\mathbf{b}_4 = (-3, 12)^T$, and they follow a horizontal trajectory from left to right. Taking the coordinates of $\mathbf{b}_1$ as the reference point on the platform, $\mathbf{p}(x, y)$, the initial point of the trajectory is $x = 0$, and the final point is $x = 8$. In Fig. 4.8, both the inverse of the 2-norm condition number, $1/\kappa(J)$, and the two relevant in-circle radii are plotted throughout the trajectory; r_1 corresponds to the triangle whose vertices are positioned at the intersection points between the lines through A_1B_1, A_2B_2, and A_3S, and r_2 corresponds to the triangle whose vertices are positioned at S, B_3, and B_4. Point S lies upon the line B_3B_4 when $x = 5$. It can be seen that r_2 approaches zero as this point is neared, however $1/k(J)$ does

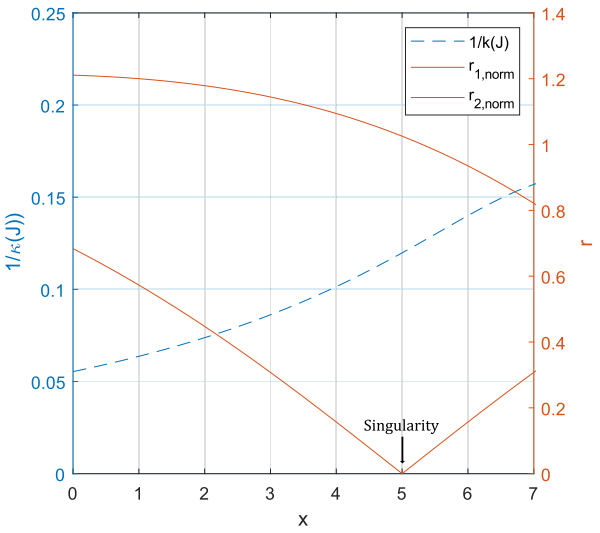

Figure 4.8: Plot of the in-circle radii and $1/k(J)$ for the mechanism presented in Schreiber and Gosselin (2018) as the mechanism passes through a singular configuration.

not approach zero. It can be verified that this configuration is singular by computing the rank of the rigidity matrix, the formula for which is given in appendix B, as the platform moves along the trajectory; the matrix is of full rank, 13, at all points except when $x = 5$, where the rank drops to 12. This demonstrates a limitation of using the Jacobian to detect a mechanism's proximity to a singularity. If the robot manipulator here follows a trajectory like the one shown in Fig. 4.8, and $1/k(J)$ is used as the index for determining the robot manipulator's proximity to a singularity, the robot manipulator would run a risk of failing near this point despite the fact that $1/k(J)$ is well above zero.

Chapter 5

A Dynamically Balanced Kinematically Redundant Planar Parallel Robot

In chapter 4, a method of singularity avoidance for kinematically redundant robots has been proposed which is more robust than conventional Jacobian-based methods. This tool provides the ability for the end-effector to move throughout the workspace without experiencing the consequences of moving into singularities, whilst the kinematically redundant parallel architecture permits high speed motions with large rotational capabilities. However, a challenge that fast moving manipulators face is that they generate large shaking forces and moments on their bases which can lead to a deterioration in the performance of the robot. A solution to eliminate these shaking forces and moments is to use dynamically balanced architectures, which are designed such that the total linear and momentum of the system is zero for any trajectory of the manipulator. Such architectures exist for non-redundant parallel mechanisms but have yet to be developed for kinematically redundant parallel robots. In this chapter, a dynamically balanced architecture of a kinematically redundant planar parallel robot is presented. The manipulator is composed of parallelogram linkages which reduces the number of counter rotary-elements required to moment balance the mechanism. The balancing conditions are derived, and the balancing parameters are optimised using Lagrange multipliers, such that the total mass and inertia of the system is minimised. The elimination of the shaking forces and moments is then verified via a simulation in the multi-body dynamic simulation software MSC Adams. The work presented in this chapter is currently under review for publication Baron et al. (2020a).

The rest of the chapter is structured as follows. In section 5.1, the methods used to

balance the mechanism are described. The architecture is introduced in section 5.2, and in 5.3 the balancing conditions are derived. The balancing parameters are optimised in section 5.4 such that the total mass and inertia added to the system is minimised. In section 5.5, a simulation is run using the multi-body dynamic simulation software MSC Adams to verify that the shaking forces and moments on the base have been eliminated; an unbalanced manipulator is also simulated to act as a point of comparison.

5.1 Balancing Methods

There are multiple methods of balancing parallel robotic mechanisms, each of which vary in terms of total mass addition to the system and complexity. Here, two methods are reviewed which are used to balance the proposed architecture. The following methods are used as they require minimal mass and inertia to be added to the system, and do not significantly complicate the design of the mechanism van der Wijk et al. (2009); van der Wijk and Herder (2009).

5.1.1 Counter-Rotary Countermasses

This method involves balancing links individually through the use of rotatable countermasses which are driven to rotate in the opposite direction to the relative rotation between the link and the previous link to which it is joined. Assuming each leg of the mechanism consists of a sequence of links joined by revolute joints, the balancing of each link is accomplished by fixing a counter mass to the other side of the revolute joint to which centre of mass (CoM) of the link is located, such that the CoM of the link and the countermass coincides with the centre of the joint. Additionally, a transmission system with a negative transmission ratio is used to drive the mass in the opposite direction to relative rotation between the link and the previous link. The moment of inertia of the countermass is determined such that the sum of the angular momentum of the link induced by its rotation relative to the previous link, and the angular momentum of the countermass are equal to zero. For example, consider a double pendulum moving in a plane balanced using this method, as shown in Fig. 5.1.

The mechanism consists of two links joined together at P_2 and link 1 is joined to the ground at P_1. The CoM of m_2 and m_3, which represent the mass of link 2 and a mass fixed to the end to the link, and the countermass, $m_{c,2}$, coincides with the centre of P_2. Similarly, the CoM of the aforementioned set of three masses, the centre of mass of m_1, the mass of link 1, and the countermass $m_{c,1}$ coincide with the centre of P_1. As the position of

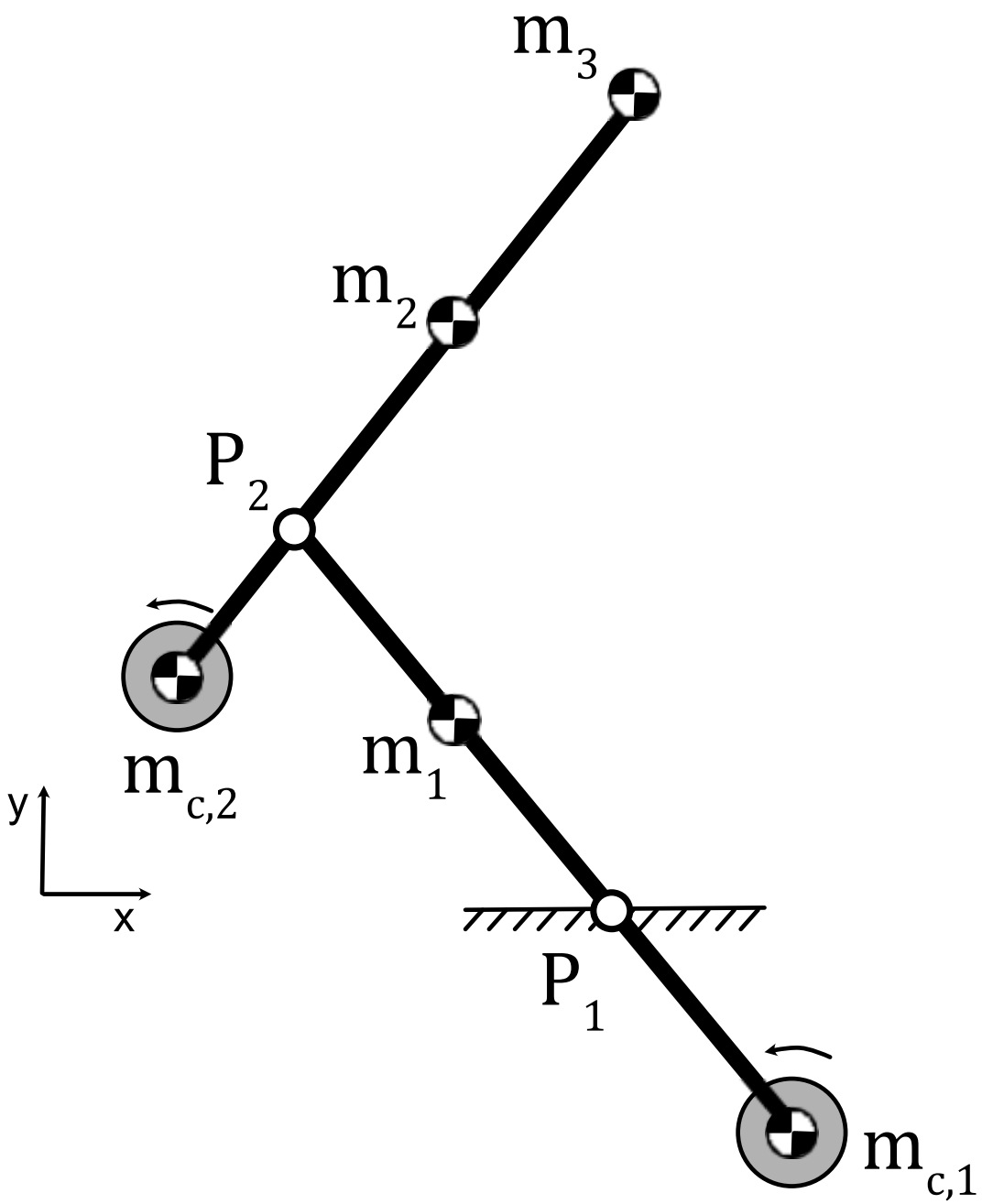

Figure 5.1: Counter-rotary countermass method used to balance a double pendulum. The countermasses are positioned such that the centre of mass of the system is constant. The countermasses are driven by negative transmission ratios such that the sum of their angular momenta and that of the rest of the system is equal to zero.

the centre of the system is constant, it is always located at the centre of P_1, the total linear momentum of the system is zero for any motion of the linkage. The linear momentum of a system of n rigid bodies can be expressed by

$$\mathbf{p} = \sum_{i=1}^{n} (m_i \dot{\mathbf{r}}_i), \tag{5.1}$$

where m_i and $\mathbf{r}_i$ denote the mass of the i^{th} body and the position of its centre of mass in the global reference frame, and dot notation is used to denote its derivative with respect to time. The total angular momentum of the system of n rigid bodies about the z-axis is computed by

$$h_z = \sum_{i=1}^{n} (I_i \dot{\theta}_i + \begin{bmatrix} 0 \\ 0 \\ 1 \end{bmatrix}^T (\mathbf{r}_i \times m_i \dot{\mathbf{r}}_i)) \tag{5.2}$$

where I_i is the moment of inertia of the i^{th} element and $\dot{\theta}_i$ is its angular velocity. By expanding this equation for all rigid bodies in the system, an expression is formed in terms of the angular velocity of each joint, and it is possible to ensure that this is equal to zero for any configuration by selecting an appropriate transmission ratio and determining the required countermass moment of inertia. The conditions for balancing a link using the counter-rotary countermass method are given in detail in section 5.3.

5.1.2 Balanced Parallelogram Legs

For parallel mechanisms with RRR type legs, that is a leg which consists of three revolute joints and where the one connected to the base is actuated, a possible method of balancing is combining pairs of legs such that they form balanced 5-bar linkages Laliberté and Gosselin (2013); van der Wijk and Herder (2009); an example is shown in Fig. 5.2. The actuated revolute joints connected to the base at P_1 and P_2 are coincident; i.e. $\mathbf{p}_1 = \mathbf{p}_2$. Two links are joined to each of the proximal links via revolute joints at P_3 and P_4, and are joined to each other via a revolute joint at P_5.

The balancing of the linear momentum of the system is performed similarly to the counter-rotary countermass method described above, except here each countermass, denoted C_i, is rigidly attached to its respective link. The masses and positions of the countermasses are set such that the centre of mass of a link, any masses joined to the end of the link, and the countermass is coincident with the revolute joint. However, the advantage of this method of balancing is that only two counter-rotary elements are required to moment balance each pair of legs; this is desirable as it reduces the complexity of the

system. This is due to the fact that opposite links in the parallelogram move with the same angular velocity as each other, and so only two counter rotary elements are required, instead of four. For example, in Fig. 5.2, the counter-rotary element CR_1 compensates the angular momentum of the links defined by P_1P_3 and P_4P_5, and their associated countermasses. Similarly, the counter-rotary element CR_2 compensates the angular momentum of the links defined by P_2P_4 and P_3P_5, and their associated countermasses. The detailed balancing conditions of the parallelogram linkage are given in section 5.3.

5.2 Architecture

In this section the architecture of the dynamically balanced parallel manipulator is presented. The architecture is based on the kinematically redundant planar parallel mechanism presented in Gosselin et al. (2015), displayed in Fig. 5.3. The former architecture, consists of a moving platform connected to the base via four $\underline{\text{P}}$RR legs, denoting an actuated prismatic joint followed by two passive revolute joints, and a redundant link (that defined by P_9P_{11}); as can been in Fig. 5.3. The four proximal joints P_i, $i = 1, .., 4$, are connected to P_j, $j = 5, ..8$, via a prismatic joint of length ρ_i which are in turn connected to each distal link via a revolute joint. The distal links connected to P_5 and P_6 are joined directly to the moving platform via a revolute joint at P_{10}, whereas those connected at P_7 and P_8 are first joined to the redundant link via a revolute joint at P_9, which is in turn connected to the moving platform via a revolute joint at P_{11}.

As stated in previous chapters, the advantage of the kinematcially redundant architecture is that the moving platform is capable of performing full rotations of the moving platform without entering singular configurations. The mechanism in Fig. 5.3 is in a singularity if two or more of the distal links in the legs become collinear, or if the links defined by $P_{10}P_{11}$ and P_9P_{11} are collinear; therefore, the robot is able to make singularity-free rotations of the moving platform as long as these conditions are not met.

In the architecture proposed here, shown in Fig. 5.4, the actuation scheme is 4-$\underline{\text{R}}$RR, denoting an actuated revolute joint followed by two passive revolute joints. The base joints at P_1 and P_2 are made to be coincident, as are those at P_3 and P_4, such that each pairing has the parallelogram structure. Each pairing of $\underline{\text{R}}$RR chains are balanced using the parallelogram method described in the previous section. Countermasses are attached to the links on each of the legs, and on the redundant link, in order to balance the linear momentum of the system. The position of the countermass attached to the link defined by joints P_i and P_j is located at C_i. C_i for which $i = 1, .., 8$ is rigidly attached to its respective

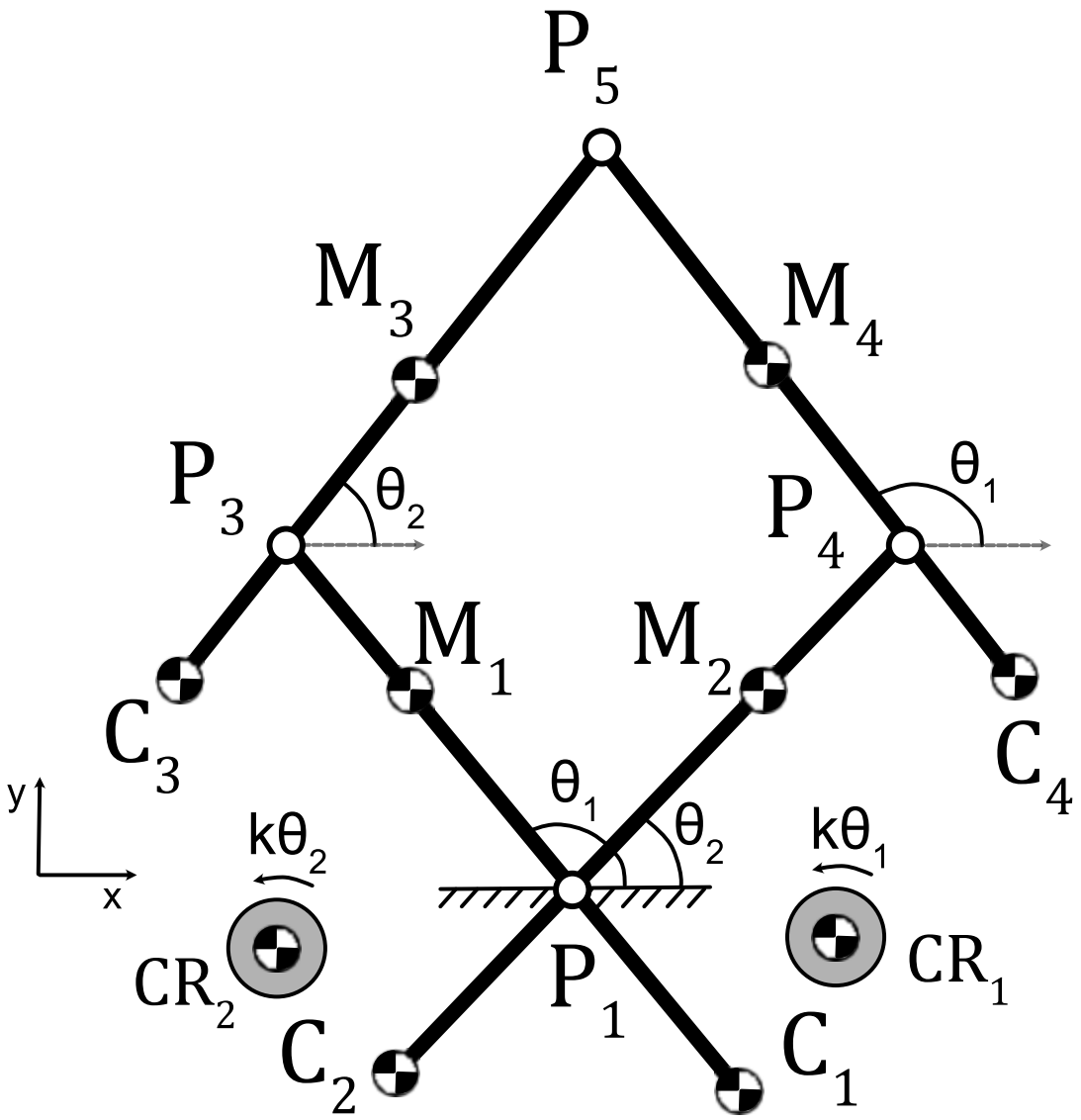

Figure 5.2: Dynamically balanced parallelogram linkage. Countermasses are rigidly attached to the links at C_i, $i = 1, .., 4$, such that the centre of mass of the linkage is constant. Two counter-rotary elements, fixed to the base at CR_1 and CR_2, are driven by the motion of the proximal links via negative transmission ratios to moment balance the linkage.

link. C_9 is attached to the redundant link, but is also driven by a transmission system which drives it to rotate with an angular velocity opposite to that of the relative rotation between the links defined by P_7P_9 and P_9P_{11}. Finally, four counter rotary elements are fixed to the base by revolute joints, at CR_i for $i = 1, .., 4$, and are driven by transmission systems such that their angular velocities are opposite to that of the four proximal links.

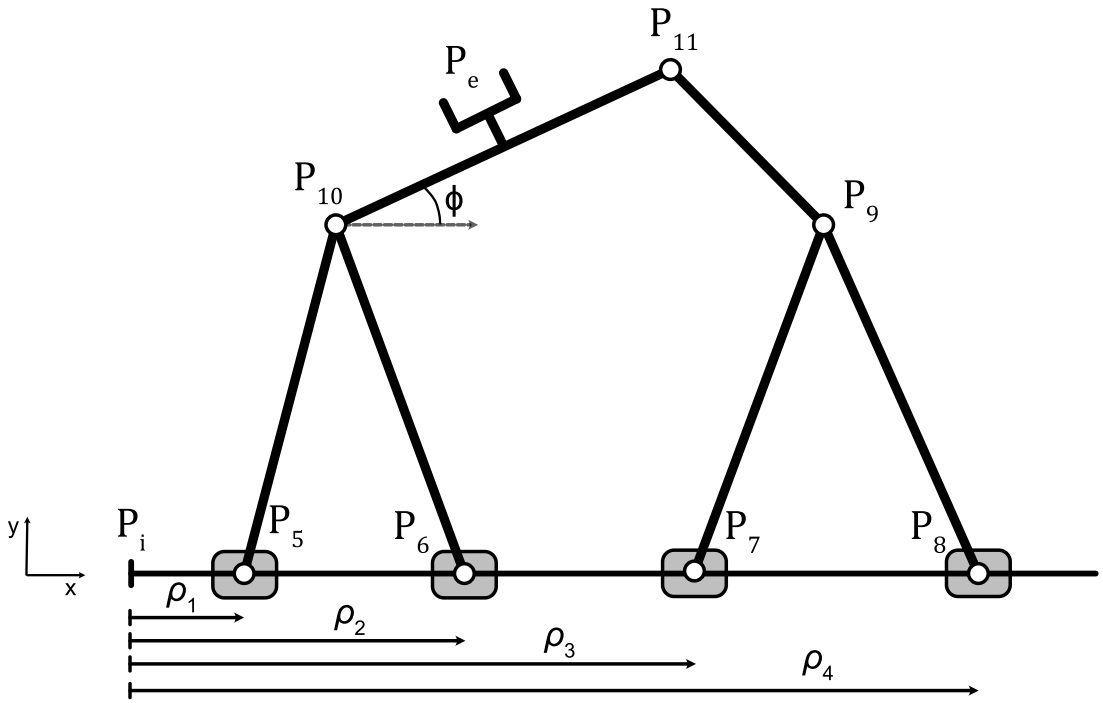

Figure 5.3: Kinematically redundant planar parallel architecture presented in Gosselin et al. (2015).

The transmission ratio and the moment of inertia of each of these counter-rotary elements are determined such that they eliminate the shaking moments transmitted to the base. The advantage of this architecture is that only five counter-rotary elements are required to moment balance the entire mechanism, four of which are joined to the base, which makes the design of the robot much more straightforward. The position of the centre of mass of the link between joints P_i and P_j is denoted by M_i.

5.3 Derivation of Balancing Conditions

In this section, the conditions required for the entire mechanism to be dynamically balanced, such that both the shaking forces and moment on the base are equal to zero, are derived. The first step that is made here is to make a dynamic equivalence between the moving platform and two individual point masses Wu and Gosselin (2007). Deriving the balancing conditions of a closed mechanism is extremely complex if it is approached by analysing the mechanism as a whole due to the kinematic coupling between the legs. A useful simplification is to treat the moving platform as individual point masses positioned at each of the joints on the platform, as shown in Fig. 5.5. The system of point masses

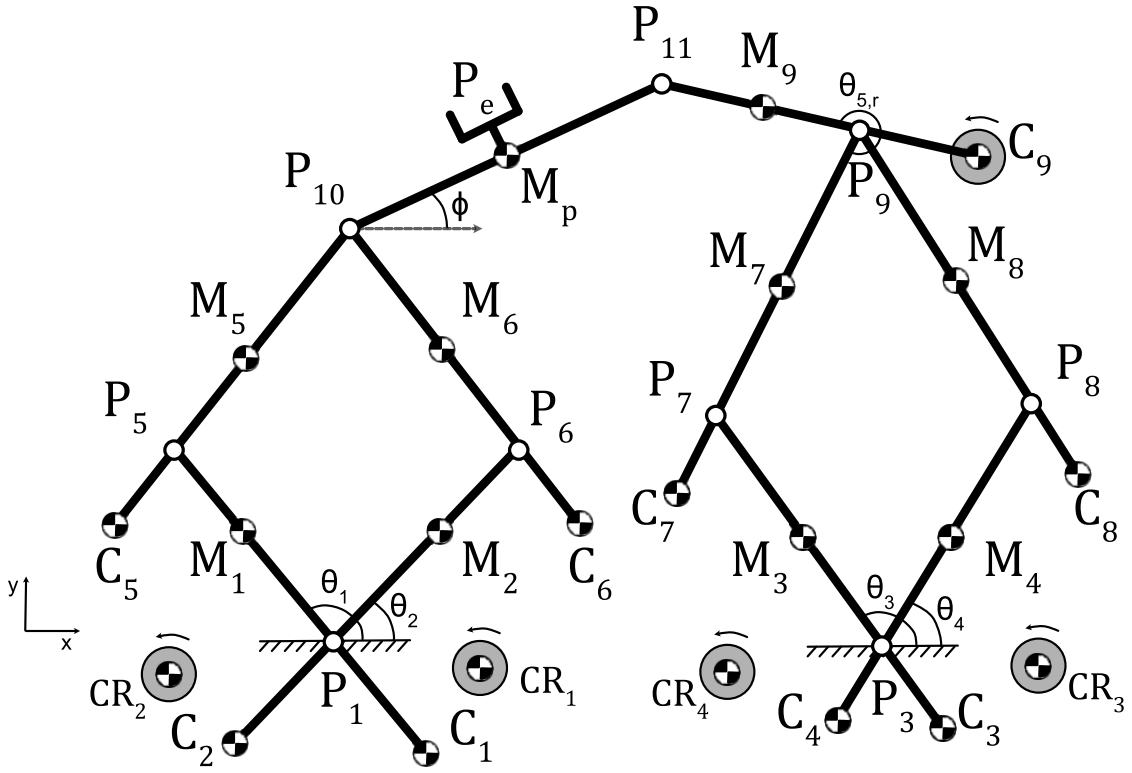

Figure 5.4: The proposed dynamically balanced kinematically redundant planar parallel architecture.

is dynamically equivalent to the moving platform if the sum of their masses are equal to the platform, if the centre of mass of the system of point masses is equal to that of the platform, and has the same inertia tensor as the platform with respect to any coordinate frame. In this case, the platform consists of revolute joints at either end, therefore it is modelled by two point masses and the above conditions are expressed by

$$m_p = m_{p,1} + m_{p,2}, \tag{5.3}$$

$$0 = m_{p,1}x_1 + m_{p,2}x_2, \tag{5.4}$$

$$m_p k_p^2 = m_{p,1}x_1^2 + m_{p,2}x_2^2, \tag{5.5}$$

where m_p, $m_{p,1}$, and $m_{p,2}$ denote the masses of the platform, and point masses 1 and 2 respectively, x_i denotes the signed distance from the centre of mass of the platform to point mass i, and k_p is the radius of gyration of the platform. The most straightforward solution is for $m_{p,1} = m_{p,2} = m_p/2$, $x_1 = -x_2$, and $k_p = x_2$.

The balancing conditions are derived separately for the two different sides of the robot which end at each of the joints on the moving platform; the first, termed the 'left hand side', consisting of the legs joined to the base at P_1 and P_2, and to the first point mass at

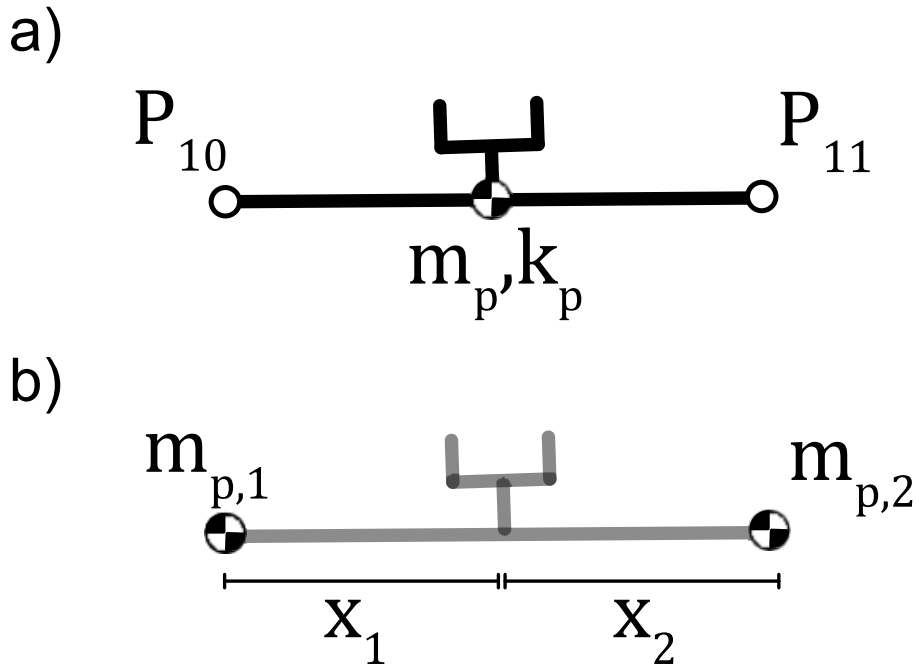

Figure 5.5: The dynamic equivalence made between the moving platform and two point masses. This equivalence holds if the point masses and the platform have the same total mass, centre of mass, and moment of inertia about any point.

P_{10}, and the second, 'the right hand side', consisting of the legs joined to the base at P_3 and P_4, to the redundant link at P_9, and to the second point mass at P_{11}. Let's consider the left hand side of the robot first, shown in Fig. 5.6. The unit vector which lies along the link between points P_i and P_j is given by $\hat{\mathbf{v}}_{i,j}$. The length of the proximal and distal links of each leg are given by l; by making the length of each link of each leg equal, the parallelogram structure of the legs is ensured and additionally the workspace of this pair of legs is maximised. The distance between the base joint $P_1 = P_2$ and the centre of mass of each proximal link is denoted by s_1. Similarly, the distance between points P_5 and P_6 and the centre of masses of the distal links to which they are attached is given by s_2.

Countermasses 1 and 2, whose positions are denoted by $\mathbf{c}_1$ and $\mathbf{c}_2$ are fixed to the proximal links, but are positioned on the other side of the revolute joint at a distance of $s_{c,1}$, such that

$$\mathbf{c}_i = \mathbf{p}_i - s_{c,1}\hat{\mathbf{v}}_{i,j} \tag{5.6}$$

for $(i, j) = (1, 5)$ and $(2, 6)$, and where $\mathbf{p}_i$ denotes the position of point P_i. Similarly, countermasses 5 and 6, whose positions are denoted by $\mathbf{c}_5$ and $\mathbf{c}_6$ are fixed to the distal links, but are positioned on the other side of the revolute joint at a distance of $s_{c,2}$, such

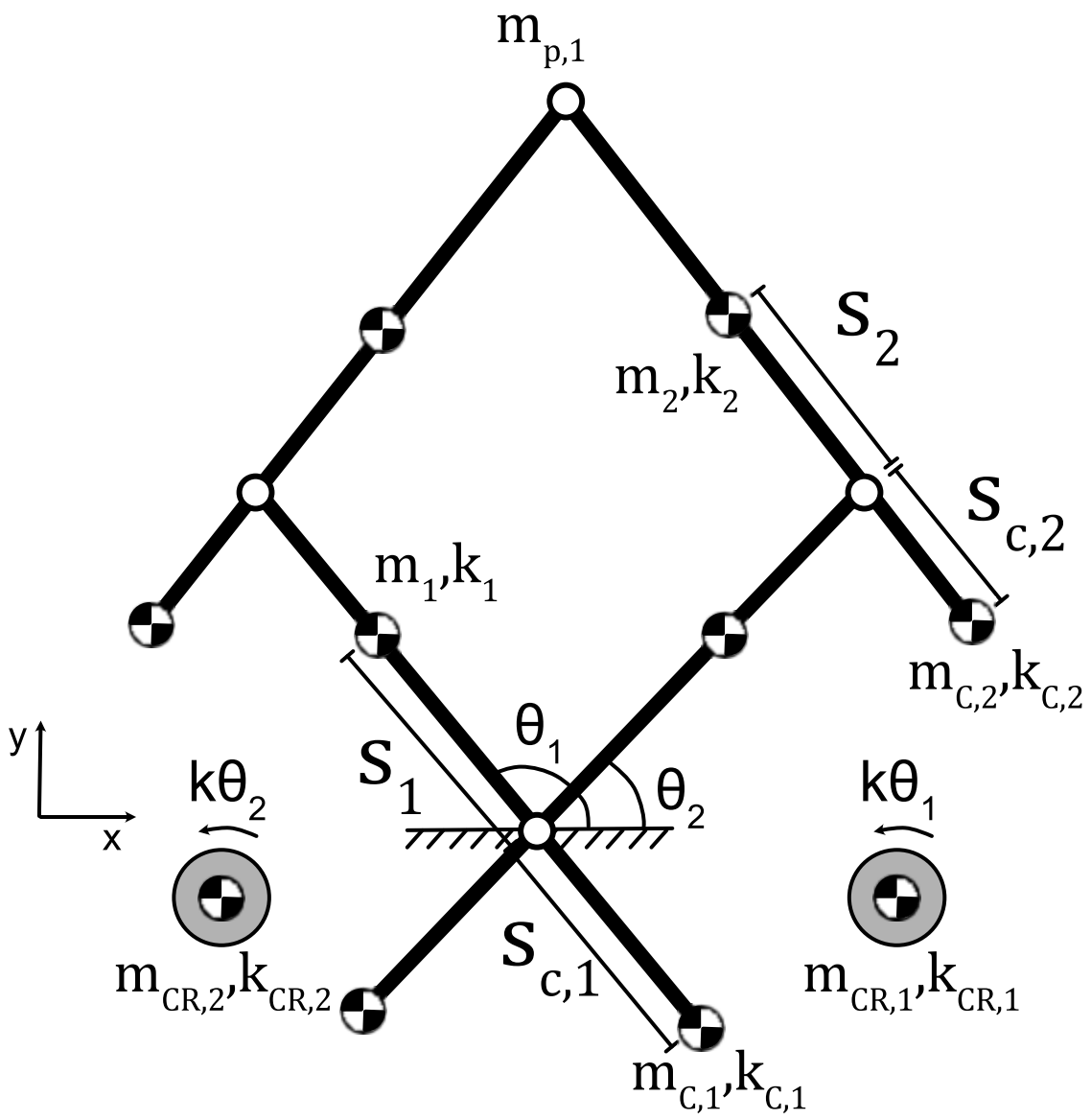

Figure 5.6: The left hand side of the manipulator, beginning at the base joint pairing of P_1 and P_2, and ends at the first point mass $m_{p,1}$, at P_{10}. Distances between CoMs and proceeding joints are labelled s_i and $s_{c,i}$, link and countermass masses are labelled m_i and $m_{c,i}$, and their respective radii of gyration k_i and $k_{c,i}$. Counter-rotary elements each have a mass of $m_{CR,i}$, radii of gyration $k_{CR,i}$, and rotate at a velocity of $k\dot{\theta}_i$, where k is a negative transmission ratio.

that

$$\mathbf{c}_i = \mathbf{p}_i - s_{c,2}\hat{\mathbf{v}}_{i,j} \tag{5.7}$$

for $(i, j) = (5, 10)$ and $(6, 10)$. Finally, the point mass is positioned at $\mathbf{p}_{10}$, and its mass is denoted by $m_{p,1}$.

The total linear momentum of the system is computed using equation (5.1). The parallelogram nature of the leg pairing allows some simplifications to be made. As the unit vectors $\hat{\mathbf{v}}_{1,5}$ and $\hat{\mathbf{v}}_{6,10}$ are always parallel, they will from herein be defined by the same unit vector, $\hat{\mathbf{v}}_1$, and their corresponding angular velocity is given by $\dot{\theta}_1$. Similarly, $\hat{\mathbf{v}}_{2,6}$ and $\hat{\mathbf{v}}_{5,10}$ from herein are defined by $\hat{\mathbf{v}}_2$ and their corresponding angular velocity is given by $\dot{\theta}_2$. Following this, the total linear of the system is given by

$$\begin{aligned}\mathbf{p}_1 = (m_1 s_1 - m_{c,1} s_{c,1})(\mathbf{E}\hat{\mathbf{v}}_1\dot{\theta}_1 + \mathbf{E}\hat{\mathbf{v}}_2\dot{\theta}_2)\\ +m_2(l\mathbf{E}\hat{\mathbf{v}}_1\dot{\theta}_1 + s_2\mathbf{E}\hat{\mathbf{v}}_2\dot{\theta}_2) + m_{c,2}(l\mathbf{E}\hat{\mathbf{v}}_1\dot{\theta}_1 - s_{c,2}\mathbf{E}\hat{\mathbf{v}}_2\dot{\theta}_2)\\ +m_2(l\mathbf{E}\hat{\mathbf{v}}_2\dot{\theta}_2 + s_2\mathbf{E}\hat{\mathbf{v}}_1\dot{\theta}_1) + m_{c,2}(l\mathbf{E}\hat{\mathbf{v}}_2\dot{\theta}_2 - s_{c,2}\mathbf{E}\hat{\mathbf{v}}_1\dot{\theta}_1)\\ +m_{p,1}(l\mathbf{E}\hat{\mathbf{v}}_1\dot{\theta}_1 + l\mathbf{E}\hat{\mathbf{v}}_2\dot{\theta}_2),\end{aligned} \tag{5.8}$$

where

$$\mathbf{E} = \begin{bmatrix} 0 & -1 \\ 1 & 0 \end{bmatrix},$$

In order for this expression to be equal to zero for any orientation or set of joint velocities, the following condition is set to zero

$$g_1 = m_1 s_1 - m_{c,1} s_{c,1} + m_2(l + s_2) + m_{c,2}(l - s_{c,2}) + m_{p,1} l = 0. \tag{5.9}$$

Now for the computation of the angular momentum of the left side of the mechanism. Firstly, the moment of inertia about the CoM of mass m_i is given by $I_i = m_i k_i^2$, and similarly that of $m_{c,i}$ and $m_{CR,i}$ are given by $I_{c,i} = m_{c,i} k_{c,i}^2$ and $I_{CR,i} = m_{CR,i} k_{CR,i}^2$, respectively. If the moment of inertia of the counter-rotary elements 1 and 2, denoted by $I_{CR,1}$ and $I_{CR,2}$, are made to be equal in order to preserve symmetry, the angular momentum is computed using equation (5.2), as

$$\begin{aligned}h_{z,1} = (I_1 + I_{c,1} + I_2 + I_{c,2} + kI_{CR,1})(\dot{\theta}_1 + \dot{\theta}_2)\\ + \begin{bmatrix} 0 \\ 0 \\ 1 \end{bmatrix}^T ((s_1\hat{\mathbf{v}}_1 \times m_1 s_1 \mathbf{E}\hat{\mathbf{v}}_1\dot{\theta}_1) + (s_1\hat{\mathbf{v}}_2 \times m_1 s_1 \mathbf{E}\hat{\mathbf{v}}_2\dot{\theta}_2)\\ +(s_{c,1}\hat{\mathbf{v}}_1 \times m_{c,1} s_{c,1} \mathbf{E}\hat{\mathbf{v}}_1\dot{\theta}_1) + (s_{c,1}\hat{\mathbf{v}}_2 \times m_{c,1} s_{c,1} \mathbf{E}\hat{\mathbf{v}}_2\dot{\theta}_2)\\ +((l\hat{\mathbf{v}}_1 + s_2\hat{\mathbf{v}}_2) \times m_2(l\mathbf{E}\hat{\mathbf{v}}_1\dot{\theta}_1 + s_2\mathbf{E}\hat{\mathbf{v}}_2\dot{\theta}_2))\\ +((l\hat{\mathbf{v}}_2 + s_2\hat{\mathbf{v}}_1) \times m_2(l\mathbf{E}\hat{\mathbf{v}}_2\dot{\theta}_2 + s_2\mathbf{E}\hat{\mathbf{v}}_1\dot{\theta}_1))\\ +((l\hat{\mathbf{v}}_1 - s_{c,2}\hat{\mathbf{v}}_2) \times m_{c,2}(l\mathbf{E}\hat{\mathbf{v}}_1\dot{\theta}_1 - s_{c,2}\mathbf{E}\hat{\mathbf{v}}_2\dot{\theta}_2))\\ +((l\hat{\mathbf{v}}_2 - s_{c,2}\hat{\mathbf{v}}_1) \times m_{c,2}(l\mathbf{E}\hat{\mathbf{v}}_2\dot{\theta}_2 - s_{c,2}\mathbf{E}\hat{\mathbf{v}}_1\dot{\theta}_1))\\ +((l\hat{\mathbf{v}}_1 + l\hat{\mathbf{v}}_2) \times m_{p,1}(l\mathbf{E}\hat{\mathbf{v}}_1\dot{\theta}_1 + l\mathbf{E}\hat{\mathbf{v}}_2\dot{\theta}_2))),\end{aligned} \tag{5.10}$$

where k is the negative transmission ratio used to drive the counter-rotary elements (this should not be confused with the radius of gyration of the counter-rotary element).

After expanding this expression, and collecting coefficients in $\dot{\theta}_1$, $\dot{\theta}_2$, and $\cos(\theta_1 - \theta_2)(\dot{\theta}_1 + \dot{\theta}_2)$, the following conditions for total angular momentum being equal to zero are formed

$$\begin{aligned} g_2 = m_1 s_1^2 + m_{c,1} s_{c,1}^2 + m_2(l^2 + s_2^2) + m_{c,2}(l^2 + s_{c,2}^2) \\ + m_{p,1} l^2 + I_1 + I_{c,1} + I_2 + I_{c,2} + k I_{CR,1} = 0, \end{aligned} \tag{5.11}$$

$$g_3 = 2m_2 l s_2 - 2m_{c,2} l s_{c,2} + m_{p,1} l^2 = 0. \tag{5.12}$$

As long as g_1, g_2, and g_3 are equal to zero, the total linear and angular momenta of the left side of the mechanism will be zero for any trajectory.

Now the balancing conditions of the right hand side of the mechanism are considered, which is depicted in Fig. 5.7. As before, the parallelogram nature of the pair of legs allows some simplifications to be made. The unit vectors from P_3 to P_7 and from P_8 to P_9, denoted by $\hat{\mathbf{v}}_{3,7}$ and $\hat{\mathbf{v}}_{8,9}$, are parallel and hence are both replaced by the same unit vector, $\hat{\mathbf{v}}_3$, and the angular velocities of the corresponding links are both $\dot{\theta}_3$. Similarly, $\hat{\mathbf{v}}_{4,8}$ and $\hat{\mathbf{v}}_{7,9}$ are replaced with $\hat{\mathbf{v}}_4$, and the angular velocity of their corresponding links is $\dot{\theta}_4$. The mass of the proximal links and their countermasses are denoted by m_3 and $m_{c,3}$, respectively, and they are positioned at distances of s_3 and $s_{c,3}$ away from their respective base joints P_3 and P_4. The mass of the distal links and their countermasses are denoted by m_4 and $m_{c,4}$, respectively, and they are positioned at distances of s_4 and $s_{c,4}$ away from their respective distal joints P_7 and P_8.

The unit vector from P_9 to P_{11}, which defines the orientation of the redundant link, is denoted by $\hat{\mathbf{v}}_5$, and its angular velocity is denoted by $\dot{\theta}_5$. The distance between P_9 and P_{11} is denoted by b. The mass of the redundant link and its countermass are m_5 and $m_{c,5}$, respectively, and they are positioned at distances of s_5 and $s_{c,5}$ away from P_9. Unlike the other moving countermasses, the countermass of the redundant link also acts as a counter-rotary element which balances the inertial effects of the relative rotation between it and the leg to which it is fixed. The transmission mechanism drives the countermass with a negative transmission ratio, k, in the opposite direction to the relative angular velocity between the link defined by P_7 and P_9, and the redundant link, denoted by $\dot{\theta}_{5,r} = \dot{\theta}_5 - \dot{\theta}_4$.

The total linear momentum of the second side of the robot is computed, using equa-

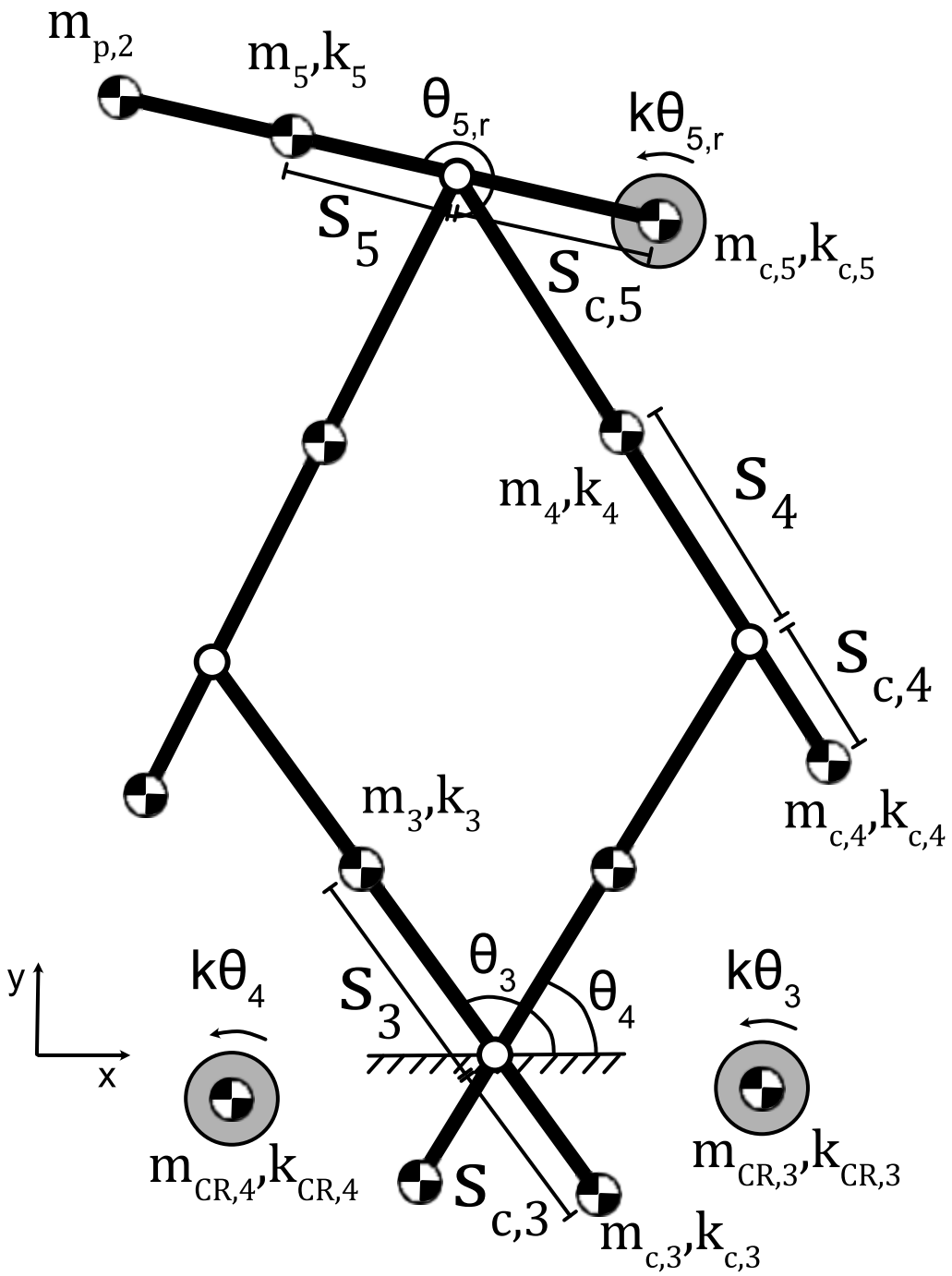

Figure 5.7: The right hand side of the manipulator, beginning at the base joint pairing of P_3 and P_4, and ends at the second point mass $m_{p,2}$, at P_{11}. The distances, masses, and radii of gyration are labelled in the same manner as the left hand side of the robot. The counter-rotary counter mass attached to the redundant link is driven by relative rotation between link P_7P_9 and P_9P_{11}, denoted by $\theta_{5,r}$.

tion (5.1), as

$$\begin{aligned}\mathbf{p}_2 = (m_3 s_3 - m_{c,3} s_{c,3})(\mathbf{E}\hat{\mathbf{v}}_3\dot{\theta}_3 + \mathbf{E}\hat{\mathbf{v}}_4\dot{\theta}_4)\\ +m_4(l\mathbf{E}\hat{\mathbf{v}}_3\dot{\theta}_3 + s_4\mathbf{E}\hat{\mathbf{v}}_4\dot{\theta}_4) + m_{c,4}(l\mathbf{E}\hat{\mathbf{v}}_3\dot{\theta}_3 - s_{c,4}\mathbf{E}\hat{\mathbf{v}}_4\dot{\theta}_4)\\ +m_4(l\mathbf{E}\hat{\mathbf{v}}_4\dot{\theta}_4 + s_4\mathbf{E}\hat{\mathbf{v}}_3\dot{\theta}_3) + m_{c,4}(l\mathbf{E}\hat{\mathbf{v}}_4\dot{\theta}_4 - s_{c,4}\mathbf{E}\hat{\mathbf{v}}_3\dot{\theta}_3)\\ +m_5(l\mathbf{E}\hat{\mathbf{v}}_3\dot{\theta}_3 + l\mathbf{E}\hat{\mathbf{v}}_4\dot{\theta}_4 + s_5\mathbf{E}\hat{\mathbf{v}}_5\dot{\theta}_5)\\ +m_{c,5}(l\mathbf{E}\hat{\mathbf{v}}_3\dot{\theta}_3 + l\mathbf{E}\hat{\mathbf{v}}_4\dot{\theta}_4 - s_{c,5}\mathbf{E}\hat{\mathbf{v}}_5\dot{\theta}_5)\\ +m_{p,2}(l\mathbf{E}\hat{\mathbf{v}}_3\dot{\theta}_3 + l\mathbf{E}\hat{\mathbf{v}}_4\dot{\theta}_4 + b\mathbf{E}\hat{\mathbf{v}}_5\dot{\theta}_5),\end{aligned} \tag{5.13}$$

where $m_{p,2}$ is the second point mass on the moving platform, positioned at P_{11}, and θ_5 is the angle between the redundant link and the horizontal axis. The conditions for the linear momentum to equal zero regardless of orientation or joint velocities are

$$\begin{aligned}g_4 = m_3 s_3 - m_{c,3} s_{c,3} + m_4(l + s_4) + m_{c,4}(l - s_{c,4}) \\ + l(m_5 + m_{c,5} + m_{p,2}) = 0,\end{aligned} \tag{5.14}$$

$$g_5 = m_5 s_5 - m_{c,5} s_{c,5} + m_{p,2} b = 0. \tag{5.15}$$

The angular momentum is computed using equation (5.2) as

$$\begin{aligned}h_{z,2} = (I_3 + I_{c,3} + I_4 + I_{c,4})(\dot{\theta}_3 + \dot{\theta}_4) + I_5\dot{\theta}_5 + I_{c,5}(\dot{\theta}_4\\ +(1+k)\dot{\theta}_{5,r}) + \begin{bmatrix}0\\0\\1\end{bmatrix}^T((s_3\hat{\mathbf{v}}_3 \times m_3 s_3 \mathbf{E}\hat{\mathbf{v}}_3\dot{\theta}_3)+\\ (s_3\hat{\mathbf{v}}_4 \times m_3 s_3 \mathbf{E}\hat{\mathbf{v}}_4\dot{\theta}_4)\\ +(s_{c,3}\hat{\mathbf{v}}_3 \times m_{c,3} s_{c,3} \mathbf{E}\hat{\mathbf{v}}_3\dot{\theta}_3) + (s_{c,3}\hat{\mathbf{v}}_4 \times m_{c,3} s_{c,3} \mathbf{E}\hat{\mathbf{v}}_4\dot{\theta}_4)\\ +((l\hat{\mathbf{v}}_3 + s_4\hat{\mathbf{v}}_4) \times m_4(l\mathbf{E}\hat{\mathbf{v}}_3\dot{\theta}_3 + s_4\mathbf{E}\hat{\mathbf{v}}_4\dot{\theta}_4))\\ +((l\hat{\mathbf{v}}_4 + s_4\hat{\mathbf{v}}_3) \times m_4(l\mathbf{E}\hat{\mathbf{v}}_4\dot{\theta}_4 + s_4\mathbf{E}\hat{\mathbf{v}}_3\dot{\theta}_3))\\ +((l\hat{\mathbf{v}}_3 - s_{c,4}\hat{\mathbf{v}}_4) \times m_{c,4}(l\mathbf{E}\hat{\mathbf{v}}_3\dot{\theta}_3 - s_{c,4}\mathbf{E}\hat{\mathbf{v}}_4\dot{\theta}_4))\\ +((l\hat{\mathbf{v}}_4 - s_{c,4}\hat{\mathbf{v}}_3) \times m_{c,4}(l\mathbf{E}\hat{\mathbf{v}}_4\dot{\theta}_4 - s_{c,4}\mathbf{E}\hat{\mathbf{v}}_3\dot{\theta}_3))\\ +((l\hat{\mathbf{v}}_3 + l\hat{\mathbf{v}}_4 + s_5\hat{\mathbf{v}}_5) \times m_5(l\mathbf{E}\hat{\mathbf{v}}_3\dot{\theta}_3 + l\mathbf{E}\hat{\mathbf{v}}_4\dot{\theta}_4\\ +s_5\mathbf{E}\hat{\mathbf{v}}_5(\dot{\theta}_4 + \dot{\theta}_{5,r}))) + ((l\hat{\mathbf{v}}_3 + l\hat{\mathbf{v}}_4 - s_{c,5}\hat{\mathbf{v}}_5) \times m_{c,5}(l\mathbf{E}\hat{\mathbf{v}}_3\dot{\theta}_3\\ +l\mathbf{E}\hat{\mathbf{v}}_4\dot{\theta}_4 - s_{c,5}\mathbf{E}\hat{\mathbf{v}}_5(\dot{\theta}_4 + \dot{\theta}_{5,r}))) + ((l\hat{\mathbf{v}}_3 + l\hat{\mathbf{v}}_4\\ +b\hat{\mathbf{v}}_5) \times m_{p,2}(l\mathbf{E}\hat{\mathbf{v}}_3\dot{\theta}_3 + l\mathbf{E}\hat{\mathbf{v}}_4\dot{\theta}_4 + b\mathbf{E}\hat{\mathbf{v}}_5(\dot{\theta}_4 + \dot{\theta}_{5,r})))).\end{aligned} \tag{5.16}$$

After expanding this expression in $\dot{\theta}_3$, $\dot{\theta}_4$, $\dot{\theta}_{5,r}$, $\cos(\theta_4 - \theta_3)(\dot{\theta}_3 + \dot{\theta}_4)$, $\cos(\theta_3 - \theta_{5,r} + \theta_4)(\dot{\theta}_3 +$

$\dot{\theta}_4 + \dot{\theta}_{5,r})$, and $\cos(\theta_{5,r})(2\dot{\theta}_4 + \dot{\theta}_{5,r})$, the following constraints are formed,

$$\begin{aligned}
g_6 &= m_3 s_3^2 + m_{c,3} s_{c,3}^2 + m_4(l^2 + s_4^2) + m_{c,4}(l^2 + s_{c,4}^2) \\
&\quad + l^2(m_5 + m_{c,5} + m_{p,2}) + I_3 + I_{c,3} + I_4 + I_{c,4} + kI_{CR,3} = 0, \\
g_7 &= m_3 s_3^2 + m_{c,3} s_{c,3}^2 + m_4(l^2 + s_4^2) + m_{c,4}(l^2 + s_{c,4}^2) \\
&\quad + m_5(l^2 + s_5^2) + m_{c,5}(l^2 + s_{c,5}^2) + m_{p,2}(l^2 + b^2) \\
&\quad + I_3 + I_{c,3} + I_4 + I_{c,4} + I_5 + I_{c,5} + kI_{CR,4} = 0, \\
g_8 &= m_5 l s_4 - m_{c,5} l s_{c,5} + m_{p,2} lb = 0 \\
g_9 &= I_5 + (1 + k)Ic, 5 + m_5 s_5^2 m_{c,5} s_{c,5}^2 + m_{p,2} b^2 = 0.
\end{aligned} \tag{5.17}$$

As long as g_i, $i = 4, .., 9$, are equal to zero, the total linear and angular momenta of the right hand side of the mechanism are nullified for any trajectory.

5.4 Mass and Inertia Optimisation

Now that the kinematic and inertial constraints for the mechanism to be dynamically balanced have been identified; the next step is to find the optimum set of balancing parameters such that the minimum amount of mass and inertia is added to the system. One of the key challenges in dynamically balancing robot manipulators is the addition of mass and inertia to the system, meaning that the actuators have to do more work. In this section, the total mass and inertia of added to the system during balancing is minimised through the use of Lagrange multipliers.

Firstly, the objective function to be minimised is composed in terms of the total mass and inertia of the system. The total mass is simply the sum of the mass of all elements in the system. The inertia is less straightforward to quantify as it is dependent on the configuration of the mechanism; here, the concept of reduced inertia is used van der Wijk et al. (2009); Laliberté and Gosselin (2013). The reduced inertia describes the inertia experienced by an actuator when all the other actuators in the mechanism are fixed. As the reduced inertia for some of the actuated joints in the mechanism is dependent on the configuration of the rest of the leg, the reduced inertia is calculated for the case where the leg is in full extension, as this is the 'worst case' scenario in terms of inertia felt by the joint. The reduced inertia, $I_{R,i}$, experienced by the i^{th} actuator of the mechanism when the other actuators' velocities are equal to zero, can be obtained from the kinetic energy expression,

$$T_{R,i} = \frac{1}{2} I_{R,i} \dot{\theta}_i^2. \tag{5.18}$$

The optimisation is carried out for each side of the mechanism separately. For the left hand side of the mechanism, the objective function to be minimised is given by

$$f_1 = \sum_i (2(m_i + m_{c,i}) + m_{CR,i}) + m_{p,1} + \sum_i I_{R,i}, \tag{5.19}$$

where $i = 1, 2$, and $I_{R,i}$ denotes the i^{th} reduced inertia of the balanced mechanism and is computed as

$$\begin{aligned} I_{R,i} = m_1 s_1^2 + m_{c,1} s_{c,1}^2 + m_2(l^2 + s_2^2) + m_{c,2}(l^2 + s_{c,2}^2) \\ + m_{p,1} l^2 + I_1 + I_{c,1} + I_2 + I_{c,2} + k^2 I_{CR,i}. \end{aligned} \tag{5.20}$$

The Lagrangian is then composed of the objective function, the dynamic constraints, g_j, and their respective Lagrange multipliers, λ_j, where $j = 1, 2, 3$, and is written as

$$\mathcal{L}_1(\mathbf{v}_1) = f_1 - \sum_j \lambda_j g_j, \tag{5.21}$$

where $\mathbf{v}_1 = [m_{c,i}, s_{c,i}, m_{CR,i}, \lambda_j]^T$ for i=1,2, and j=1,2,3, is the vector of balancing parameters and Lagrange multipliers to be optimised. The radii of gyration of the countermasses and the counter-rotary elements have not been included in this vector as the optimisation of these values is straightforward; the radii of gyration of the countermasses should be as small as possible and that of the counter-rotary elements should be as large as possible. The aim is to find the set of negative values for the Lagrange multipliers, such that each element of the partial derivative of the Lagrangian is equal to zero,

$$\frac{\partial \mathcal{L}_1}{\partial \mathbf{v}_1} = \begin{bmatrix} \lambda_1 s_{c,1} - \lambda_2(k_{c,1}^2 + s_{c,1}^2) + 2k_{c,1}^2 + 2s_{c,1}^2 + 2 \\ 2k_{c,2}^2 - \lambda_2\sigma_1 - \lambda_1\sigma_2 + 2l^2 + 2s_{c,2}^2 + l\lambda_3 s_{c,2} + 2 \\ 2k^2 k_{c,r}^2 + \lambda_2 k k_{c,r}^2 + 2 \\ m_{c,1}(\lambda_1 + 4s_{c,1} - 2\lambda_2 s_{c,1}) \\ m_{c,2}(\lambda_1 + 4s_{c,2} + l\lambda_3 - 2\lambda_2 s_{c,2}) \\ \sigma_3 - l m_{c,2} - l m_{p,1} - m_1 s_1 - m_2 s_2 - l m_2 \\ \sigma_4 - l^2 m_2 - l^2 m_{c,2} - l^2 m_{p,1} + \sigma_5 \\ -(l(2l m_{p,1} + 4m_2 s_2 - 4m_{c,2} s_{c,2}))/2 \end{bmatrix} = \mathbf{0} \tag{5.22}$$

where

$$\begin{aligned} \sigma_1 &= k_{c,2}^2 + l^2 + s_{c,2}^2, \\ \sigma_2 &= (l - s_{c,2}), \\ \sigma_3 &= m_{c,1} s_{c,1} + m_{c,2} s_{c,2}, \\ \sigma_4 &= k k_{CR}^2 m_{CR} - k_2^2 m_2 - k_{c,1}^2 m_{c,1} - k_{c,2}^2 m_{c,2}, \\ \sigma_5 &= -m_{c,1} s_{c,1}^2 - m_{c,2} s_{c,2}^2 - k_1^2 m_1 - m_1 s_1^2 - m_2 s_2^2. \end{aligned}$$

If (5.22) is satisfied, then it is ensured, for the left hand side of the mechanism, that the balancing conditions are met such that the mass and inertia added to the system is minimised.

For the right side of the mechanism, the reduced inertias, $I_{R,3}$, $I_{R,4}$, and $I_{R,5}$ are computed for the linkage when $\dot{\theta}_4 = \dot{\theta}_{5,r} = 0$, $\dot{\theta}_3 = \dot{\theta}_{5,r} = 0$, and $\dot{\theta}_3 = \dot{\theta}_4 = 0$, respectively.

$$\begin{aligned} I_{R,i} = m_3 s_3^2 + m_{c,3} s_{c,3}^2 + m_4 (l + s_4)^2 + m_4 s_4^2 + m_{c,4} (l - s_{c,4})^2 \\ + m_{c,4} s_{c,4}^2 + m_5 (2l + s_5)^2 + m_{c,5} (2l - s_{c,5})^2 \\ + m_{p,2} (2l + b)^2 + I_3 + I_{c,3} + 2(I_4 + I_{c,4}) + I_5 + I_{c,5} + k^2 I_{CR,i} \end{aligned} \tag{5.23}$$

for $i = 3, 4$, and

$$I_{R,5} = I_5 + (1 + k)^2 I_{c,5} + m_5 s_5^2 + m_{c,5} s_{c,5}^2 + m_{p,2} b^2. \tag{5.24}$$

It should be noted that the reduced inertia $I_{R,5}$, in contrast to the definition given earlier, is not the experienced inertia felt by an actuated joint, however the concept still holds because it describes the contributed inertia due to the angular velocity $\dot{\theta}_{5,r}$.

The objective function is then formed, like for the left hand side, as the combination of the total mass and reduced inertia of the system, as

$$\begin{aligned} f_2 = \sum_{i=3}^{4} (2(m_i + m_{c,i}) + m_{CR,i}) + m_5 + m_{c,5} \\ + m_{p,2} + \sum_{j=3}^{5} I_{R,j}. \end{aligned} \tag{5.25}$$

The Lagrangian is then formed as

$$\mathcal{L}_2(\mathbf{v}_2) = f_2 - \sum_h \lambda_h g_h, \tag{5.26}$$

where $\mathbf{v}_2 = [m_{c,i}, m_{CR,j}, s_{c,i}, \lambda_h]^T$, and $i = 3, 4, 5$, $j = 3, 4$, $h = 4, .., 9$. The radii of gyration of the countermasses and counter-rotary elements have not been included for the

same reasons given before. The derivative of the Lagrangian is computed as

$$\frac{\partial \mathcal{L}_2}{\partial \mathbf{v}_2} = \begin{bmatrix} \lambda_1 s_{c,3} - \lambda_3\sigma_6 - \lambda_4\sigma_6 + 2k_{c,3}^2 + 2s_{c,3}^2 + 2 \\ \sigma_9 - \lambda_3\sigma_7 - \lambda_4\sigma_7 - \lambda_1\sigma_8 + 2\sigma_8^2 \\ \sigma_{10} + \sigma_{11} + s_{c,5}^2 - \lambda_6((1-k)k_{c,5}^2 + s_{c,5}^2) + 1 \\ k^2k_{CR}^2 + \lambda_3 k k_{CR}^2 + 1 \\ k^2k_{CR}^2 + \lambda_4 k k_{CR}^2 + 1 \\ m_{c,3}(\lambda_1 + 4s_{c,3} - 2\lambda_3 s_{c,3} - 2\lambda_4 s_{c,3}) \\ -m_{c,4}(4l - \lambda_1 - 8s_{c,4} - 2l\lambda_5 + 2\lambda_3 s_{c,4} + 2\lambda_4 s_{c,4}) \\ -m_{c,5}(8l - \lambda_2 - 6s_{c,5} + 2\lambda_4 s_{c,5} + 2\lambda_6 s_{c,5}) \\ \sigma_{12} - lm_{p,2} - m_3 s_3 - m_4 s_4 - lm_4 + m_{c,4}s_{c,4} \\ m_{c,5}s_{c,5} - m_5 s_5 - bm_{p,2} \\ \sigma_{13} + \sigma_{14} - m_{c,3}s_{c,3}^2 - m_{c,4}s_{c,4}^2 - k_3^2 m_3 \\ \sigma_{15} + \sigma_{16} + \sigma_{17} + \sigma_{18} \\ -l\sigma_{19}/2 \\ \sigma_{20} - m_5 s_5^2 - m_{c,5}s_{c,5}^2 - b^2 m_{p,2} \end{bmatrix} = \mathbf{0}, \tag{5.27}$$

where

$$\begin{aligned}
\sigma_6 &= k_{c,3}^2 + s_{c,3}^2, \\
\sigma_7 &= k_{c,4}^2 + l^2 + s_{c,4}^2, \\
\sigma_8 &= l - s_{c,4}, \\
\sigma_9 &= 4k_{c,4}^2 + 2s_{c,4}^2 + 2l\lambda_5 s_{c,4} + 2, \\
\sigma_{10} &= \lambda_2 s_{c,5} - l\lambda_1 + k_{c,5}^2(k-1)^2 + 2(2l - s_{c,5})^2, \\
\sigma_{11} &= -\lambda_4(k_{c,5}^2 + l^2 + s_{c,5}^2) - l^2\lambda_3 - l^2\lambda_5 + 2k_{c,5}^2, \\
\sigma_{12} &= m_{c,3}s_{c,3} - lm_5 - lm_{c,4} - lm_{c,5}, \\
\sigma_{13} &= kk_{CR}^2 m_{CR,3} - k_4^2 m_4 - k_{c,3}^2 m_{c,3} - k_{c,4}^2 m_{c,4}, \\
\sigma_{14} &= -l^2 m_4 - l^2 m_5 - l^2 m_{c,4} - l^2 m_{c,5} - l^2 m_{p,2} - m_3 s_3^2 - m_4 s_4^2, \\
\sigma_{15} &= kk_{CR}^2 m_{CR,4} - k_3^2 m_3 - k_4^2 m_4, \\
\sigma_{16} &= -k_5^2 m_5 - k_{c,3}^2 m_{c,3} - k_{c,4}^2 m_{c,4} - k_{c,5}^2 m_{c,5} - l^2 m_4 - l^2 m_5, \\
\sigma_{17} &= -l^2 m_{c,4} - l^2 m_{c,5} - l^2 m_{p,2} - m_3 s_3^2 - m_4 s_4^2 - m_5 s_5^2, \\
\sigma_{18} &= -m_{c,3}s_{c,3}^2 - m_{c,4}s_{c,4}^2 - m_{c,5}s_{c,5}^2 - b^2 m_{p,2}, \\
\sigma_{19} &= 2lm_5 + 2lm_{c,5} + 2lm_{p,2} + 4m_4 s_4 - 4m_{c,4}s_{c,4}, \\
\sigma_{20} &= -m_5 k_5^2 + m_{c,5}(k-1)k_{c,5}^2.
\end{aligned}$$

The analytical solutions for each of the balancing parameters are not given here for the

sake of brevity. Instead, let's consider an example mechanism, and obtain the optimum set of balancing parameters in order to dynamically balance the robot with minimal added mass and inertia.

Consider the mechanism with the following kinematic and inertial parameters: $l = 0.4$, $b = 0.4$, $s_i = 0.075$, $m_1 = 0.6$, $m_2 = 0.2$, $m_3 = 0.6$, $m_4 = 0.2$, $m_5 = 0.1$, $m_{p,1} = m_{p,2} = 0.05$, $k = 16$, $k_i = 0.1$, $k_{c,i} = 0.1$, and $k_{CR,j} = 0.2$, for $i = 1, .., 5$, and $j = 1, ..4$. All distances and masses are given in m and kg, respectively. Firstly, equation (5.22) is solved to obtain values of $m_{c,1} = 0.59$, $m_{c,2} = 0.038$, $m_{CR} = 0.19$, $s_{c,1} = 0.25$, $s_{c,2} = 0.65$, $\lambda_1 = -18.77$, $\lambda_2 = -35.13$, and $\lambda_3 = -74.25$.

Next, equation (5.27) is solve to obtain values of $m_{c,3} = 0.87$, $m_{c,4} = 0.11$, $m_{c,5} = 0.11$, $m_{CR,3} = 0.33$, $m_{CR,4} = 0.36$, $s_{c,3} = 0.25$, $s_{c,4} = 0.64$, $s_{c,5} = 0.25$, $\lambda_4 = -18.77$, $\lambda_5 = -59.98$, $\lambda_6 = -17.56$, $\lambda_7 = -17.56$, $\lambda_8 = -36.77$, and $\lambda_9 = -105.45$.

5.5 Simulation

In this section, the dynamic balancing of the robot is verified numerically through the use of a multi-body dynamic simulation software, MSC ADAMS. The simulation was set up using the optimised kinematic and inertial parameters computed in section 5.4, and the base joints of the legs are positioned at $\mathbf{p}_1 = \mathbf{p}_2 = [-0.5, 0]^T$ and $\mathbf{p}_3 = \mathbf{p}_4 = [0.3, 0]^T$. The trajectory of the moving platform of the robot is a full rotation about a fixed point; a trajectory that is not possible for non-redundant architectures without encountering kinematic singularities. The redundant link's orientation remains fixed with respect to the moving platform throughout the trajectory. The end-effector is centred at the origin throughout the trajectory, the moving platform rotates about this point with a constant angular velocity of $\dot{\phi} = 1$ and an initial orientation of $\phi = 0$. The orientation of the redundant link, ψ, is fixed at a perpendicular angle to the moving platform throughout the trajectory. The described trajectory is written as

$$\dot{\mathbf{p}}_e = \begin{bmatrix} 0 \\ 0 \end{bmatrix}, \qquad \dot{\phi} = 1, \qquad \dot{\psi} = 1, \tag{5.28}$$

where the initial conditions are given by $\mathbf{p}_e = [0, 0]^T$, $\phi = 0$, and $\psi = -\pi/2$.

The actuated joint velocities, $\dot{\theta}_1, .., \dot{\theta}_4$, for this trajectory are computed using the Jacobian matrix of the mechanism. Given that the angular velocity of the redundant link has been set to be equal to that of the moving platform, the joint velocities are computed as

$$\dot{\theta} = \mathbf{K}^{-1}\mathbf{J} \begin{bmatrix} \dot{\mathbf{p}}_e \\ \dot{\phi} \end{bmatrix}, \tag{5.29}$$

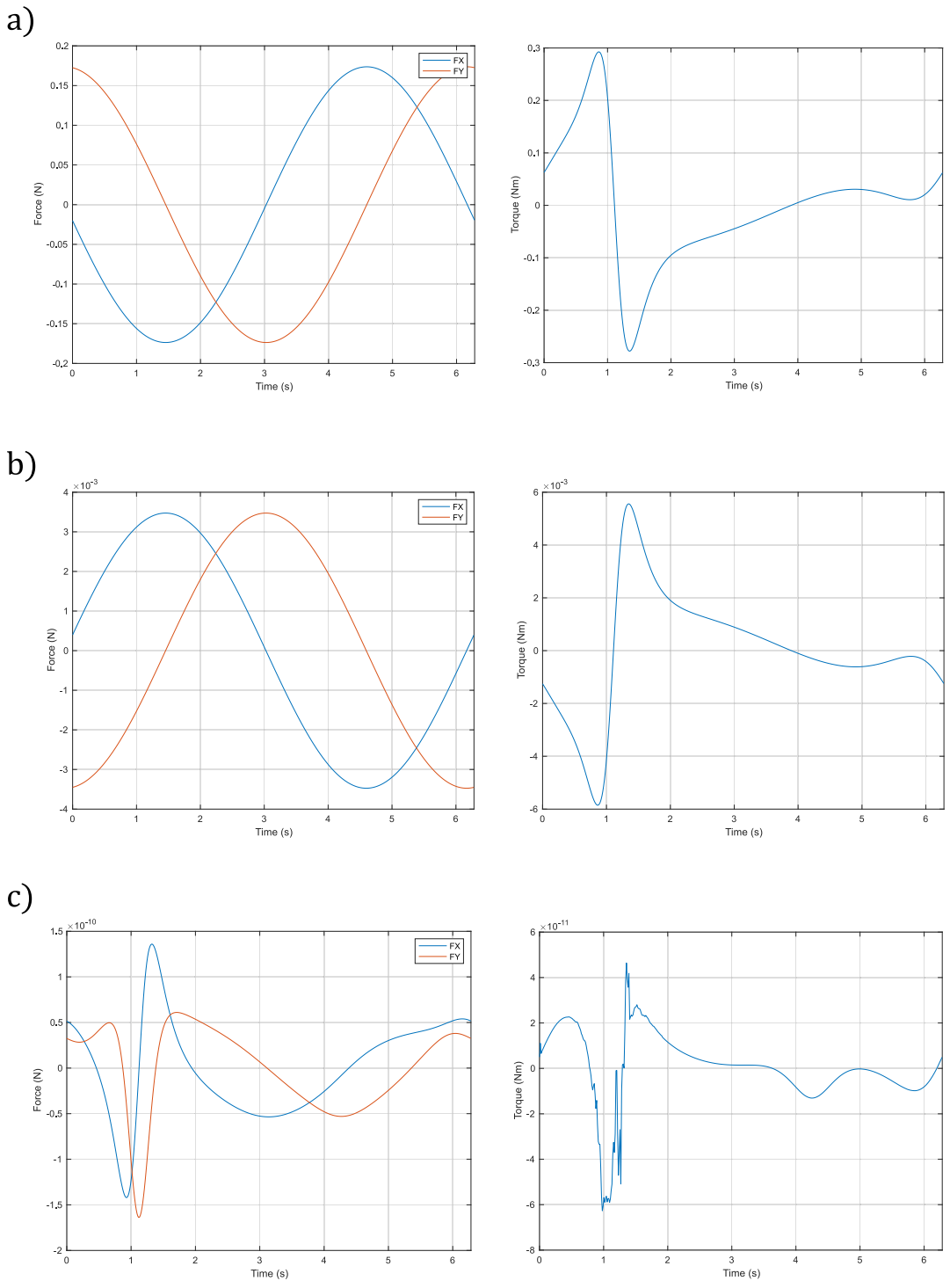

Figure 5.8: Results of the MSC ADAMS simulation for (a) the unbalanced manipulator, (b) the balanced manipulator with imposed countermass errors of 2%, and (c) the balanced manipulator. The left hand graphs show the shaking force imposed by the manipulator upon the base along the x and y axes, denoted by FX and FY. The right hand graphs show the shaking torque imposed upon the base by the manipulator.

where

$$\mathbf{J} = \begin{bmatrix} \mathbf{p}_{5,10}^T & -\mathbf{p}_{5,10}^T \mathbf{E} \mathbf{p}_{10,e} \\ \mathbf{p}_{6,10}^T & -\mathbf{p}_{6,10}^T \mathbf{E} \mathbf{p}_{10,e} \\ \mathbf{p}_{7,9}^T & \mathbf{p}_{7,9}^T \mathbf{E} (\mathbf{p}_{e,11} - \mathbf{p}_{9,11}) \\ \mathbf{p}_{8,9}^T & \mathbf{p}_{8,9}^T \mathbf{E} (\mathbf{p}_{e,11} - \mathbf{p}_{9,11}) \end{bmatrix},$$

$$\mathbf{K} = \begin{bmatrix} \mathbf{p}_{5,10}^T \mathbf{E} \mathbf{p}_{1,5} & 0 & 0 & 0 \\ 0 & \mathbf{p}_{6,10}^T \mathbf{E} \mathbf{p}_{2,6} & 0 & 0 \\ 0 & 0 & \mathbf{p}_{7,9}^T \mathbf{E} \mathbf{p}_{3,7} & 0 \\ 0 & 0 & 0 & \mathbf{p}_{8,9}^T \mathbf{E} \mathbf{p}_{4,8} \end{bmatrix},$$

$\dot{\theta} = [\dot{\theta}_1, \dot{\theta}_2, \dot{\theta}_3, \dot{\theta}_4]^T$, and $\mathbf{p}_{i,j} = \mathbf{p}_j - \mathbf{p}_i$. To act as a point of comparison, an unbalanced mechanism is simulated to follow the same trajectory, described by equation (5.28), and with the same computed joint velocities using equation (5.29). The unbalanced manipulator is identical to the balanced manipulator, except the countermasses and counter-rotary elements are removed.

The results of the simulation are given in Fig. 5.8; row (a) shows the results of the unbalanced manipulator and row (c) shows the results of the balanced manipulator. The left hand graphs show the force imposed on the base by the manipulator throughout the trajectory, along the x and y axes. The graphs on the right hand side show the torque imposed on the base by the manipulator throughout the trajectory (measured about P_1). It can be seen that the force and torque exerted on the base for the unbalanced manipulator are in the order of 10^{-1} N and Nm, respectively. However, the force and torque exerted on the base for the balanced manipulator are in the order of 10^{-10} N and Nm, respectively. The shaking forces and torques are virtually eliminated for the balanced architecture, whilst the kinematic redundancy of the system allows full rotations of the end-effector to take place without encountering any singularities. The small forces and torques imposed on the base by the balanced manipulator are due to small modelling errors.

Although the simulation reported in Fig.5.8 shows that manipulator imposed no shaking forces or torques on the base when the countermasses are put in place with the correct balancing parameters, it is important to know what the effects are when a degree of error is introduced to the system. A challenge when creating a physical prototype is the degree of precision and accuracy which can be achieved in simulation can not always be achieved in reality, and so it is important to know how this can effect the outcome of the system. To explore the effect of this, the balanced manipulator was simulated to follow the same trajectory as before, however with a small degree of error added to the system. In this

simulation, the masses of each countermass and counter-rotary element were increased by 2%. The results of this simulation are shown in row (b) of Fig. 5.8. It can be seen that the shaking forces and torques imposed on the base are reduced by roughly two orders of magnitude throughout the trajectory. It is concluded that if a physical prototype of the proposed balanced manipulator were constructed, the shaking forces and torques generated would be greatly reduced compared to a similar unbalanced manipulator, even if the level of accuracy in the manufacturing of the balancing components is limited.

Chapter 6

Conclusion

The work presented in this thesis addresses some key challenges in order for kinematically redundant parallel robots to be used more frequently in high performance applications. The first challenge is that there needs to be a greater number of architectures in order for developers to design kinematically redundant parallel robots for a greater range of applications. The next challenge is that conventional methods of singularity analysis for parallel robots are unreliable when applied to kinematically redundant architectures with non-serially connected actuators, this is a huge issue that needed to be addressed as Jacobian-based methods of singularity, the most commonly used approaches, would both fail to detect some singularities and incorrectly identify other configurations as singularities when they are not. The result of this is that the feasible workspace of the manipulator is needlessly restricted in order to avoid false positive singularities, whilst still including false negative singularities in which the performance of the robot can deteriorate significantly. This issue had previously remained unaddressed in the literature and so the first aim was to investigate the conditions which lead to the Jacobian failing as a means of singularity analysis. With this analysis carried out, the next challenge was to develop a more reliable method of singularity analysis which does not exhibit these shortcomings. Additionally, using this robust method of singularity analysis, a method of utilising the kinematically redundant degree of freedom for optimising the mechanism's proximity from a singularity for any given pose of the end-effector would allow the potential of kinematically redundant architectures to be unlocked. Finally, kinematic redundant parallel architectures provide a solution to develop fast-moving manipulators with large rotational capabilities and workspaces. However, a drawback of fast-moving manipulators is that they can accumulate large shaking forces and moments onto their bases. It is therefore important to develop architectures which eliminate these effects, such that the high performance of the robot is

not detracted from by these shaking forces and moments.

6.1 Summary of Main Contributions

In chapter 2, a novel kinematically redundant planar parallel robot manipulator has been presented whose architecture is a fundamental truss and is able to complete 2π rotations of the end-effector without producing singularities. Achieving such a combination of characteristics had remained elusive in the literature. Fundamental architectures of parallel manipulators are important because they constitute the general instance of a family of robot manipulators. For the proposed parallel manipulator, the bilateration method was used to solve the inverse kinematics and forward kinematics problems. The singularity analysis was carried out by describing the geometric conditions that lead to the loss of the rigidity of the robot manipulator by using a method based on the computations of instantaneous centres of rotations of the sub-mechanisms of mobility 1. An example trajectory with a full rotation of the moving platform was tested both numerically and experimentally, these results are reported and a link to an online video recording of the prototype performing the trajectory is also provided; the actuator values used to complete the predefined trajectory were calculated by solving the inverse kinematics. This video also consists of an example of singularity avoidance thanks to redundancy and a potential application of the full rotation capabilities.

In chapter 3, the shortcomings of using Jacobian-based methods of singularity analysis on kinematically redundant parlallel robots which exhibit no actuators connected in series are detailed. Three example mechanisms are examined in particular configurations where the Jacobian fails as a means of singularity analysis, in one case the determinant of the Jacobian equals zero when the robot is not in a singularity (false positive), in the other cases it fails to go to zero as the robot approaches a singularity (false negative). The robot is determined herein to be in a singularity by computing the rank of the rigidity matrix of the underlying graph of the mechanism; this matrix becomes rank deficient if the mechanism enters a type-II singularity and is full rank when in a non-singular configuration. The problems with the Jacobian for these types of parallel robots arise due to the need to eliminate a redundant variable(s). The chapter is summarised by instructing developers of parallel robots with similar architectures to use non-Jacobian based methods of singularity detection or path planning algorithms.

Chapter 4 presented a geometric method of singularity avoidance for kinematically redundant planar parallel robots which does not exhibit the same limitations that Jacobian-

based approaches do when applied to these architectures. The singularity analysis is performed by firstly determining the positions of the relevant instantaneous centres of rotation of the mechanism from the positions and orientations of the links, and secondly by determining the relevant in-circle radii formed by these ICRs; these radii act as a measure of how close two ICRs are to coinciding or how close an ICR is to becoming indeterminable – both of which indicate that the robot manipulator is in a singularity. The robot manipulator's distance from a singularity is given by the minimum normalised value of these in-circle radii, r_{min}. A configuration of the kinematically redundant mechanism that is further away from a singularity is calculated by formulating r_{min} in terms of the redundant parameter. A predictor-corrector method is then implemented to find a value of this parameter which gives an increased value of r_{min} without crossing a singularity to get there – a point where $r_{min} = 0$.

Finally, the in-circle method is compared with a conventional method of singularity analysis, the calculation of the inverse of the condition number of the Jacobian, $1/k(J)$. The in-circle method is shown to be more robust than using $1/k(J)$ as a means of measuring proximity to a singularity; two examples are shown to demonstrate these advantages. Firstly, both methods are used on a non-singular configuration of the mechanism proposed in Baron et al. (2018); the Jacobian matrix is singular however the in-circle method suggests that the robot manipulator is not in a singularity, and the corresponding rigidity matrix of the mechanism is of full rank which verifies this. In the second example, the mechanism proposed in Schreiber and Gosselin (2018) is moved toward a singularity, however $1/k(J)$ does not approach zero as this point is neared, whereas r_{min} does. It is concluded that the proposed geometric method is more reliable than conventional Jacobian-based methods when applied to kinematically redundant architectures for the reasons described above. Future work may involve geometric methods of singularity analysis for kinematically redundant spatial manipulators.

Chapter 5 presented a novel, dynamically balanced kinematically redundant planar parallel robot. Firstly, the method of balancing is presented and is applied on the kinematically redundant architecture of the robot. The balancing conditions are then derived, such that the shaking forces and moments imposed on the base are zero for any trajectory of the manipulator. The set of balancing parameters are then optimised such that the total amount of mass and inertia added to the system is minimised. The performance of the balanced manipulator is verified numerically via a simulation using the multi-body dynamic simulation software MSC ADAMS.

6.1.1 Directions for Future Work

The main aim of this thesis is to address some of the fundamental challenges that kinematically redundant parallel robots face so that they can be developed for many applications where high performance is a requirement. Some possible directions for future work are listed below.

- **The Development of Spatial Architectures:** The novel architectures presented in this thesis were both planar ones, which are useful for many applications, however there are many applications which require that the end-effector is not confined to move just in a single plane. In order to enhance the potential for kinematically redundant parallel robots to be used more frequently, e.g. in industry, more spatial architectures must be developed.

- **Singularity Analysis for Spatial Architectures:** The issues of conventional, Jacobian-based methods of singularity analysis were addressed in this thesis, and an example of the Jacobian failing to detect a singularity was shown in chapter 3. The robust method of singularity analysis that was presented in chapter 4 is applicable to planar architectures, however it is not applicable to spatial architectures. Along with the development of spatial architectures, a method of robust singularity analysis must be developed which can be applied to spatial kinematically redundant robots.

- **Prototype of the Dynamically Balanced Kinematically Redundant Architecture:** The balanced architecture presented in chapter 5 was evaluated using the multi-body dynamic simulation software MSC Adams. However, before further research on this mechanism can be conducted, a physical mechanism needs to be built in order to prove the elimination of shaking forces and moments can be achieved in reality.

- **Workspace Optimisation:** The development of kinematically redundant parallel architectures opens a door to parallel robots to be used in many more applications as it greatly enhances their potential workspaces and rotational capabilities. Following this, an important next step is to develop algorithms which can be used in the design process which optimise the workspaces of these mechanisms. This could include the reachable workspace of the mechanism, i.e. the total area which the end-effector can reach, or the dexterous workspace, i.e. the total area in which the end-effector is capable of achieving full cycle rotations. A start on this topic

was recently made in Cheung et al. (2019), where an algorithm of computing the 'singularity-safe' workspace of a kinetically redundant robot was presented.

- **Path Planning Algorithms:** Multiple path planning algorithms have been developed for parallel robots; it is common to try and optimise some performance index, such as the condition number of the Jacobian matrix, along a particular path. However, as highlighted in this thesis, this is unreliable when applied to kinematically redundant parallel robots with non-seriall connected actuators. A robust method of singularity avoidance was presented in this thesis which optimises the robot's configuration for a given pose of the end-effector. In addition to this, it would be useful for path planning algorithms to be developed for these types of architectures where a reliable performance index, such as r_{min}, can optimised over an entire trajectory.

Bibliography

Abedinnasab, M. H. and Vossoughi, G. (2009). Analysis of a 6-dof redundantly actuated 4-legged parallel mechanism. *Nonlinear Dynamics*, 58(4):611. 6

Arakelian, V. H. and Smith, M. (2005a). Shaking force and shaking moment balancing of mechanisms: a historical review with new examples. *J. Mech. Des.*, 127(2):334–339. 11

Arakelian, V. H. and Smith, M. (2005b). Shaking force and shaking moment balancing of mechanisms: a historical review with new examples. *J. Mech. Des.*, 127(2):334–339. 11

Asimow, L. and Roth, B. (1978). The rigidity of graphs. *Transactions of the American Mathematical Society*, 245:279–289. 34, 54

Asimow, L. and Roth, B. (1979). The rigidity of graphs, ii. *Journal of Mathematical Analysis and Applications*, 68(1):171–190. 34, 54

Bagci, C. (1982). Complete shaking force and shaking moment balancing of link mechanisms using balancing idler loops. *ASME Journal of Mechanical Design*, 104(2):482–493. 11

Baret, M. (1978). Six degrees of freedom large motion system for flight simulators. *AGARD Piloted Aircraft Environ. Simulation Tech. 8 p(SEE N 79-15973 07-09)*. 3

Baron, N., Philippides, A., and Rojas, N. (2018). A Geometric Method of Singularity Avoidance for Kinematically Redundant Planar Parallel Robots. In *International Symposium on Advances in Robot Kinematics*, pages 187–194. Springer. xii, xiii, 15, 36, 39, 47, 54, 55, 56, 93

Baron, N., Philippides, A., and Rojas, N. (2019). A novel kinematically redundant planar parallel robot manipulator with full rotatability. *Journal of Mechanisms and Robotics*, 11(1). 13, 14, 50

Baron, N., Philippides, A., and Rojas, N. (2020a). A dynamically balanced kinematically redundant planar parallel robot. *Under Review*. 13, 69

Baron, N., Philippides, A., and Rojas, N. (2020b). On the false positives and false negatives of the jacobian matrix in kinematically redundant parallel mechanisms. *IEEE Transactions on Robotics*, 36:951–958. 13, 33

Baron, N., Philippides, A., and Rojas, N. (2020c). A robust geometric method of singularity avoidance for kinematically redundant planar parallel robot manipulators. *Mechanism and Machine Theory*, 151:103863. 13, 53

Berenson, D., Srinivasa, S., and Kuffner, J. (2011). Task space regions: A framework for pose-constrained manipulation planning. *The International Journal of Robotics Research*, 30(12):1435–1460. 10

Berkof, R. and Lowen, G. (1969). A new method for completely force balancing simple linkages. *ASME Journal of Engineering for Industry*, 91(1):21–26. 11

Berkof, R. and Lowen, G. (1971). Theory of shaking moment optimization of force-balanced four-bar linkages. *ASME Journal of Engineering for Industry*, 93(1):53–60. 11

Bhattacharya, S., Hatwal, H., and Ghosh, A. (1998). Comparison of an exact and an approximate method of singularity avoidance in platform type parallel manipulators. *Mechanism and Machine Theory*, 33(7):965–974. 10

Bohigas, O., Henderson, M. E., Ros, L., Manubens, M., and Porta, J. M. (2013). Planning singularity-free paths on closed-chain manipulators. *IEEE Transactions on Robotics*, 29(4):888–898. 10

Bohigas, O., Henderson, M. E., Ros, L., and Porta, J. M. (2012). A singularity-free path planner for closed-chain manipulators. In *2012 IEEE International Conference on Robotics and Automation*, pages 2128–2134. IEEE. 10

Bonev, I. A. and Ryu, J. (2001). A new approach to orientation workspace analysis of 6-dof parallel manipulators. *Mechanism and machine theory*, 36(1):15–28. 4

Briot, S. and Bonev, I. A. (2007). Are parallel robots more accurate than serial robots? *Transactions of the Canadian Society for Mechanical Engineering*, 31(4):445–455. 3

Briot, S. and Bonev, I. A. (2008). Accuracy analysis of 3-dof planar parallel robots. *Mechanism and Machine Theory*, 43(4):445–458. 3

Carp-Ciocardia, D. et al. (2003). Dynamic analysis of clavel's delta parallel robot. In *2003 IEEE international conference on robotics and automation (Cat. No. 03CH37422)*, volume 3, pages 4116–4121. IEEE. 4

Carretero, J., Ebrahimi, I., and Boudreau, R. (2008). A comparison between two motion planning strategies for kinematically redundant parallel manipulators. In *Advances in Robot Kinematics: Analysis and Design*, pages 243–252. Springer. 10

Carretero, J. A., Ebrahimi, I., and Boudreau, R. (2012). Overall motion planning for kinematically redundant parallel manipulators. *Journal of Mechanisms and Robotics*, 4(2):024502. 10

Cha, S.-H., Lasky, T. A., and Velinsky, S. A. (2007). Kinematically-Redundant Variations of the 3-RRR Mechanism and Local Optimization-Based Singularity Avoidance. *Mechanics based design of structures and machines*, 35(1):15–38. 7, 10

Chakarov, D. (2004). Study of the antagonistic stiffness of parallel manipulators with actuation redundancy. *Mechanism and machine theory*, 39(6):583–601. 6

Cheng, H. (2001). *Dynamics and control of parallel manipulators with actuation redundancy*. PhD thesis, Hong Kong University of Science and Technology. 7

Cheng, H., Yiu, Y.-K., and Li, Z. (2003). Dynamics and control of redundantly actuated parallel manipulators. *IEEE/ASME Transactions on mechatronics*, 8(4):483–491. 7

Cheung, Y. H., Baron, N., and Rojas, N. (2019). Full-rotation singularity-safe workspace for kinematically redundant parallel robots. In *Annual Conference Towards Autonomous Robotic Systems*, pages 436–447. Springer. 95

Clavel, R. (1988). A fast robot with parallel geometry. In *Proc. Int. Symposium on Industrial Robots*, pages 91–100. 3

Collins, C. L. (1997). *Singularity analysis and design of parallel manipulators*. PhD thesis, University of California, Irvine. 6

Cortés, J. and Siméon, T. (2004). Sampling-based motion planning under kinematic loop-closure constraints. In *Algorithmic Foundations of Robotics VI*, pages 75–90. Springer. 10

Daniali, H. (2005). Instantaneous center of rotation and singularities of planar parallel manipulators. *International Journal of Mechanical Engineering Education*, 33:251–259. 23, 50, 55

Daniali, H. M., Zsombor-Murray, P., and Angeles, J. (1995). Singularity analysis of planar parallel manipulators. *Mechanism and Machine Theory*, 30(5):665–678. 5

Dasgupta, B. and Mruthyunjaya, T. (1998a). Force redundancy in parallel manipulators: theoretical and practical issues. *Mechanism and Machine Theory*, 33(6):727–742. 6

Dasgupta, B. and Mruthyunjaya, T. (1998b). Singularity-free path planning for the stewart platform manipulator. *Mechanism and Machine Theory*, 33(6):711–725. 10

Dash, A. K., Chen, I.-M., Yeo, S. H., and Yang, G. (2005). Workspace generation and planning singularity-free path for parallel manipulators. *Mechanism and Machine Theory*, 40(7):776–805. 10

Di Gregorio, R. (2009). A novel method for the singularity analysis of planar mechanisms with more than one degree of freedom. *Mechanism and Machine Theory*, 44(1):83–102. 50, 55

Dresig, H., Rockhausen, L., and Naake, S. (1992). Balancing conditions for planar mechanism. *Flexible Mechanisms, Dynamics and Analysis*, 47:67–73. 12

Ebrahimi, I., Carretero, J. A., and Boudreau, R. (2007). 3-PRRR redundant planar parallel manipulator: Inverse displacement, workspace and singularity analyses. *Mechanism and Machine Theory*, 42(8):1007–1016. 5, 7

Ebrahimi, I., Carretero, J. A., and Boudreau, R. (2008). Kinematic analysis and path planning of a new kinematically redundant planar parallel manipulator. *Robotica*, 26(3):405–413. 10, 26, 58, 59

Firmani, F. and Podhorodeski, R. P. (2004). Force-unconstrained poses for a redundantly-actuated planar parallel manipulator. *Mechanism and Machine Theory*, 39(5):459–476. 6

Foucault, S. and Gosselin, C. m. M. (2004). Synthesis, design, and prototyping of a planar three degree-of-freedom reactionless parallel mechanism. *J. Mech. Des.*, 126(6):992–999. 11

Garg, V., Nokleby, S. B., and Carretero, J. A. (2009). Wrench capability analysis of redundantly actuated spatial parallel manipulators. *Mechanism and machine theory*, 44(5):1070–1081. 6

Gomes, A., Voiculescu, I., Jorge, J., Wyvill, B., and Galbraith, C. (2009). *Implicit curves and surfaces: mathematics, data structures and algorithms*. Springer Science & Business Media. 63

Gosselin, C. and Angeles, J. (1990). Singularity Analysis of Closed-Loop Kinematic Chains. *IEEE Transactions on Robotics*, 6:281–290. 4, 5, 9

Gosselin, C., Laliberté, T., and Veillette, A. (2015). Singularity-Free Kinematically Redundant Planar Parallel Mechanisms With Unlimited Rotational Capability. *IEEE Transactions on Robotics*, 31:457–467. xiv, 8, 14, 23, 33, 54, 73, 75

Gosselin, C. and Schreiber, L.-T. (2016). Kinematically redundant spatial parallel mechanisms for singularity avoidance and large orientational workspace. *IEEE Transactions on Robotics*, 32(2):286–300. xii, 33, 36, 37, 41, 42, 46

Gosselin, C. and Schreiber, L.-T. (2018). Redundancy in parallel mechanisms: A review. *Applied Mechanics Reviews*, 70(1). 5, 6

Gosselin, C. M., Vollmer, F., Côté, G., and Wu, Y. (2004). Synthesis and design of reactionless three-degree-of-freedom parallel mechanisms. *IEEE Transactions on Robotics and Automation*, 20(2):191–199. 11

Gough, V. E. (1962). Universal tyre test machine. *Proc. FISITA 9th Int. Technical Congr., London, 1962*, pages 117–137. 3

Guan, L., Wang, J., Yun, Y., and Wang, L. (2004). Kinematics of a tricept-like parallel robot. In *2004 IEEE International Conference on Systems, Man and Cybernetics (IEEE Cat. No. 04CH37583)*, volume 6, pages 5312–5316. IEEE. 3

Gupta, K. (1986). On the nature of robot workspace. *The International journal of robotics research*, 5(2):112–121. 4

Han, L. (2000). A kinematics-based probabilistic roadmap method for closed chain systems. In *In Proc. Int. Workshop on Algorithmic Foundations of Robotics (WAFR*. Citeseer. 10

Harada, T. and Nagase, M. (2010). Impedance Control of a Redundantly Actuated 3-DOF Planar Parallel Link Mechanism Using Direct Drive Linear Motors. In *Robotics and Biomimetics (ROBIO), 2010 IEEE International Conference on*, pages 501–506, Tianjin, China. 7

Hartenberg, R. S. and Denavit, J. (1964). *Kinematic Synthesis of Linkages*, chapter 4. McGraw-Hill, New York, NY. 23, 56

Hendrickson, B. (1992). Conditions for Unique Graph Realizations. *SIAM Journal on Computing*, 21(1):65–84. 28, 34, 54

Herder, J. L. and Gosselin, C. M. (2004). A counter-rotary counterweight (crcw) for light-weight dynamic balancing. In *International Design Engineering Technical Conferences and Computers and Information in Engineering Conference*, volume 46954, pages 659–667. 12

Huang, Z. and Kong, X. (1995). Kinematic analysis on the spatial parallel mechanisms with redundant degree of freedom. *Chin. J. Mech. Eng*, 31(3):44–50. 7

Hunt, K. (1983). Structural Kinematics of In-Parallel-Actuated Robot-Arms. *ASME Journal of Mechanisms, Transmissions, and Automation in Design*, 105:705–712. 19

Jáuregui, J. C., Hernández, E. E., Ceccarelli, M., López-Cajún, C., and García, A. (2013). Kinematic calibration of precise 6-dof stewart platform-type positioning systems for radio telescope applications. *Frontiers of Mechanical Engineering*, 8(3):252–260. 4

Jean, M. and Gosselin, C. M. (1996). Static balancing of planar parallel manipulators. In *Proceedings of IEEE International Conference on Robotics and Automation*, volume 4, pages 3732–3737. IEEE. 11

Kochev, I. (2000). General theory of complete shaking moment balancing of planar linkages: a critical review. *Mechanism and Machine Theory*, 35(11):1501–1514. 12

Kock, S. and Schumacher, W. (1998). A parallel xy manipulator with actuation redundancy for high-speed and active-stiffness applications. In *Proceedings. 1998 IEEE International Conference on Robotics and Automation (Cat. No. 98CH36146)*, volume 3, pages 2295–2300. IEEE. 6

Krut, S., Pierrot, F., et al. (2004). Velocity performances indexes for parallel mechanisms with actuation redundancy. *Robotica*, 22(Part 2):129–139. 6

Kumar, V. (1992). Instantaneous kinematics of parallel-chain robotic mechanisms. *Journal of Mechanical Design*, 114(3):349–358. 4

Kurtz, R., Hayward, V., et al. (1992). Multiple-goal kinematic optimization of a parallel spherical mechanism with actuator redundancy. *IEEE Transactions on Robotics and Automation*, 8(5):644–651. 6

Lai, Z. and Yang, D. (1986). A new method for the singularity analysis of simple six-link manipulators. *The International journal of robotics research*, 5(2):66–74. 5

Laliberté, T. and Gosselin, C. (2013). Dynamic balancing of two-dof parallel mechanisms using a counter-mechanism. In *ASME 2013 International Design Engineering Technical Conferences and Computers and Information in Engineering Conference*. American Society of Mechanical Engineers Digital Collection. 72, 83

Lee, J. H., Yi, B.-J., Oh, S.-R., and Suh, I. H. (1998). Optimal design of a five-bar finger with redundant actuation. In *Proceedings. 1998 IEEE International Conference on Robotics and Automation (Cat. No. 98CH36146)*, volume 3, pages 2068–2074. IEEE. 6

Lee, S. and Kim, S. (1993). Kinematic analysis of generalized parallel manipulator systems. In *Decision and Control, 1993., Proceedings of the 32nd IEEE Conference on*, pages 1097–1102, San Antonio, TX, USA. 5

Liao, H., Li, T., and Tang, X. (2004). Singularity analysis of redundant parallel manipulators. In *2004 IEEE International Conference on Systems, Man and Cybernetics*, volume 5, pages 4214–4220. IEEE. 9

Lowen, G. and Berkof, R. (1968). Survey of investigations into the balancing of linkages. *Journal of mechanisms*, 3(4):221–231. 11

Luces, M., Mills, J. K., and Benhabib, B. (2017). A review of redundant parallel kinematic mechanisms. *Journal of Intelligent & Robotic Systems*, 86(2):175–198. 6

MacCalion, H. and Pham, D. (1979). The analysis of a six degrees of freedom work station for mechanized assembly. In *Proc. 5th Word Congress on Theory of Machines and Mechanisms*, pages 6–11. 3

Marquet, F., Krut, S., Company, O., and Pierrot, F. (2001). ARCHI: A New Redundant Parallel Mechanism-Modeling, Control and First Results. In *Intelligent Robots and Systems, 2001. Proceedings. 2001 IEEE/RSJ International Conference on*, pages 183–188, Maui, HI, USA. 6

Merlet, J. (1987). Parallel manipulator, part 1: Theory, design, kinematic and control. *INRIA Research Report*, 646. 3

Merlet, J. (1988). Parallel manipulator part 2: Singular configurations and grassmann geometry. *Technical report*. 3

Merlet, J. (2006). *Parallel Robots*, chapter 2. Springer Science & Business Media, Dordrecht, The Netherlands. 3, 34

Merlet, J.-P. (1989). Singular configurations of parallel manipulators and grassmann geometry. *The international journal of robotics research*, 8(5):45–56. 5

Merlet, J.-P. (1996). Redundant parallel manipulators. *Laboratory Robotics and Automation*, 8(1):17–24. 9

Merlet, J.-P., Gosselin, C. M., and Mouly, N. (1998). Workspaces of planar parallel manipulators. *Mechanism and Machine Theory*, 33(1-2):7–20. 4

Miller, K. (2004). Optimal design and modeling of spatial parallel manipulators. *The International Journal of Robotics Research*, 23(2):127–140. 4

Mohamed, M. and Duffy, J. (1985). A direct determination of the instantaneous kinematics of fully parallel robot manipulators. *Journal of Mechanical Design*, 107(2):226–229. 3

Mohamed, M. G. and Gosselin, C. M. (2005). Design and analysis of kinematically redundant parallel manipulators with configurable platforms. *IEEE Transactions on Robotics*, 21(3):277–287. 7

Mueller, A. (2013). On the terminology and geometric aspects of redundant parallel manipulators. *Robotica*, 31(1):137–147. 6

Müller, A. (2009). Generic mobility of rigid body mechanisms. *Mechanism and Machine Theory*, 44(6):1240 – 1255. 17

Niu, X.-M., Gao, G.-Q., Liu, X.-J., and Bao, Z.-D. (2013). Dynamics and control of a novel 3-dof parallel manipulator with actuation redundancy. *International Journal of Automation and Computing*, 10(6):552–562. 7

Nokleby, S. B., Firmani, F., Zibil, A., and Podhorodeski, R. P. (2007). An Analysis of the Force-Moment Capabilities of Branch-Redundant Planar-Parallel Manipulators. In *Proceedings of the 2007 ASME Design Engineering Technical Conference, ASME, Las Vegas, NV, USA,(Sept. 4-7, 2007)*, pages 1013–1020, Las Vegas, Nevada, USA. 7

Notash, L. and Podhorodeski, R. P. (1994). Uncertainty configurations of three-branch parallel manipulators: Identification and elimination. *Robotics: Kinematics, Dynamics and Controls*, 72:459–466. 6

Park, F. and Kim, J. W. (1999). Singularity analysis of closed kinematic chains. *Journal of Mechnical Design*, 121(1):32–38. 4, 5

Patel, Y., George, P., et al. (2012). Parallel manipulators applications—a survey. *Modern Mechanical Engineering*, 2(03):57. 3

Pierrot, F., Dauchez, P., and Fournier, A. (1991). Fast parallel robots. *Journal of Robotic Systems*, 8(6):829–840. 4

Pierrot, F., Reynaud, C., and Fournier, A. (1990). Delta: a simple and efficient parallel robot. *Robotica*, 8(2):105–109. 4

Porta, J. M., Cortés, J., Ros, L., and Thomas, F. (2007). A space decomposition method for path planning of loop linkages. In *2007 IEEE/RSJ International Conference on Intelligent Robots and Systems*, pages 1882–1888. IEEE. 10

Porta, J. M., Jaillet, L., and Bohigas, O. (2012). Randomized path planning on manifolds based on higher-dimensional continuation. *The International Journal of Robotics Research*, 31(2):201–215. 10

Pradipta, J., Klünder, M., Weickgenannt, M., and Sawodny, O. (2013). Development of a pneumatically driven flight simulator stewart platform using motion and force control. In *2013 IEEE/ASME International Conference on Advanced Intelligent Mechatronics*, pages 158–163. IEEE. 4

Rey, L. and Clavel, R. (1999). The delta parallel robot. In *Parallel Kinematic Machines*, pages 401–417. Springer. 4

Ricard, R. and Gosselin, C. M. (2000). On the development of reactionless parallel manipulators. In *Proceedings of ASME Design Engineering Technical Conferences, MECH-14098*. 11

Rojas, N. (2012). *Distance-Based Formulations for the Position Analysis Of Kinematic Chains*. PhD thesis, Universitat Politècnica de Catalunya, Barcelona. 8, 14, 18

Rojas, N. and Dollar, A. (2016). Gross Motion Analysis of Fingertip-Based Within-Hand Manipulation. *IEEE Transactions on Robotics*, 32:1009–1016. 16, 57

Rojas, N. and Thomas, F. (2011). The Forward Kinematics of 3-RPR Planar Robots: A Review And A Distance-Based Formulation. *IEEE Transactions on Robotics*, 27:143–150. 19

Rojas, N. and Thomas, F. (2012). On closed-form solutions to the position analysis of baranov trusses. *Mechanism and Machine Theory*, 50:179–196. 62

Rojas, N. and Thomas, F. (2018). Forward kinematics of the general triple-arm robot using a distance-based formulation. In *Computational Kinematics*, pages 257–264. Springer. 36

Ryu, S.-J., Kim, J. W., Hwang, J. C., Park, C., Cho, H. S., Lee, K., Lee, Y., Cornel, U., Park, F., and Kim, J. (1999). Eclipse: An overactuated parallel mechanism for rapid machining. In *Parallel Kinematic Machines*, pages 441–455. Springer. 6

Saglia, J. A., Dai, J. S., and Caldwell, D. G. (2008). Geometry and kinematic analysis of a redundantly actuated parallel mechanism that eliminates singularities and improves dexterity. *Journal of Mechanical Design*, 130(12). 6

Saglia, J. A., Tsagarakis, N. G., Dai, J. S., and Caldwell, D. G. (2009). A high-performance redundantly actuated parallel mechanism for ankle rehabilitation. *The International Journal of Robotics Research*, 28(9):1216–1227. 6

Schreiber, L.-T. and Gosselin, C. (2018). Kinematically redundant planar parallel mechanisms: Kinematics, workspace and trajectory planning. *Mechanism and Machine Theory*, 119:91–105. xii, xiii, 8, 14, 15, 27, 33, 36, 37, 44, 51, 54, 66, 67, 68, 93

Schreiber, L.-T. and Gosselin, C. (2019). Exploiting the kinematic redundancy of a (6+3) degrees-of-freedom parallel mechanism. *Journal of Mechanisms and Robotics*, 11(2):021005. 51

Sen, S., Dasgupta, B., and Mallik, A. K. (2003). Variational approach for singularity-free path-planning of parallel manipulators. *Mechanism and Machine Theory*, 38(11):1165–1183. 10

Song, J., Mou, J.-I., and King, C. (1999). Error modeling and compensation for parallel kinematic machines. In *Parallel Kinematic Machines*, pages 171–187. Springer. 3

Stewart, D. (1965). A platform with six degrees of freedom. *Proceedings of the institution of mechanical engineers*, 180(1):371–386. 3

Su, Y. X., Duan, B. Y., Zheng, C. H., Zhang, Y., Chen, G., and Mi, J. (2004). Disturbance-rejection high-precision motion control of a stewart platform. *IEEE transactions on control systems technology*, 12(3):364–374. 4

Van der Wijk, V., Herder, J., Demeulenaere, B., and Gosselin, C. (2008). Comparative analysis and optimization for low-mass and low-inertia dynamic balancing of a 1-dof rotatable link balanced by a counter-rotary counter-mass. *TOWARDS LOW MASS AND LOW INERTIA DYNAMIC BALANCING OF MECHANISMS*, page 19. 12

van der Wijk, V. and Herder, J. L. (2009). Synthesis of dynamically balanced mechanisms by using counter-rotary countermass balanced double pendula. *Journal of mechanical design*, 131(11). 12, 70, 72

van der Wijk, V. and Herder, J. L. (2012). Inherently balanced 4r four-bar based linkages. In *Latest Advances in Robot Kinematics*, pages 309–316. Springer. 12

Van der Wijk, V. and Herder, J. L. (2012). Synthesis method for linkages with center of mass at invariant link point—pantograph based mechanisms. *Mechanism and machine theory*, 48:15–28. 12

van der Wijk, V., Herder, J. L., and Demeulenaere, B. (2009). Comparison of various dynamic balancing principles regarding additional mass and additional inertia. *Journal of mechanisms and robotics*, 1(4). 12, 70, 83

Van Der Wijk, V., Krut, S., Pierrot, F., and Herder, J. L. (2013). Design and experimental evaluation of a dynamically balanced redundant planar 4-rrr parallel manipulator. *The International Journal of Robotics Research*, 32(6):744–759. 12

Van Silfhout, R. G. (1999). High-precision hydraulic stewart platform. *Review of scientific instruments*, 70(8):3488–3494. 4

Varalakshmi, K. and Srinivas, J. (2014). Optimized configurations of kinematically redundant planar parallel manipulator following a desired trajectory. *Procedia Technology*, 14:133–140. 10

Waldron, K., Wang, S.-L., and Bolin, S. (1985). A study of the jacobian matrix of serial manipulators. *Journal of Mechnical Design*, 107(2):230–237. 5

Wang, J. and Gosselin, C. m. M. (2004). Kinematic analysis and design of kinematically redundant parallel mechanisms. *J. Mech. Des.*, 126(1):109–118. 7

Wapler, M., Urban, V., Weisener, T., Stallkamp, J., Dürr, M., and Hiller, A. (2003). A stewart platform for precision surgery. *Transactions of the Institute of Measurement and Control*, 25(4):329–334. 4

Watson, P. (1984). Flight simulators-the grand illusion. *Electron. Aust*, 46(4):12–17. 3

Wavering, A. J. (1999). Parallel kinematic machine research at nist: past, present, and future. In *Parallel kinematic machines*, pages 17–31. Springer. 4

Wen, J. T. and O'Brien, J. F. (2003). Singularities in three-legged platform-type parallel mechanisms. *IEEE Transactions on Robotics and Automation*, 19(4):720–726. 5

Wu, J., Wang, J., Wang, L., and Li, T. (2009). Dynamics and control of a planar 3-dof parallel manipulator with actuation redundancy. *Mechanism and Machine Theory*, 44(4):835–849. 6

Wu, Y. and Gosselin, C. (2005). Design of reactionless 3-dof and 6-dof parallel manipulators using parallelepiped mechanisms. *IEEE Transactions on Robotics*, 21(5):821–833. 11

Wu, Y. and Gosselin, C. M. (2007). On the dynamic balancing of multi-dof parallel mechanisms with multiple legs. *ASME Journal of Mechanical Design*, 129(2):234–238. 12, 75

Yakey, J. H., LaValle, S. M., and Kavraki, L. E. (2001). Randomized path planning for linkages with closed kinematic chains. *IEEE Transactions on Robotics and Automation*, 17(6):951–958. 10

Zanganeh, K. E. and Angeles, J. (1994a). Instantaneous kinematics and design of a novel redundant parallel manipulator. In *Proceedings of the 1994 IEEE International Conference on Robotics and Automation*, pages 3043–3048. IEEE. 5

Zanganeh, K. E. and Angeles, J. (1994b). Mobility and position analyses of a novel redundant parallel manipulator. In *Proceedings of the 1994 IEEE International Conference on Robotics and Automation*, pages 3049–3054. IEEE. 7

Zlatanov, D., Bonev, I. A., and Gosselin, C. M. (2002). Constraint singularities of parallel mechanisms. In *Proceedings 2002 IEEE International Conference on Robotics and Automation*, volume 1, pages 496–502. IEEE. 33

Zlatanov, D., Fenton, R. G., and Benhabib, B. (1994). Singularity analysis of mechanisms and robots via a motion-space model of the instantaneous kinematics. In *Proceedings of the 1994 IEEE International Conference on Robotics and Automation*, pages 980–985. IEEE. 4, 5, 9

Zlatanov, D. S. (1999). *Generalized singularity analysis of mechanisms.* University of Toronto. 4

Appendix A

Detailed Jacobian Calculations

A.1 1^{st} Planar Case

Firstly, the following vector loop equations are formed:

$$\mathbf{p}_e = \mathbf{p}_1 + \mathbf{p}_{1,6} + \mathbf{p}_{6,e} \tag{A.1}$$

$$\mathbf{p}_e = \mathbf{p}_2 + \mathbf{p}_{2,7} + \mathbf{p}_{7,e} \tag{A.2}$$

$$\mathbf{p}_e = \mathbf{p}_3 + \mathbf{p}_{3,4} + \mathbf{p}_{4,6} + \mathbf{p}_{6,e} \tag{A.3}$$

$$\mathbf{p}_e = \mathbf{p}_3 + \mathbf{p}_{3,5} + \mathbf{p}_{5,7} + \mathbf{p}_{7,e} \tag{A.4}$$

where $\mathbf{p}_{i,j}$ denotes the vector from P_i to P_j, $\mathbf{p}_e$ denotes the position vector of P_e, and $\mathbf{p}_i$ denotes the position vector of P_i. Then, as the distance between the end revolute joints of leg i is given by ρ_i, the following relation is obtained

$$\rho_i^2 = (\mathbf{p}_k - \mathbf{p}_j)^T(\mathbf{p}_k - \mathbf{p}_j) \tag{A.5}$$

where $\mathbf{p}_j$ and $\mathbf{p}_k$ denote the end revolute joints of leg i. Given this, equations (A.1-A.4) can be transformed into

$$\mathbf{p}_{1,6}^T(\mathbf{p}_e - \mathbf{p}_1 - \mathbf{p}_{6,e}) = \rho_1^2, \tag{A.6}$$

$$\mathbf{p}_{2,7}^T(\mathbf{p}_e - \mathbf{p}_2 - \mathbf{p}_{7,e}) = \rho_2^2, \tag{A.7}$$

$$\mathbf{p}_{4,6}^T(\mathbf{p}_e - \mathbf{p}_3 - \mathbf{p}_{3,4} - \mathbf{p}_{6,e}) = \rho_3^2, \tag{A.8}$$

$$\mathbf{p}_{5,7}^T(\mathbf{p}_e - \mathbf{p}_3 - \mathbf{p}_{3,5} - \mathbf{p}_{7,e}) = \rho_4^2 \tag{A.9}$$

and by differentiating, we obtain

$$\mathbf{p}_{1,6}^T(\dot{\mathbf{p}}_e - \dot{\mathbf{p}}_{6,e}) = \rho_1\dot{\rho}_1, \tag{A.10}$$

$$\mathbf{p}_{2,7}^T(\dot{\mathbf{p}}_e - \dot{\mathbf{p}}_{7,e}) = \rho_2\dot{\rho}_2, \tag{A.11}$$

$$\mathbf{p}_{4,6}^T(\dot{\mathbf{p}}_e - \dot{\mathbf{p}}_{3,4} - \dot{\mathbf{p}}_{6,e}) = \rho_3\dot{\rho}_3, \tag{A.12}$$

$$\mathbf{p}_{5,7}^T(\dot{\mathbf{p}}_e - \dot{\mathbf{p}}_{3,5} - \dot{\mathbf{p}}_{7,e}) = \rho_4\dot{\rho}_4. \tag{A.13}$$

Since the output of the robot is the 3-dimensional velocity vector, $\dot{\mathbf{c}} = (\dot{x}, \dot{y}, \dot{\phi})^T$, and the input is the 4-dimensional velocity vector, $\dot{\mathbf{q}} = (\dot{\rho}_1, \dot{\rho}_2, \dot{\rho}_3, \dot{\rho}_4)^T$, the Jacobian matrices, $\mathbf{J}$ and $\mathbf{K}$, are of dimension 3×3 and 3×4, respectively. The first two rows are formed by equations (A.10) and (A.11), whereas the third row is formed by combining equations (A.12) and (A.13) through the elimination of $\dot{\mathbf{p}}_{3,5}$; the vector which corresponds to the redundant output variable.

Since P_3, P_4, and P_5 are all connected to the same ternary link, the following relation exists:

$$\mathbf{p}_{3,4} = \lambda\mathbf{M}\mathbf{p}_{3,5} \tag{A.14}$$

where

$$\lambda = \frac{d_{3,4}}{d_{3,5}},$$

$$\mathbf{M} = \begin{bmatrix} cos(\delta) & -sin(\delta) \\ sin(\delta) & cos(\delta) \end{bmatrix},$$

and δ is the angle taken anti-clockwise from $\mathbf{p}_{3,5}$ to $\mathbf{p}_{3,4}$. Using this relation, equations (A.12) and (A.13) can be combined to obtain

$$\begin{bmatrix} \mathbf{p}_{4,6}^T(\dot{\mathbf{p}}_e - \dot{\mathbf{p}}_{6,e}) - \rho_3\dot{\rho}_3 \\ \mathbf{p}_{5,7}^T(\dot{\mathbf{p}}_e - \dot{\mathbf{p}}_{7,e}) - \rho_4\dot{\rho}_4 \end{bmatrix} = \begin{bmatrix} \mathbf{p}_{4,6}^T\lambda\mathbf{M} \\ \mathbf{p}_{5,7}^T \end{bmatrix} \dot{\mathbf{p}}_{3,5}, \tag{A.15}$$

and then $\dot{\mathbf{p}}_{3,5}$ can be made the subject by

$$\dot{\mathbf{p}}_{3,5} = \mathbf{N} \begin{bmatrix} \mathbf{p}_{4,6}^T(\dot{\mathbf{p}}_e - \dot{\mathbf{p}}_{6,e}) - \rho_3\dot{\rho}_3 \\ \mathbf{p}_{5,7}^T(\dot{\mathbf{p}}_e - \dot{\mathbf{p}}_{7,e}) - \rho_4\dot{\rho}_4 \end{bmatrix}, \tag{A.16}$$

where

$$\mathbf{N} = \begin{bmatrix} \mathbf{p}_{4,6}^T\lambda\mathbf{M} \\ \mathbf{p}_{5,7}^T \end{bmatrix}^{-1}.$$

Since the distance between P_3 and P_5 is constant,

$$\mathbf{p}_{3,5}^T\dot{\mathbf{p}}_{3,5} = 0. \tag{A.17}$$

Given that

$$\dot{\mathbf{p}}_e = \begin{bmatrix} \dot{x} \\ \dot{y} \end{bmatrix}, \tag{A.18}$$

$$\dot{\mathbf{p}}_{i,e} = \mathbf{E}\mathbf{p}_{i,e}\dot{\phi}, \qquad i = 6, 7, \tag{A.19}$$

where

$$\mathbf{E} = \begin{bmatrix} 0 & -1 \\ 1 & 0 \end{bmatrix},$$

by substituting (A.16) into (A.17), and expanding the velocity vectors, we obtain

$$\mathbf{p}_{3,5}^T\mathbf{N}\begin{bmatrix} \mathbf{p}_{4,6}^T \\ \mathbf{p}_{5,7}^T \end{bmatrix}\begin{bmatrix} \dot{x} \\ \dot{y} \end{bmatrix} - \mathbf{p}_{3,5}^T\mathbf{N}\begin{bmatrix} \mathbf{p}_{4,6}^T\mathbf{E}\mathbf{p}_{6,e} \\ \mathbf{p}_{5,7}^T\mathbf{E}\mathbf{p}_{7,e} \end{bmatrix}\dot{\phi} = \mathbf{p}_{3,5}^T\mathbf{N}\begin{bmatrix} \rho_3\dot{\rho}_3 \\ \rho_4\dot{\rho}_4 \end{bmatrix}. \tag{A.20}$$

By similarly expanding the velocity vectors of equations (A.6) and (A.7), the Jacobian matrices $\mathbf{J}$ and $\mathbf{K}$ are formed.

$$\mathbf{J} = \begin{bmatrix} \mathbf{p}_{1,6}^T & -\mathbf{p}_{1,6}^T\mathbf{E}\mathbf{p}_{6,e} \\ \mathbf{p}_{2,7}^T & -\mathbf{p}_{2,7}^T\mathbf{E}\mathbf{p}_{7,e} \\ \mathbf{p}_{3,5}^T\mathbf{N}\begin{bmatrix} \mathbf{p}_{4,6}^T \\ \mathbf{p}_{5,7}^T \end{bmatrix} & -\mathbf{p}_{3,5}^T\mathbf{N}\begin{bmatrix} \mathbf{p}_{4,6}^T\mathbf{E}\mathbf{p}_{6,e} \\ \mathbf{p}_{5,7}^T\mathbf{E}\mathbf{p}_{7,e} \end{bmatrix} \end{bmatrix} \tag{A.21}$$

and

$$\mathbf{K} = \begin{bmatrix} \rho_1 & 0 & 0 & 0 \\ 0 & \rho_2 & 0 & 0 \\ 0 & 0 & \mathbf{p}_{3,5}^T\mathbf{N}\begin{bmatrix} \rho_3 & 0 \\ 0 & \rho_4 \end{bmatrix} \end{bmatrix} \tag{A.22}$$

A.2 Spatial Case

A unit vector, $\mathbf{e}_i$, is defined along the axis which passes through the base joints of redundant leg i, such that

$$\mathbf{e}_i = \frac{\mathbf{a}_{i,2} - \mathbf{a}_{i,1}}{\|\mathbf{a}_{i,2} - \mathbf{a}_{i,1}\|}. \tag{A.23}$$

The positions of the joints on the platform in the base frame are described by the position of the origin of the moving frame, $\mathbf{p}_i$, the orientation of the platform, given by the rotation matrix $\mathbf{Q}$, and the positions of the platform joints in the moving frame, $\mathbf{v}_{i,0}$, such that

$$\mathbf{b}_i = \mathbf{p} + \mathbf{Q}\mathbf{v}_{i,0} \tag{A.24}$$

where $i = 1, ..., 6$. The length between the end joints of the i^{th} non-redundant leg, ρ_i, is described by the relation

$$(\mathbf{b}_i - \mathbf{a}_i)^T(\mathbf{b}_i - \mathbf{a}_i) = \rho_i^2, \qquad i = 4, 5, 6 \tag{A.25}$$

and by differentiating this equation, one obtains

$$(\mathbf{b}_i - \mathbf{a}_i)^T \dot{\mathbf{b}}_i = \rho_i \dot{\rho}_i. \tag{A.26}$$

Taking the derivative of (A.24) and substituting the result into (A.26), the following is obtained;

$$(\mathbf{b}_i - \mathbf{a}_i)^T \dot{\mathbf{p}} + [\mathbf{Q}\mathbf{v}_{i,0} \times (\mathbf{b}_i - \mathbf{a}_i)]^T \boldsymbol{\omega} = \rho_i \dot{\rho}_i. \tag{A.27}$$

Equation (A.27) is used to construct the rows of the Jacobian which correspond to the non-redundant legs of the manipulator. In this case, the output and input velocity vectors of $\mathbf{J}\dot{\mathbf{c}} = \mathbf{K}\dot{\mathbf{q}}$ are given by $\dot{\mathbf{c}} = (\dot{\mathbf{p}}^T, \boldsymbol{\omega}^T)^T$, describing the linear and angular velocity of the platform, and $\dot{\mathbf{q}} = (\dot{\rho}_{1,1}, \dot{\rho}_{1,2}, \dot{\rho}_{2,1}, \dot{\rho}_{2,2}, \dot{\rho}_{3,1}, \dot{\rho}_{3,2}, \dot{\rho}_4, \dot{\rho}_5, \dot{\rho}_6)^T$, describing the vector of active joint velocities.

For the i^{th} redundant leg, the following constraint equations are written

$$(\mathbf{s}_i - \mathbf{a}_{i,j})^T (\mathbf{s}_i - \mathbf{a}_{i,j}) = \rho_{i,j}^2, \qquad i = 1, 2, 3, \tag{A.28}$$

$$(\mathbf{s}_i - \mathbf{b}_i)^T (\mathbf{s}_i - \mathbf{b}_i) = l_i^2, \qquad i = 1, 2, 3, \tag{A.29}$$

where l_i denotes the length of the link which joins S_i and B_i, and $j = 1, 2$. Given that the joints $A_{i,1}$, $A_{i,2}$, S_i, and B_i are coplanar, the following relationship must hold

$$[(\mathbf{b}_i - \mathbf{a}_{i,1}) \times \mathbf{e}_i]^T (\mathbf{s}_i - \mathbf{a}_{i,1}) = 0. \tag{A.30}$$

By differentiating equations (A.28) and (A.30), the following is obtained

$$\mathbf{H}_i \dot{\mathbf{s}}_i = \mathbf{w}_i, \tag{A.31}$$

where

$$\mathbf{H}_i = \begin{bmatrix} (\mathbf{s}_i - \mathbf{a}_{i,1})^T \\ (\mathbf{s}_i - \mathbf{a}_{i,2})^T \\ [(\mathbf{b}_i - \mathbf{a}_{i,1}) \times \mathbf{e}_i]^T \end{bmatrix}, \tag{A.32}$$

and

$$\mathbf{w}_i = \begin{bmatrix} \rho_{i,1}\dot{\rho}_{i,1} \\ \rho_{i,2}\dot{\rho}_{i,2} \\ [(\mathbf{s}_i - \mathbf{a}_{i,1}) \times \mathbf{e}_i]^T \dot{\mathbf{b}}_i \end{bmatrix}. \tag{A.33}$$

Equation (A.31) is solved for $\dot{\mathbf{s}}_i$ by taking the matrix inverse of $\mathbf{H}_i$, such that

$$\dot{\mathbf{s}}_i = \mathbf{H}_i^{-1} \mathbf{w}_i, \tag{A.34}$$

where $\mathbf{H}_i^{-1}$ can be expressed as

$$\mathbf{H}_i^{-1} = \frac{Adj(\mathbf{H}_i)}{det(\mathbf{H}_i)}, \tag{A.35}$$

$Adj(\mathbf{H}_i)$ is the adjoint of matrix $\mathbf{H}_i$ and $det(\mathbf{H}_i)$ is the determinant, which herein will be denoted by μ_i. These can be expressed algebraically by

$$det(\mathbf{H}_i) = \mu_i = [(\mathbf{s}_i - \mathbf{a}_{i,1}) \times (\mathbf{s}_i - \mathbf{a}_{i,2})]^T [(\mathbf{b}_i - \mathbf{a}_{i,1}) \times \mathbf{e}_i] \tag{A.36}$$

and

$$Adj(\mathbf{H}_i) = \begin{bmatrix} \mathbf{h}_{i,1} & \mathbf{h}_{i,2} & \mathbf{h}_{i,3} \end{bmatrix} \tag{A.37}$$

where

$$\mathbf{h}_{i,1} = (\mathbf{s}_i - \mathbf{a}_{i,2}) \times [(\mathbf{b}_i - \mathbf{a}_{i,1}) \times \mathbf{e}_i], \tag{A.38}$$

$$\mathbf{h}_{i,2} = [(\mathbf{b}_i - \mathbf{a}_{i,1}) \times \mathbf{e}_i] \times (\mathbf{s}_i - \mathbf{a}_{i,1}), \tag{A.39}$$

$$\mathbf{h}_{i,3} = (\mathbf{s}_i - \mathbf{a}_{i,1}) \times (\mathbf{s}_i - \mathbf{a}_{i,2}). \tag{A.40}$$

Now equation (A.34) can be rewritten as

$$\dot{\mathbf{s}}_i = \frac{1}{\mu_i}(\mathbf{h}_{i,1}\rho_{i,1}\dot{\rho}_{i,1} + \mathbf{h}_{i,2}\rho_{i,2}\dot{\rho}_{i,2} + \mathbf{h}_{i,3}[(\mathbf{s}_i - \mathbf{a}_{i,1}) \times \mathbf{e}_i]^T \dot{\mathbf{b}}_i). \tag{A.41}$$

By taking the derivative of (A.29), one obtains

$$(\mathbf{s}_i - \mathbf{b}_i)^T \dot{\mathbf{s}}_i = (\mathbf{s}_i - \mathbf{b}_i)^T \dot{\mathbf{b}}_i, \tag{A.42}$$

and substituting (A.41) and the derivative of (A.24) into (A.42) gives

$$(\mathbf{s}_i - \mathbf{b}_i)^T \dot{\mathbf{p}} + [\mathbf{Q}\mathbf{v}_{i,0} \times (\mathbf{s}_i - \mathbf{b}_i)]^T \boldsymbol{\omega} = (\mathbf{s}_i - \mathbf{b}_i)^T \mathbf{m}_i \dot{\rho}_{i,1} + (\mathbf{s}_i - \mathbf{b}_i)^T \mathbf{n}_i \dot{\rho}_{i,2} \tag{A.43}$$

where

$$\mathbf{m}_i = \frac{\rho_{i,1}}{\mu_i}[(\mathbf{s}_i - \mathbf{a}_{i,2}) \times [(\mathbf{b}_i - \mathbf{a}_{i,1}) \times \mathbf{e}_i]], \tag{A.44}$$

$$\mathbf{n}_i = \frac{\rho_{i,2}}{\mu_i}[[(\mathbf{b}_i - \mathbf{a}_{i,1}) \times \mathbf{e}_i] \times (\mathbf{s}_i - \mathbf{a}_{i,1})]. \tag{A.45}$$

Equation (A.43) is used to construct the first three rows of the Jacobian which correspond to the redundant legs, and equation (A.27) makes up the latter three rows, corresponding to the non-redundant legs, such that the resulting Jacobian matrices $\mathbf{J}$ and $\mathbf{K}$, which are of dimension 6×6 and 6×9, are given by

$$\mathbf{J} = \begin{bmatrix} (\mathbf{s}_1 - \mathbf{b}_1)^T & [\mathbf{Q}\mathbf{v}_{1,0} \times (\mathbf{s}_1 - \mathbf{b}_1)^T] \\ (\mathbf{s}_2 - \mathbf{b}_2)^T & [\mathbf{Q}\mathbf{v}_{2,0} \times (\mathbf{s}_2 - \mathbf{b}_2)^T] \\ (\mathbf{s}_3 - \mathbf{b}_3)^T & [\mathbf{Q}\mathbf{v}_{3,0} \times (\mathbf{s}_3 - \mathbf{b}_3)^T] \\ (\mathbf{b}_4 - \mathbf{a}_4)^T & [\mathbf{Q}\mathbf{v}_{4,0} \times (\mathbf{b}_4 - \mathbf{a}_4)^T] \\ (\mathbf{b}_5 - \mathbf{a}_5)^T & [\mathbf{Q}\mathbf{v}_{5,0} \times (\mathbf{b}_5 - \mathbf{a}_5)^T] \\ (\mathbf{b}_6 - \mathbf{a}_6)^T & [\mathbf{Q}\mathbf{v}_{6,0} \times (\mathbf{b}_6 - \mathbf{a}_6)^T] \end{bmatrix} \tag{A.46}$$

and

$$\mathbf{K} = \begin{bmatrix} \mathbf{K}_1 & \mathbf{0} \\ \mathbf{0} & \mathbf{K}_2 \end{bmatrix} \tag{A.47}$$

where

$$\mathbf{K}_1 = \begin{bmatrix} \mathbf{r}_1^T\mathbf{m}_1 & \mathbf{r}_1^T\mathbf{n}_1 & 0 & 0 \\ 0 & \mathbf{r}_2^T\mathbf{m}_2 & \mathbf{r}_2^T\mathbf{n}_2 & 0 \\ 0 & 0 & \mathbf{r}_3^T\mathbf{m}_3 & \mathbf{r}_3^T\mathbf{n}_3 \end{bmatrix}, \tag{A.48}$$

$\mathbf{r}_i = (\mathbf{s}_i - \mathbf{b}_i)$, and $\mathbf{K}_2 = diag[\rho_4, \rho_5, \rho_6]$.

A.3 2^{nd} Planar Case

Rotation matrices $\mathbf{Q}$ and $\mathbf{R}$ are formed to define the orientation of the platform and link A_3S,

$$\mathbf{Q} = \begin{bmatrix} cos(\phi) & -sin(\phi) \\ sin(\phi) & cos(\phi) \end{bmatrix}, \tag{A.49}$$

$$\mathbf{R} = \begin{bmatrix} cos(\gamma) & -sin(\gamma) \\ sin(\gamma) & cos(\gamma) \end{bmatrix}. \tag{A.50}$$

The positions of the platform joints and point S are given by

$$\mathbf{b}_i = \mathbf{p} + \mathbf{Q}\boldsymbol{\nu}_{0,i}, \tag{A.51}$$

$$\mathbf{s} = \mathbf{a}_3 + \mathbf{R}\mathbf{s}_0, \tag{A.52}$$

where $\boldsymbol{\nu}_{0,i}$ and $\mathbf{s}_0$ are the positions of joints B_i in the moving frame and joint S in the fixed frame, respectively. The following constraint equations are then formed

$$(\mathbf{b}_i - \mathbf{a}_i)^T(\mathbf{b}_i - \mathbf{a}_i) = \rho_i^2, \qquad i = 1, 2 \tag{A.53}$$

$$(\mathbf{b}_i - \mathbf{s})^T(\mathbf{b}_i - \mathbf{s}) = \rho_i^2, \qquad i = 3, 4 \tag{A.54}$$

$$(\mathbf{s} - \mathbf{a}_3)^T(\mathbf{s} - \mathbf{a}_3) = l^2. \tag{A.55}$$

Then by differentiating (A.51)-(A.55) with respect to time, the following are obtained

$$(\mathbf{b}_i - \mathbf{a}_i)^T(\dot{\mathbf{p}} + \dot{\phi}\mathbf{E}\nu_i) = \rho_i\dot{\rho}_i, \qquad i = 1, 2 \tag{A.56}$$

$$\mathbf{f}^T(\dot{\mathbf{p}} + \dot{\phi}\mathbf{E}\nu_3 - \dot{\mathbf{s}}) = \rho_3\dot{\rho}_3, \tag{A.57}$$

$$\mathbf{m}^T(\dot{\mathbf{p}} + \dot{\phi}\mathbf{E}\nu_4 - \dot{\mathbf{s}}) = \rho_4\dot{\rho}_4, \tag{A.58}$$

$$(\mathbf{s} - \mathbf{a}_3)^T\dot{\mathbf{s}} = 0, \tag{A.59}$$

where

$$\mathbf{f} = \mathbf{b}_3 - \mathbf{s},$$
$$\mathbf{m} = \mathbf{b}_4 - \mathbf{s},$$
$$\boldsymbol{\nu}_i = \mathbf{Q}\boldsymbol{\nu}_{0,i}.$$

Equations (A.57) and (A.58) are then combined to form the matrix equation

$$\mathbf{G}\dot{\mathbf{c}} - \mathbf{h} = \mathbf{H}\dot{\mathbf{s}} \tag{A.60}$$

where

$$\mathbf{H} = \begin{bmatrix} \mathbf{f}^T \\ \mathbf{m}^T \end{bmatrix},$$
$$\mathbf{h} = \begin{bmatrix} \rho_3\dot{\rho}_3 \\ \rho_4\dot{\rho}_4 \end{bmatrix},$$
$$\mathbf{G} = \begin{bmatrix} \mathbf{f}^T & \mathbf{f}^T\mathbf{E}\boldsymbol{\nu}_3 \\ \mathbf{m}^T & \mathbf{m}^T\mathbf{E}\boldsymbol{\nu}_4 \end{bmatrix}.$$

Equation (A.60) is then rearranged to make $\dot{\mathbf{s}}$ the subject by taking the inverse of matrix $\mathbf{H}$, such that

$$\dot{\mathbf{s}} = \mathbf{N}(\mathbf{G}\dot{\mathbf{c}} - \mathbf{h}) \tag{A.61}$$

where

$$\mathbf{N} = \mathbf{H}^{-1} = \frac{1}{\mathbf{f}^T\mathbf{E}\mathbf{m}} \begin{bmatrix} \mathbf{E}\mathbf{m} & -\mathbf{E}\mathbf{f} \end{bmatrix}.$$

Substituting (A.61) into (A.59) then gives

$$(\mathbf{s} - \mathbf{a}_3)^T\mathbf{N}\mathbf{G}\dot{\mathbf{c}} = (\mathbf{s} - \mathbf{a}_3)^T \begin{bmatrix} \frac{\mathbf{E}\mathbf{m}\rho_3}{\mathbf{f}^T\mathbf{E}\mathbf{m}} & \frac{-\mathbf{E}\mathbf{f}\rho_4}{\mathbf{f}^T\mathbf{E}\mathbf{m}} \end{bmatrix} \begin{bmatrix} \dot{\rho}_3 \\ \dot{\rho}_4 \end{bmatrix} \tag{A.62}$$

where

$$\mathbf{N}\mathbf{G} = \frac{\mathbf{E}}{\mathbf{f}^T\mathbf{E}\mathbf{m}} \begin{bmatrix} (\mathbf{m}\mathbf{f}^T - \mathbf{f}\mathbf{m}^T) & (\mathbf{m}\mathbf{f}^T\mathbf{E}\boldsymbol{\nu}_3 - \mathbf{f}\mathbf{m}^T\mathbf{E}\boldsymbol{\nu}_4) \end{bmatrix}. \tag{A.63}$$

Since

$$\mathbf{m}\mathbf{f}^T - \mathbf{f}\mathbf{m}^T = -(\mathbf{f}^T\mathbf{E}\mathbf{m})\mathbf{E}, \tag{A.64}$$
$$\boldsymbol{\nu}_3 = \mathbf{s} - \mathbf{p} + \mathbf{f}, \tag{A.65}$$
$$\boldsymbol{\nu}_4 = \mathbf{s} - \mathbf{p} + \mathbf{m}, \tag{A.66}$$

one may obtain

$$\begin{aligned}\mathbf{m}\mathbf{f}^T\mathbf{E}\boldsymbol{\nu}_3 - \mathbf{f}\mathbf{m}^T\mathbf{E}\boldsymbol{\nu}_4 = & \\ & (\mathbf{m}\mathbf{f}^T\mathbf{E}(\mathbf{s}-\mathbf{p}+\mathbf{f}) - \mathbf{f}\mathbf{m}^T\mathbf{E}(\mathbf{s}-\mathbf{p}+\mathbf{m})) \qquad \text{(A.67)}\\ & = (\mathbf{f}^T\mathbf{E}\mathbf{m})(\mathbf{s}-\mathbf{p}) \qquad \text{(A.68)}\end{aligned}$$

which means that (A.63) becomes

$$\mathbf{NG} = \begin{bmatrix}\mathbf{1} & \mathbf{E}(\mathbf{s}-\mathbf{p})\end{bmatrix} \tag{A.69}$$

where $\mathbf{1}$ denotes the 2×2 identity matrix. The first two rows of the Jacobian Matrices, $\mathbf{J}$ and $\mathbf{K}$, are then formed from (A.56), and the third row is obtained by substituting (A.69) into (A.62), such that

$$\mathbf{J} = \begin{bmatrix}(\mathbf{b}_1-\mathbf{a}_1)^T & (\mathbf{b}_1-\mathbf{a}_1)^T\mathbf{E}\nu_1 \\ (\mathbf{b}_2-\mathbf{a}_2)^T & (\mathbf{b}_2-\mathbf{a}_2)^T\mathbf{E}\nu_2 \\ (\mathbf{s}-\mathbf{a}_3)^T & (\mathbf{s}-\mathbf{a}_3)^T\mathbf{E}(\mathbf{s}-\mathbf{p})\end{bmatrix} \tag{A.70}$$

and

$$\mathbf{K} = \begin{bmatrix}\rho_1 & 0 & 0 & 0 \\ 0 & \rho_2 & 0 & 0 \\ 0 & 0 & k_{33} & k_{34}\end{bmatrix} \tag{A.71}$$

where

$$k_{33} = \frac{(\mathbf{s}-\mathbf{a}_3)^T\mathbf{E}\mathbf{m}\rho_3}{\mathbf{f}^T\mathbf{E}\mathbf{m}} \tag{A.72}$$

and

$$k_{34} = \frac{-(\mathbf{s}-\mathbf{a}_3)^T\mathbf{E}\mathbf{f}\rho_4}{\mathbf{f}^T\mathbf{E}\mathbf{m}}. \tag{A.73}$$

Appendix B

Rigidity Matrices

B.1 1^{st} Planar Case

The columns correspond to the coordinates of the vertices v_1 to v_7, which correspond to the joints P_1 to P_7 of the mechanism. Each row corresponds to the an edge, where the term $e_{i,j}$ denotes the transpose of the two-dimensional position vector from v_i to v_j, such that $e_{i,j} = (v_{j,x} - v_{i,x}, v_{j,y} - v_{i,y})$, and 0 denotes the two-dimensional row vector of zeros.

$$M = \begin{array}{c} \begin{matrix} v_1 & v_2 & v_3 & v_4 & v_5 & v_6 & v_7 \end{matrix} \\ \begin{pmatrix} e_{1,2} & -e_{1,2} & 0 & 0 & 0 & 0 & 0 \\ e_{1,3} & 0 & -e_{1,3} & 0 & 0 & 0 & 0 \\ e_{1,6} & 0 & 0 & 0 & 0 & -e_{1,6} & 0 \\ 0 & e_{2,3} & -e_{2,3} & 0 & 0 & 0 & 0 \\ 0 & e_{2,7} & 0 & 0 & 0 & 0 & -e_{2,7} \\ 0 & 0 & e_{3,4} & -e_{3,4} & 0 & 0 & 0 \\ 0 & 0 & e_{3,5} & 0 & -e_{3,5} & 0 & 0 \\ 0 & 0 & 0 & e_{4,5} & -e_{4,5} & 0 & 0 \\ 0 & 0 & 0 & e_{4,6} & 0 & -e_{4,6} & 0 \\ 0 & 0 & 0 & 0 & e_{5,7} & 0 & -e_{5,7} \\ 0 & 0 & 0 & 0 & 0 & e_{6,7} & -e_{6,7} \end{pmatrix} \end{array}.$$

B.2 Spatial Case

The rigidity matrix of the spatial case is slightly more complex. Unlike the planar cases, there is not a straight one-to-one mapping between the joints and the vertices, as discussed in section 2 of chapter 3. When the prismatic actuators are locked, the manipulator

consists of 15 joints (counting coincident joints only once), whereas the corresponding graph is made up of 36 vertices (labelled $v1$ to $v36$). This is because only the spherical joints correspond to single vertices, the revolute joints on the other hand correspond to two vertices and the universal joints correspond to three vertices, as discussed in section 2 of chapter 3.

Each universal joint corresponds to the vertex triple (v_i,v_j,v_k), where the axis attached to the base is defined by (v_i,v_j) and the other axis is defined by (v_j,v_k). Vertex triples (v_1,v_2,v_{19}), (v_3,v_4,v_{20}), (v_5,v_6,v_{21}), (v_7,v_8,v_{22}), (v_9,v_{10},v_{23}), (v_{11},v_{12},v_{24}), (v_{13},v_{14},v_{25}), (v_{15},v_{16},v_{26}), and (v_{17},v_{18},v_{27}) denote $A_{1,1}$, $A_{1,2}$, $A_{2,1}$, $A_{2,2}$, $A_{3,1}$, $A_{3,2}$, A_4, A_5, and A_6, respectively. The revolute joints at S_1, S_2, and S_3 are defined by the vertex pairings (v_{28},v_{29}), (v_{30},v_{31}), and (v_{32},v_{33}), and the spherical joints on the platform, B_1, B_2, and B_3, are defined by v_{34}, v_{35}, and v_{36}.

The columns correspond to the coordinates of the vertices, and each row corresponds to an edge, where the term $e_{i,j}$ denotes the transpose of the three-dimensional position vector from v_i to v_j, such that $e_{i,j} = (v_{j,x} - v_{i,x}, v_{j,y} - v_{i,y}, v_{j,z} - v_{i,z})$, and 0 denotes the three-dimensional row vector of zeros.

Firstly, we compose the rigidity matrix of the graph corresponding to the base joints, $\mathbf{M}_1$.

$$M_1 = \begin{array}{c} \begin{array}{cccccccccccccccccc} v_1 & v_2 & v_3 & v_4 & v_5 & v_6 & v_7 & v_8 & v_9 & v_{10} & v_{11} & v_{12} & v_{13} & v_{14} & v_{15} & v_{16} & v_{17} & v_{18} \end{array} \\ \begin{pmatrix} e_{1,2} & -e_{1,2} & 0 & 0 & 0 & 0 & 0 & 0 & 0 & 0 & 0 & 0 & 0 & 0 & 0 & 0 & 0 & 0 \\ e_{1,12} & 0 & 0 & 0 & 0 & 0 & 0 & 0 & 0 & 0 & 0 & -e_{1,12} & 0 & 0 & 0 & 0 & 0 & 0 \\ e_{1,14} & 0 & 0 & 0 & 0 & 0 & 0 & 0 & 0 & 0 & 0 & 0 & 0 & -e_{1,14} & 0 & 0 & 0 & 0 \\ e_{1,18} & 0 & 0 & 0 & 0 & 0 & 0 & 0 & 0 & 0 & 0 & 0 & 0 & 0 & 0 & 0 & 0 & -e_{1,18} \\ 0 & e_{2,7} & 0 & 0 & 0 & 0 & -e_{2,7} & 0 & 0 & 0 & 0 & 0 & 0 & 0 & 0 & 0 & 0 & 0 \\ 0 & e_{2,8} & 0 & 0 & 0 & 0 & 0 & -e_{2,8} & 0 & 0 & 0 & 0 & 0 & 0 & 0 & 0 & 0 & 0 \\ 0 & e_{2,11} & 0 & 0 & 0 & 0 & 0 & 0 & 0 & 0 & -e_{2,11} & 0 & 0 & 0 & 0 & 0 & 0 & 0 \\ 0 & e_{2,13} & 0 & 0 & 0 & 0 & 0 & 0 & 0 & 0 & 0 & 0 & -e_{2,13} & 0 & 0 & 0 & 0 & 0 \\ 0 & e_{2,16} & 0 & 0 & 0 & 0 & 0 & 0 & 0 & 0 & 0 & 0 & 0 & 0 & 0 & -e_{2,16} & 0 & 0 \\ 0 & e_{2,17} & 0 & 0 & 0 & 0 & 0 & 0 & 0 & 0 & 0 & 0 & 0 & 0 & 0 & 0 & -e_{2,17} & 0 \\ 0 & 0 & e_{3,4} & -e_{3,4} & 0 & 0 & 0 & 0 & 0 & 0 & 0 & 0 & 0 & 0 & 0 & 0 & 0 & 0 \\ 0 & 0 & e_{3,10} & 0 & 0 & 0 & 0 & 0 & 0 & -e_{3,10} & 0 & 0 & 0 & 0 & 0 & 0 & 0 & 0 \\ 0 & 0 & e_{3,11} & 0 & 0 & 0 & 0 & 0 & 0 & 0 & -e_{3,11} & 0 & 0 & 0 & 0 & 0 & 0 & 0 \\ 0 & 0 & e_{3,15} & 0 & 0 & 0 & 0 & 0 & 0 & 0 & 0 & 0 & 0 & 0 & -e_{3,15} & 0 & 0 & 0 \\ 0 & 0 & e_{3,16} & 0 & 0 & 0 & 0 & 0 & 0 & 0 & 0 & 0 & 0 & 0 & 0 & -e_{3,16} & 0 & 0 \\ 0 & 0 & 0 & e_{4,8} & 0 & 0 & 0 & -e_{4,8} & 0 & 0 & 0 & 0 & 0 & 0 & 0 & 0 & 0 & 0 \\ 0 & 0 & 0 & e_{4,9} & 0 & 0 & 0 & 0 & -e_{4,9} & 0 & 0 & 0 & 0 & 0 & 0 & 0 & 0 & 0 \\ 0 & 0 & 0 & e_{4,10} & 0 & 0 & 0 & 0 & 0 & -e_{4,10} & 0 & 0 & 0 & 0 & 0 & 0 & 0 & 0 \\ 0 & 0 & 0 & e_{4,15} & 0 & 0 & 0 & 0 & 0 & 0 & 0 & 0 & 0 & 0 & -e_{4,15} & 0 & 0 & 0 \\ 0 & 0 & 0 & 0 & e_{5,6} & -e_{5,6} & 0 & 0 & 0 & 0 & 0 & 0 & 0 & 0 & 0 & 0 & 0 & 0 \\ 0 & 0 & 0 & 0 & e_{5,11} & 0 & 0 & 0 & 0 & 0 & -e_{5,11} & 0 & 0 & 0 & 0 & 0 & 0 & 0 \\ 0 & 0 & 0 & 0 & e_{5,12} & 0 & 0 & 0 & 0 & 0 & 0 & -e_{5,12} & 0 & 0 & 0 & 0 & 0 & 0 \\ 0 & 0 & 0 & 0 & e_{5,14} & 0 & 0 & 0 & 0 & 0 & 0 & 0 & 0 & -e_{5,14} & 0 & 0 & 0 & 0 \\ 0 & 0 & 0 & 0 & e_{5,15} & 0 & 0 & 0 & 0 & 0 & 0 & 0 & 0 & 0 & -e_{5,15} & 0 & 0 & 0 \\ 0 & 0 & 0 & 0 & e_{5,17} & 0 & 0 & 0 & 0 & 0 & 0 & 0 & 0 & 0 & 0 & 0 & -e_{5,17} & 0 \\ 0 & 0 & 0 & 0 & 0 & e_{6,7} & -e_{6,7} & 0 & 0 & 0 & 0 & 0 & 0 & 0 & 0 & 0 & 0 & 0 \\ 0 & 0 & 0 & 0 & 0 & e_{6,12} & 0 & 0 & 0 & 0 & 0 & -e_{6,12} & 0 & 0 & 0 & 0 & 0 & 0 \\ 0 & 0 & 0 & 0 & 0 & e_{6,13} & 0 & 0 & 0 & 0 & 0 & 0 & -e_{6,13} & 0 & 0 & 0 & 0 & 0 \\ 0 & 0 & 0 & 0 & 0 & e_{6,17} & 0 & 0 & 0 & 0 & 0 & 0 & 0 & 0 & 0 & 0 & -e_{6,17} & 0 \\ 0 & 0 & 0 & 0 & 0 & 0 & e_{7,8} & -e_{7,8} & 0 & 0 & 0 & 0 & 0 & 0 & 0 & 0 & 0 & 0 \\ 0 & 0 & 0 & 0 & 0 & 0 & e_{7,18} & 0 & 0 & 0 & 0 & 0 & 0 & 0 & 0 & 0 & 0 & -e_{7,18} \\ 0 & 0 & 0 & 0 & 0 & 0 & 0 & e_{8,13} & 0 & 0 & 0 & 0 & -e_{8,13} & 0 & 0 & 0 & 0 & 0 \\ 0 & 0 & 0 & 0 & 0 & 0 & 0 & e_{8,14} & 0 & 0 & 0 & 0 & 0 & -e_{8,14} & 0 & 0 & 0 & 0 \\ 0 & 0 & 0 & 0 & 0 & 0 & 0 & e_{8,17} & 0 & 0 & 0 & 0 & 0 & 0 & 0 & 0 & -e_{8,17} & 0 \\ 0 & 0 & 0 & 0 & 0 & 0 & 0 & 0 & e_{9,10} & -e_{9,10} & 0 & 0 & 0 & 0 & 0 & 0 & 0 & 0 \\ 0 & 0 & 0 & 0 & 0 & 0 & 0 & 0 & e_{9,16} & 0 & 0 & 0 & 0 & 0 & 0 & -e_{9,16} & 0 & 0 \\ 0 & 0 & 0 & 0 & 0 & 0 & 0 & 0 & e_{9,17} & 0 & 0 & 0 & 0 & 0 & 0 & 0 & -e_{9,17} & 0 \\ 0 & 0 & 0 & 0 & 0 & 0 & 0 & 0 & 0 & e_{10,14} & 0 & 0 & 0 & -e_{10,14} & 0 & 0 & 0 & 0 \\ 0 & 0 & 0 & 0 & 0 & 0 & 0 & 0 & 0 & e_{10,15} & 0 & 0 & 0 & 0 & -e_{10,15} & 0 & 0 & 0 \\ 0 & 0 & 0 & 0 & 0 & 0 & 0 & 0 & 0 & e_{10,16} & 0 & 0 & 0 & 0 & 0 & -e_{10,16} & 0 & 0 \\ 0 & 0 & 0 & 0 & 0 & 0 & 0 & 0 & 0 & 0 & e_{11,12} & -e_{11,12} & 0 & 0 & 0 & 0 & 0 & 0 \\ 0 & 0 & 0 & 0 & 0 & 0 & 0 & 0 & 0 & 0 & e_{11,17} & 0 & 0 & 0 & 0 & 0 & -e_{11,17} & 0 \\ 0 & 0 & 0 & 0 & 0 & 0 & 0 & 0 & 0 & 0 & e_{11,18} & 0 & 0 & 0 & 0 & 0 & 0 & -e_{11,18} \\ 0 & 0 & 0 & 0 & 0 & 0 & 0 & 0 & 0 & 0 & 0 & e_{12,13} & -e_{12,13} & 0 & 0 & 0 & 0 & 0 \\ 0 & 0 & 0 & 0 & 0 & 0 & 0 & 0 & 0 & 0 & 0 & e_{12,18} & 0 & 0 & 0 & 0 & 0 & -e_{12,18} \\ 0 & 0 & 0 & 0 & 0 & 0 & 0 & 0 & 0 & 0 & 0 & 0 & e_{13,14} & -e_{13,14} & 0 & 0 & 0 & 0 \\ 0 & 0 & 0 & 0 & 0 & 0 & 0 & 0 & 0 & 0 & 0 & 0 & 0 & 0 & e_{15,16} & -e_{15,16} & 0 & 0 \\ 0 & 0 & 0 & 0 & 0 & 0 & 0 & 0 & 0 & 0 & 0 & 0 & 0 & 0 & 0 & 0 & e_{17,18} & -e_{17,18} \end{pmatrix} \end{array}.$$

The rigidity matrix corresponding to the remaining links in the mechanism has been divided into matrices $\mathbf{M}_2$ and $\mathbf{M}_3$, such that

$$
M_2 = \begin{array}{c}
\begin{array}{cccccccccccccccccc} v_1 & v_2 & v_3 & v_4 & v_5 & v_6 & v_7 & v_8 & v_9 & v_{10} & v_{11} & v_{12} & v_{13} & v_{14} & v_{15} & v_{16} & v_{17} & v_{18} \end{array} \\
\begin{pmatrix}
e_{1,19} & 0 & 0 & 0 & 0 & 0 & 0 & 0 & 0 & 0 & 0 & 0 & 0 & 0 & 0 & 0 & 0 & 0 \\
0 & e_{2,19} & 0 & 0 & 0 & 0 & 0 & 0 & 0 & 0 & 0 & 0 & 0 & 0 & 0 & 0 & 0 & 0 \\
0 & 0 & e_{3,20} & 0 & 0 & 0 & 0 & 0 & 0 & 0 & 0 & 0 & 0 & 0 & 0 & 0 & 0 & 0 \\
0 & 0 & 0 & e_{4,20} & 0 & 0 & 0 & 0 & 0 & 0 & 0 & 0 & 0 & 0 & 0 & 0 & 0 & 0 \\
0 & 0 & 0 & 0 & e_{5,21} & 0 & 0 & 0 & 0 & 0 & 0 & 0 & 0 & 0 & 0 & 0 & 0 & 0 \\
0 & 0 & 0 & 0 & 0 & e_{6,21} & 0 & 0 & 0 & 0 & 0 & 0 & 0 & 0 & 0 & 0 & 0 & 0 \\
0 & 0 & 0 & 0 & 0 & 0 & e_{7,22} & 0 & 0 & 0 & 0 & 0 & 0 & 0 & 0 & 0 & 0 & 0 \\
0 & 0 & 0 & 0 & 0 & 0 & 0 & e_{8,22} & 0 & 0 & 0 & 0 & 0 & 0 & 0 & 0 & 0 & 0 \\
0 & 0 & 0 & 0 & 0 & 0 & 0 & 0 & e_{9,23} & 0 & 0 & 0 & 0 & 0 & 0 & 0 & 0 & 0 \\
0 & 0 & 0 & 0 & 0 & 0 & 0 & 0 & 0 & e_{10,23} & 0 & 0 & 0 & 0 & 0 & 0 & 0 & 0 \\
0 & 0 & 0 & 0 & 0 & 0 & 0 & 0 & 0 & 0 & e_{11,24} & 0 & 0 & 0 & 0 & 0 & 0 & 0 \\
0 & 0 & 0 & 0 & 0 & 0 & 0 & 0 & 0 & 0 & 0 & e_{12,24} & 0 & 0 & 0 & 0 & 0 & 0 \\
0 & 0 & 0 & 0 & 0 & 0 & 0 & 0 & 0 & 0 & 0 & 0 & e_{13,25} & 0 & 0 & 0 & 0 & 0 \\
0 & 0 & 0 & 0 & 0 & 0 & 0 & 0 & 0 & 0 & 0 & 0 & 0 & e_{14,25} & 0 & 0 & 0 & 0 \\
0 & 0 & 0 & 0 & 0 & 0 & 0 & 0 & 0 & 0 & 0 & 0 & 0 & 0 & e_{15,26} & 0 & 0 & 0 \\
0 & 0 & 0 & 0 & 0 & 0 & 0 & 0 & 0 & 0 & 0 & 0 & 0 & 0 & 0 & e_{16,26} & 0 & 0 \\
0 & 0 & 0 & 0 & 0 & 0 & 0 & 0 & 0 & 0 & 0 & 0 & 0 & 0 & 0 & 0 & e_{17,27} & 0 \\
0 & 0 & 0 & 0 & 0 & 0 & 0 & 0 & 0 & 0 & 0 & 0 & 0 & 0 & 0 & 0 & 0 & e_{18,27} \\
0 & e_{2,28} & 0 & 0 & 0 & 0 & 0 & 0 & 0 & 0 & 0 & 0 & 0 & 0 & 0 & 0 & 0 & 0 \\
0 & 0 & 0 & 0 & 0 & 0 & 0 & 0 & 0 & 0 & 0 & 0 & 0 & 0 & 0 & 0 & 0 & 0 \\
0 & e_{2,29} & 0 & 0 & 0 & 0 & 0 & 0 & 0 & 0 & 0 & 0 & 0 & 0 & 0 & 0 & 0 & 0 \\
0 & 0 & 0 & 0 & 0 & 0 & 0 & 0 & 0 & 0 & 0 & 0 & 0 & 0 & 0 & 0 & 0 & 0 \\
0 & 0 & 0 & e_{4,28} & 0 & 0 & 0 & 0 & 0 & 0 & 0 & 0 & 0 & 0 & 0 & 0 & 0 & 0 \\
0 & 0 & 0 & 0 & 0 & 0 & 0 & 0 & 0 & 0 & 0 & 0 & 0 & 0 & 0 & 0 & 0 & 0 \\
0 & 0 & 0 & e_{4,29} & 0 & 0 & 0 & 0 & 0 & 0 & 0 & 0 & 0 & 0 & 0 & 0 & 0 & 0 \\
0 & 0 & 0 & 0 & 0 & 0 & 0 & 0 & 0 & 0 & 0 & 0 & 0 & 0 & 0 & 0 & 0 & 0 \\
0 & 0 & 0 & 0 & 0 & 0 & 0 & 0 & 0 & 0 & 0 & 0 & 0 & 0 & 0 & 0 & 0 & 0 \\
0 & 0 & 0 & 0 & 0 & 0 & 0 & e_{8,30} & 0 & 0 & 0 & 0 & 0 & 0 & 0 & 0 & 0 & 0 \\
0 & 0 & 0 & 0 & 0 & 0 & 0 & 0 & 0 & 0 & 0 & 0 & 0 & 0 & 0 & 0 & 0 & 0 \\
0 & 0 & 0 & 0 & 0 & 0 & 0 & e_{8,31} & 0 & 0 & 0 & 0 & 0 & 0 & 0 & 0 & 0 & 0 \\
0 & 0 & 0 & 0 & 0 & 0 & 0 & 0 & 0 & 0 & 0 & 0 & 0 & 0 & 0 & 0 & 0 & 0 \\
0 & 0 & 0 & 0 & 0 & 0 & 0 & 0 & 0 & 0 & 0 & 0 & 0 & 0 & 0 & 0 & 0 & 0 \\
0 & 0 & 0 & 0 & 0 & 0 & 0 & 0 & 0 & e_{10,30} & 0 & 0 & 0 & 0 & 0 & 0 & 0 & 0 \\
0 & 0 & 0 & 0 & 0 & 0 & 0 & 0 & 0 & 0 & 0 & 0 & 0 & 0 & 0 & 0 & 0 & 0 \\
0 & 0 & 0 & 0 & 0 & 0 & 0 & 0 & 0 & e_{10,31} & 0 & 0 & 0 & 0 & 0 & 0 & 0 & 0 \\
0 & 0 & 0 & 0 & 0 & 0 & 0 & 0 & 0 & 0 & 0 & 0 & 0 & 0 & 0 & 0 & 0 & 0 \\
0 & 0 & 0 & 0 & 0 & 0 & 0 & 0 & 0 & 0 & 0 & 0 & 0 & e_{14,32} & 0 & 0 & 0 & 0 \\
0 & 0 & 0 & 0 & 0 & 0 & 0 & 0 & 0 & 0 & 0 & 0 & 0 & 0 & 0 & 0 & 0 & 0 \\
0 & 0 & 0 & 0 & 0 & 0 & 0 & 0 & 0 & 0 & 0 & 0 & 0 & e_{14,33} & 0 & 0 & 0 & 0 \\
0 & 0 & 0 & 0 & 0 & 0 & 0 & 0 & 0 & 0 & 0 & 0 & 0 & 0 & 0 & 0 & 0 & 0 \\
0 & 0 & 0 & 0 & 0 & 0 & 0 & 0 & 0 & 0 & 0 & 0 & 0 & 0 & 0 & e_{16,32} & 0 & 0 \\
0 & 0 & 0 & 0 & 0 & 0 & 0 & 0 & 0 & 0 & 0 & 0 & 0 & 0 & 0 & 0 & 0 & 0 \\
0 & 0 & 0 & 0 & 0 & 0 & 0 & 0 & 0 & 0 & 0 & 0 & 0 & 0 & 0 & e_{16,33} & 0 & 0 \\
0 & 0 & 0 & 0 & 0 & 0 & 0 & 0 & 0 & 0 & 0 & 0 & 0 & 0 & 0 & 0 & 0 & 0 \\
0 & 0 & 0 & 0 & 0 & 0 & 0 & 0 & 0 & 0 & 0 & 0 & 0 & 0 & 0 & 0 & 0 & 0 \\
0 & 0 & 0 & 0 & 0 & 0 & 0 & 0 & 0 & 0 & 0 & 0 & 0 & 0 & 0 & 0 & 0 & e_{18,34} \\
0 & 0 & 0 & 0 & 0 & 0 & 0 & 0 & 0 & 0 & 0 & 0 & 0 & 0 & 0 & 0 & 0 & 0 \\
0 & 0 & 0 & 0 & 0 & 0 & 0 & 0 & 0 & 0 & 0 & 0 & 0 & 0 & 0 & 0 & 0 & 0 \\
0 & 0 & 0 & 0 & 0 & 0 & 0 & 0 & 0 & 0 & 0 & 0 & 0 & 0 & 0 & 0 & 0 & 0 \\
0 & 0 & 0 & 0 & 0 & e_{6,35} & 0 & 0 & 0 & 0 & 0 & 0 & 0 & 0 & 0 & 0 & 0 & 0 \\
0 & 0 & 0 & 0 & 0 & 0 & 0 & 0 & 0 & 0 & 0 & 0 & 0 & 0 & 0 & 0 & 0 & 0 \\
0 & 0 & 0 & 0 & 0 & 0 & 0 & 0 & 0 & 0 & 0 & 0 & 0 & 0 & 0 & 0 & 0 & 0 \\
0 & 0 & 0 & 0 & 0 & 0 & 0 & 0 & 0 & 0 & 0 & 0 & 0 & 0 & 0 & 0 & 0 & 0 \\
0 & 0 & 0 & 0 & 0 & 0 & 0 & 0 & 0 & 0 & 0 & e_{12,36} & 0 & 0 & 0 & 0 & 0 & 0 \\
0 & 0 & 0 & 0 & 0 & 0 & 0 & 0 & 0 & 0 & 0 & 0 & 0 & 0 & 0 & 0 & 0 & 0 \\
0 & 0 & 0 & 0 & 0 & 0 & 0 & 0 & 0 & 0 & 0 & 0 & 0 & 0 & 0 & 0 & 0 & 0 \\
0 & 0 & 0 & 0 & 0 & 0 & 0 & 0 & 0 & 0 & 0 & 0 & 0 & 0 & 0 & 0 & 0 & 0 \\
0 & 0 & 0 & 0 & 0 & 0 & 0 & 0 & 0 & 0 & 0 & 0 & 0 & 0 & 0 & 0 & 0 & 0 \\
0 & 0 & 0 & 0 & 0 & 0 & 0 & 0 & 0 & 0 & 0 & 0 & 0 & 0 & 0 & 0 & 0 & 0 \\
0 & 0 & 0 & 0 & 0 & 0 & 0 & 0 & 0 & 0 & 0 & 0 & 0 & 0 & 0 & 0 & 0 & 0
\end{pmatrix}
\end{array},
$$

$$M_3 = \begin{array}{c} \begin{array}{cccccccccccccccccc} v_{19} & v_{20} & v_{21} & v_{22} & v_{23} & v_{24} & v_{25} & v_{26} & v_{27} & v_{28} & v_{29} & v_{30} & v_{31} & v_{32} & v_{33} & v_{34} & v_{35} & v_{36} \end{array} \\ \begin{pmatrix} -e_{1,19} & 0 & 0 & 0 & 0 & 0 & 0 & 0 & 0 & 0 & 0 & 0 & 0 & 0 & 0 & 0 & 0 & 0 \\ -e_{2,19} & 0 & 0 & 0 & 0 & 0 & 0 & 0 & 0 & 0 & 0 & 0 & 0 & 0 & 0 & 0 & 0 & 0 \\ 0 & -e_{3,20} & 0 & 0 & 0 & 0 & 0 & 0 & 0 & 0 & 0 & 0 & 0 & 0 & 0 & 0 & 0 & 0 \\ 0 & -e_{4,20} & 0 & 0 & 0 & 0 & 0 & 0 & 0 & 0 & 0 & 0 & 0 & 0 & 0 & 0 & 0 & 0 \\ 0 & 0 & -e_{5,21} & 0 & 0 & 0 & 0 & 0 & 0 & 0 & 0 & 0 & 0 & 0 & 0 & 0 & 0 & 0 \\ 0 & 0 & -e_{6,21} & 0 & 0 & 0 & 0 & 0 & 0 & 0 & 0 & 0 & 0 & 0 & 0 & 0 & 0 & 0 \\ 0 & 0 & 0 & -e_{7,22} & 0 & 0 & 0 & 0 & 0 & 0 & 0 & 0 & 0 & 0 & 0 & 0 & 0 & 0 \\ 0 & 0 & 0 & -e_{8,22} & 0 & 0 & 0 & 0 & 0 & 0 & 0 & 0 & 0 & 0 & 0 & 0 & 0 & 0 \\ 0 & 0 & 0 & 0 & -e_{9,23} & 0 & 0 & 0 & 0 & 0 & 0 & 0 & 0 & 0 & 0 & 0 & 0 & 0 \\ 0 & 0 & 0 & 0 & -e_{10,23} & 0 & 0 & 0 & 0 & 0 & 0 & 0 & 0 & 0 & 0 & 0 & 0 & 0 \\ 0 & 0 & 0 & 0 & 0 & -e_{11,24} & 0 & 0 & 0 & 0 & 0 & 0 & 0 & 0 & 0 & 0 & 0 & 0 \\ 0 & 0 & 0 & 0 & 0 & -e_{12,24} & 0 & 0 & 0 & 0 & 0 & 0 & 0 & 0 & 0 & 0 & 0 & 0 \\ 0 & 0 & 0 & 0 & 0 & 0 & -e_{13,25} & 0 & 0 & 0 & 0 & 0 & 0 & 0 & 0 & 0 & 0 & 0 \\ 0 & 0 & 0 & 0 & 0 & 0 & -e_{14,25} & 0 & 0 & 0 & 0 & 0 & 0 & 0 & 0 & 0 & 0 & 0 \\ 0 & 0 & 0 & 0 & 0 & 0 & 0 & -e_{15,26} & 0 & 0 & 0 & 0 & 0 & 0 & 0 & 0 & 0 & 0 \\ 0 & 0 & 0 & 0 & 0 & 0 & 0 & -e_{16,26} & 0 & 0 & 0 & 0 & 0 & 0 & 0 & 0 & 0 & 0 \\ 0 & 0 & 0 & 0 & 0 & 0 & 0 & 0 & -e_{17,27} & 0 & 0 & 0 & 0 & 0 & 0 & 0 & 0 & 0 \\ 0 & 0 & 0 & 0 & 0 & 0 & 0 & 0 & -e_{18,27} & 0 & 0 & 0 & 0 & 0 & 0 & 0 & 0 & 0 \\ 0 & 0 & 0 & 0 & 0 & 0 & 0 & 0 & 0 & -e_{2,28} & 0 & 0 & 0 & 0 & 0 & 0 & 0 & 0 \\ e_{19,28} & 0 & 0 & 0 & 0 & 0 & 0 & 0 & 0 & -e_{19,28} & 0 & 0 & 0 & 0 & 0 & 0 & 0 & 0 \\ 0 & 0 & 0 & 0 & 0 & 0 & 0 & 0 & 0 & 0 & -e_{2,29} & 0 & 0 & 0 & 0 & 0 & 0 & 0 \\ e_{19,29} & 0 & 0 & 0 & 0 & 0 & 0 & 0 & 0 & 0 & -e_{19,29} & 0 & 0 & 0 & 0 & 0 & 0 & 0 \\ 0 & 0 & 0 & 0 & 0 & 0 & 0 & 0 & 0 & -e_{4,28} & 0 & 0 & 0 & 0 & 0 & 0 & 0 & 0 \\ 0 & e_{20,28} & 0 & 0 & 0 & 0 & 0 & 0 & 0 & -e_{20,28} & 0 & 0 & 0 & 0 & 0 & 0 & 0 & 0 \\ 0 & 0 & 0 & 0 & 0 & 0 & 0 & 0 & 0 & 0 & -e_{4,29} & 0 & 0 & 0 & 0 & 0 & 0 & 0 \\ 0 & e_{20,29} & 0 & 0 & 0 & 0 & 0 & 0 & 0 & 0 & -e_{20,29} & 0 & 0 & 0 & 0 & 0 & 0 & 0 \\ 0 & 0 & 0 & 0 & 0 & 0 & 0 & 0 & 0 & e_{28,29} & -e_{28,29} & 0 & 0 & 0 & 0 & 0 & 0 & 0 \\ 0 & 0 & 0 & 0 & 0 & 0 & 0 & 0 & 0 & 0 & 0 & -e_{8,30} & 0 & 0 & 0 & 0 & 0 & 0 \\ 0 & 0 & 0 & e_{22,30} & 0 & 0 & 0 & 0 & 0 & 0 & 0 & -e_{22,30} & 0 & 0 & 0 & 0 & 0 & 0 \\ 0 & 0 & 0 & 0 & 0 & 0 & 0 & 0 & 0 & 0 & 0 & 0 & -e_{8,31} & 0 & 0 & 0 & 0 & 0 \\ 0 & 0 & 0 & e_{22,31} & 0 & 0 & 0 & 0 & 0 & 0 & 0 & 0 & -e_{22,31} & 0 & 0 & 0 & 0 & 0 \\ 0 & 0 & 0 & 0 & 0 & 0 & 0 & 0 & 0 & 0 & 0 & e_{30,31} & -e_{30,31} & 0 & 0 & 0 & 0 & 0 \\ 0 & 0 & 0 & 0 & 0 & 0 & 0 & 0 & 0 & 0 & 0 & -e_{10,30} & 0 & 0 & 0 & 0 & 0 & 0 \\ 0 & 0 & 0 & 0 & e_{23,30} & 0 & 0 & 0 & 0 & 0 & 0 & -e_{23,30} & 0 & 0 & 0 & 0 & 0 & 0 \\ 0 & 0 & 0 & 0 & 0 & 0 & 0 & 0 & 0 & 0 & 0 & 0 & -e_{10,31} & 0 & 0 & 0 & 0 & 0 \\ 0 & 0 & 0 & 0 & e_{23,31} & 0 & 0 & 0 & 0 & 0 & 0 & 0 & -e_{23,31} & 0 & 0 & 0 & 0 & 0 \\ 0 & 0 & 0 & 0 & 0 & 0 & 0 & 0 & 0 & 0 & 0 & 0 & 0 & -e_{14,32} & 0 & 0 & 0 & 0 \\ 0 & 0 & 0 & 0 & 0 & 0 & e_{25,32} & 0 & 0 & 0 & 0 & 0 & 0 & -e_{25,32} & 0 & 0 & 0 & 0 \\ 0 & 0 & 0 & 0 & 0 & 0 & 0 & 0 & 0 & 0 & 0 & 0 & 0 & 0 & -e_{14,33} & 0 & 0 & 0 \\ 0 & 0 & 0 & 0 & 0 & 0 & e_{25,33} & 0 & 0 & 0 & 0 & 0 & 0 & 0 & -e_{25,33} & 0 & 0 & 0 \\ 0 & 0 & 0 & 0 & 0 & 0 & 0 & 0 & 0 & 0 & 0 & 0 & 0 & -e_{16,32} & 0 & 0 & 0 & 0 \\ 0 & 0 & 0 & 0 & 0 & 0 & 0 & e_{26,32} & 0 & 0 & 0 & 0 & 0 & -e_{26,32} & 0 & 0 & 0 & 0 \\ 0 & 0 & 0 & 0 & 0 & 0 & 0 & 0 & 0 & 0 & 0 & 0 & 0 & 0 & -e_{16,33} & 0 & 0 & 0 \\ 0 & 0 & 0 & 0 & 0 & 0 & 0 & e_{26,33} & 0 & 0 & 0 & 0 & 0 & 0 & -e_{26,33} & 0 & 0 & 0 \\ 0 & 0 & 0 & 0 & 0 & 0 & 0 & 0 & 0 & 0 & 0 & 0 & 0 & e_{32,33} & -e_{32,33} & 0 & 0 & 0 \\ 0 & 0 & 0 & 0 & 0 & 0 & 0 & 0 & 0 & 0 & 0 & 0 & 0 & 0 & 0 & -e_{18,34} & 0 & 0 \\ 0 & 0 & 0 & 0 & 0 & 0 & 0 & 0 & e_{27,34} & 0 & 0 & 0 & 0 & 0 & 0 & -e_{27,34} & 0 & 0 \\ 0 & 0 & 0 & 0 & 0 & 0 & 0 & 0 & 0 & e_{28,34} & 0 & 0 & 0 & 0 & 0 & -e_{28,34} & 0 & 0 \\ 0 & 0 & 0 & 0 & 0 & 0 & 0 & 0 & 0 & 0 & e_{29,34} & 0 & 0 & 0 & 0 & -e_{29,34} & 0 & 0 \\ 0 & 0 & 0 & 0 & 0 & 0 & 0 & 0 & 0 & 0 & 0 & 0 & 0 & 0 & 0 & 0 & -e_{6,35} & 0 \\ 0 & 0 & e_{21,35} & 0 & 0 & 0 & 0 & 0 & 0 & 0 & 0 & 0 & 0 & 0 & 0 & 0 & -e_{21,35} & 0 \\ 0 & 0 & 0 & 0 & 0 & 0 & 0 & 0 & 0 & 0 & 0 & e_{30,35} & 0 & 0 & 0 & 0 & -e_{30,35} & 0 \\ 0 & 0 & 0 & 0 & 0 & 0 & 0 & 0 & 0 & 0 & 0 & 0 & e_{31,35} & 0 & 0 & 0 & -e_{31,35} & 0 \\ 0 & 0 & 0 & 0 & 0 & 0 & 0 & 0 & 0 & 0 & 0 & 0 & 0 & 0 & 0 & 0 & 0 & -e_{12,36} \\ 0 & 0 & 0 & 0 & 0 & e_{24,36} & 0 & 0 & 0 & 0 & 0 & 0 & 0 & 0 & 0 & 0 & 0 & -e_{24,36} \\ 0 & 0 & 0 & 0 & 0 & 0 & 0 & 0 & 0 & 0 & 0 & 0 & 0 & e_{32,36} & 0 & 0 & 0 & -e_{32,36} \\ 0 & 0 & 0 & 0 & 0 & 0 & 0 & 0 & 0 & 0 & 0 & 0 & 0 & 0 & e_{33,36} & 0 & 0 & -e_{33,36} \\ 0 & 0 & 0 & 0 & 0 & 0 & 0 & 0 & 0 & 0 & 0 & 0 & 0 & 0 & 0 & e_{34,35} & -e_{34,35} & 0 \\ 0 & 0 & 0 & 0 & 0 & 0 & 0 & 0 & 0 & 0 & 0 & 0 & 0 & 0 & 0 & e_{34,36} & 0 & -e_{34,36} \\ 0 & 0 & 0 & 0 & 0 & 0 & 0 & 0 & 0 & 0 & 0 & 0 & 0 & 0 & 0 & 0 & e_{35,36} & -e_{35,36} \end{pmatrix} \end{array}.$$

The rigidity matrix of the entire mechanism is then constructed by

$$\mathbf{M} = \begin{bmatrix} \mathbf{M}_1 & \mathbf{0} \\ \mathbf{M}_2 & \mathbf{M}_3 \end{bmatrix}$$

where $\mathbf{0}$ denotes the 48×54 matrix of zeros.

The rigidity matrix $\mathbf{M}_1$, describing the graph corresponding to the base joints, has a maximum rank of 48, which is equal to the number of edges required for the structure to be rigid (see equation 2 of chapter 3). For the mechanism used in example 2, all of the base joints are coplanar and so the rank of $\mathbf{M}_1$ in this example is 34, 14 below full rank. The base is rigid by definition, so the drop in rank of this matrix is irrelevant. In example 2, the rank of the rigidity matrix $\mathbf{M}$ is 88 at all points during the trajectory, which is 14 less than the minimum number of edges required for this graph to be rigid, except when in the last pose, the singularity, when the rank drops to 87.

B.3 2^{nd} Planar Case

The columns correspond to the coordinates of the vertices v_1 to v_8; where vertices v_1 to v_3 correspond to the base joints A_1 to A_3, vertices v_4 to v_7 correspond to the platform joints B_1 to B_4, and vertex v_8 corresponds to joint S. Just like in the first planar example, each row corresponds to the an edge, $e_{i,j}$, denoting the transpose of the two-dimensional position vector from v_i to v_j, and 0 denotes the two-dimensional row vector of zeros.

$$M = \begin{array}{c} \begin{matrix} v_1 & v_2 & v_3 & v_4 & v_5 & v_6 & v_7 & v_8 \end{matrix} \\ \begin{pmatrix} e_{1,2} & -e_{1,2} & 0 & 0 & 0 & 0 & 0 & 0 \\ e_{1,3} & 0 & -e_{1,3} & 0 & 0 & 0 & 0 & 0 \\ e_{1,4} & 0 & 0 & -e_{1,4} & 0 & 0 & 0 & 0 \\ 0 & e_{2,3} & -e_{2,3} & 0 & 0 & 0 & 0 & 0 \\ 0 & e_{2,5} & 0 & 0 & -e_{2,5} & 0 & 0 & 0 \\ 0 & 0 & e_{3,8} & 0 & 0 & 0 & 0 & -e_{3,8} \\ 0 & 0 & 0 & e_{4,5} & -e_{4,5} & 0 & 0 & 0 \\ 0 & 0 & 0 & e_{4,7} & 0 & 0 & -e_{4,7} & 0 \\ 0 & 0 & 0 & 0 & e_{5,6} & -e_{5,6} & 0 & 0 \\ 0 & 0 & 0 & 0 & e_{5,7} & 0 & -e_{5,7} & 0 \\ 0 & 0 & 0 & 0 & 0 & e_{6,7} & -e_{6,7} & 0 \\ 0 & 0 & 0 & 0 & 0 & e_{6,8} & 0 & -e_{6,8} \\ 0 & 0 & 0 & 0 & 0 & 0 & e_{7,8} & -e_{7,8} \end{pmatrix} \end{array}.$$